Review

Polarimetric remote sensing of atmospheric aerosols: Instruments, methodologies, results, and perspectives

Oleg Dubovik [a,*], Zhengqiang Li [b,*], Michael I. Mishchenko [c], Didier Tanré [a], Yana Karol [d], Bojan Bojkov [e], Brian Cairns [c], David J. Diner [f], W. Reed Espinosa [g,h], Philippe Goloub [a], Xingfa Gu [b], Otto Hasekamp [i], Jin Hong [j], Weizhen Hou [b], Kirk D. Knobelspiesse [h], Jochen Landgraf [i], Li Li [b], Pavel Litvinov [d], Yi Liu [k], Anton Lopatin [d], Thierry Marbach [e], Hal Maring [l], Vanderlei Martins [g], Yasjka Meijer [m], Gennadi Milinevsky [n], Sonoyo Mukai [o], Frederic Parol [a], Yanli Qiao [j], Lorraine Remer [g], Jeroen Rietjens [i], Itaru Sano [p], Piet Stammes [q], Snorre Stamnes [r], Xiaobing Sun [j], Pierre Tabary [s], Larry D. Travis [c], Fabien Waquet [a], Feng Xu [f], Changxiang Yan [t], Dekui Yin [u]

[a] Laboratoire d'Optique Atmosphérique, CNRS/Université Lille, Villeneuve d'Ascq, France
[b] State Environmental Protection Key Laboratory of Satellite Remote Sensing, Institute of Remote Sensing and Digital Earth, Chinese Academy of Sciences, Beijing, China
[c] NASA Goddard Institute for Space Studies, New York, NY, USA
[d] GRASP-SAS, Villeneuve d'Ascq, France
[e] European Organisation for the Exploitation of Meteorological Satellites (EUMETSAT), Darmstadt, Germany
[f] Jet Propulsion Laboratory, California Institute of Technology, Pasadena, CA, USA
[g] University of Maryland, Baltimore County, Baltimore, USA
[h] NASA Goddard Space Flight Center, Greenbelt, MD, USA
[i] SRON Netherlands Institute for Space Research, Utrecht, The Netherlands
[j] Anhui Institute of Optics and Fine Mechanics, Chinese Academy of Sciences, Hefei, China
[k] Institute of Atmospheric Physics, Chinese Academy of Sciences, Beijing, China
[l] Earth Science Division, Science Mission Directorate, NASA Headquarters, Washington, DC, USA
[m] European Space Agency (ESA), Keplerlaan 1, 2201 AZ Noordwijk, The Netherlands
[n] Taras Shevchenko National University of Kyiv, Kyiv, Ukraine
[o] Kyoto College of Graduate Studies for Informatics, Kyoto, Japan
[p] Faculty of Science and Engineering, Kindai University, Osaka, Japan
[q] Royal Netherlands Meteorological Institute, De Bilt, The Netherlands
[r] NASA Langley Research Center, Hampton, VA, USA
[s] CNES–Direction de l'Innovation des Applications et de la Science (DIA), Toulouse, France
[t] Changchun Institute of Optics, Fine Mechanics and Physics, Chinese Academy of Sciences, Changchun, China
[u] Shanghai Institute of Technical Physics, Chinese Academy of Sciences, Shanghai, China

ARTICLE INFO

ABSTRACT

Polarimetry is one of the most promising types of remote sensing for improved characterization of atmospheric aerosol. Indeed, aerosol particles constitute a highly variable atmospheric component characterized by a large number of parameters describing particle sizes, morphologies (including shape and internal structure), absorption and scattering properties, amounts, horizontal and vertical distribution, etc. Reliable monitoring of all these parameters is very challenging, and therefore the aerosol effects on climate and environment are considered to be among the most uncertain factors in climate and environmental research. In this regard, observations that provide both the angular distribution of the scattered atmospheric radiation as well as its polarization state at multiple wavelengths covering the UV–SWIR spectral range carry substantial implicit information on the atmospheric composition. Therefore, high expectations in improving aerosol characterization are associated with detailed passive photopolarimetric observations.

* Corresponding authors.
  E-mail addresses: oleg.dubovik@univ-lille.fr (O. Dubovik), lizq@radi.ac.cn (Z. Li).

The critical need to use space-borne polarimetry for global accurate monitoring of detailed aerosol properties was first articulated in the late 1980s and early 1990s. By now, several orbital instruments have already provided polarization observations from space, and a number of advanced missions are scheduled for launch in the coming years by international and national space agencies. The first and most extensive record of polarimetric imagery was provided by POLDER-I, POLDER-II, and POLDER/PARASOL multi-angle multi-spectral polarization sensors. Polarimetric observations with the POLDER-like design intended for collecting extensive multi-angular multi-spectral measurements will be provided by several instruments, such as the MAI/TG-2, CAPI/TanSat, and DPC/GF-5 sensors recently launched by the Chinese Space Agency. Instruments such as the 3MI/MetOp-SG, MAIA, SpexOne and HARP2 on PACE, POSP, SMAC, PCF, DPC–Lidar, ScanPol and MSIP/Aerosol-UA, MAP/Copernicus CO2 Monitoring, etc. are planned to be launched by different space agencies in the coming decade. The concepts of these future instruments, their technical designs, and the accompanying algorithm development have been tested intensively and analyzed using diverse airborne prototypes. Certain polarimetric capabilities have also been implemented in such satellite sensors as GOME-2/MetOp and SGLI/GCOM-C.

A number of aerosol retrieval products have been developed based on the available measurements and successfully used for different scientific applications. However, the completeness and accuracy of aerosol data operationally derived from polarimetry do not yet appear to have reached the accuracy levels implied by theoretical sensitivity studies that analyzed the potential information content of satellite polarimetry. As a result, the dataset provided by MODIS is still most frequently used by the scientific community, yet this sensor has neither polarimetric nor multi-angular capabilities. Admittedly polarimetric multi-angular observations are highly complex and have extra sensitivities to aerosol particle morphology, vertical variability of aerosol properties, polarization of surface reflectance, etc. As such, they necessitate state-of-the-art forward modeling based on first-principles physics which remains rare, and conventional retrieval approaches based on look-up tables turn out to be unsuitable to fully exploit the information implicit in the measurements. Several new-generation retrieval approaches have recently been proposed to address these challenges. These methods use improved forward modeling of atmospheric (polarized) radiances and implement a search in the continuous space of solutions using rigorous statistically optimized inversions. Such techniques provide more accurate retrievals of the main aerosol parameters such as aerosol optical thickness and yield additional parameters such as aerosol absorption. However, the operational implementation of advanced retrieval approaches generally requires a significant extra effort, and the forward-modeling part of such retrievals still needs to be substantially improved.

Ground-based passive polarimetric measurements have also been evolving over the past decade. Although polarimetry helps improve aerosol characterization, especially of the fine aerosol mode, the operators of major observational networks such as AERONET remain reluctant to include polarimetric measurements as part of routine retrievals owing to their high complexity and notable increase in effort required to acquire and interpret polarization data.

In addition to remote-sensing observations, polarimetric characteristics of aerosol scattering have been measured in situ as well as in the laboratory using polar nephelometers. Such measurements constitute direct observations of single scattering with no contributions from multiple scattering effects and therefore provide unique data for the validation of aerosol optical models and retrieval concepts.

This article overviews the above-mentioned polarimetric observations, their history and expected developments, and the state of resulting aerosol products. It also discusses the main achievements and challenges in the exploitation of polarimetry for the improved characterization of atmospheric aerosols.

1. Introduction

Over the past five decades, remote sensing has been extensively exploited for deriving the global distribution of radiative properties of the Earth's atmosphere and surface. Yet the potential of improving the volume and accuracy of retrieved information and expectations of further evolution of remote-sensing techniques remain high [1,2]. In particular, future progress in the comprehensive characterization of atmospheric aerosol properties is often associated with the advancement of multi-angular multi-spectral polarimetry [3].

Aerosol particles range from a few tenths to several tens of micrometers in size. Particles of such dimensions are usually invisible to the human eye, however they efficiently interact with solar radiation and affect strongly its distribution throughout the atmosphere as well as influence the total atmospheric energy budget, atmospheric visibility, and climate dynamics. They also have important impacts on the environment, air quality and safety, and other aspects of human life.

Yet accounting for the effects of aerosol particles is very difficult since they represent one of the most complex atmospheric constituents. For example, it has widely been recognized that the lingering uncertainty in the knowledge of aerosol properties drives the global climate change estimation uncertainly (e.g., IPCC[1] reports [4,5]). Indeed, aerosol is a mixture of small particles of different sizes, shapes, morphologies, and compositions. The physical and chemical, as well as the resulting optical and radiative, properties of such mixtures can be quite complex and must be described by a large number of parameters. In addition, aerosol properties exhibit a very strong temporal and spatial variability. For example, the loading and composition of aerosol particles over a 10×10 km scene can change dramatically within just half an hour, that is, much faster and much stronger than most atmospheric gases. Therefore, for a reliable characterization of aerosol, a large number of aerosol parameters need to be retrieved simultaneously at rather fine temporal and spatial scales.

Multi-angular multi-spectral polarimeters are widely considered as instruments that can provide most of the requisite information about global and regional properties of aerosols. Indeed,

---

[1] All acronyms along with their definitions are listed alphabetically in Table 1.

simultaneous spectral, angular, and polarimetric measurements of atmospheric radiation should maximize the sensitivity of observations to detailed aerosol properties. Numerous theoretical studies have concluded that polarimetry is an approach that can provide accurate characterization of aerosols with the detail and accuracy sufficient for many important applications. Specifically, the studies by Mishchenko and Travis [6,7], Mishchenko et al. [8], and Hasekamp and Landgraf [9,10] were among the first to suggest that aerosol amount, type, and other detailed properties such as the ability to absorb solar radiation can be derived from polarimetry with an accuracy sufficient for the requisite reduction of the uncertainty in aerosol climate forcing [11]. A number of other independent analyses have supported the conclusion about the strong potential of polarimetric observations for reliable monitoring of various aerosol parameters (e.g., Refs. [12,13], etc.).

The critical need to use space-borne polarimetry for global accurate monitoring of detailed aerosol properties was first articulated in the late 1980s and early 1990s [14,15] based on previous tremendous successes of planetary polarimetry (see, e.g., Refs. [16–20]). As a consequence, the EOSP was included in the NASA EOS payload. Unfortunately, this instrument was later descoped because of budget constraints and expectations that radiometers like MODIS and MISR would provide the requisite aerosol information.

Routine orbital polarimetric observations of the terrestrial atmosphere started in 1996 with the launch of the POLDER instrument [21] on the ADEOS-1 platform. This observational record was continued by two subsequent POLDER instruments launched on the ADEOS-2 and PARASOL satellite platforms (e.g., see Ref. [22]). A dedicated aerosol polarimeter, the NASA APS [23], was lost during unsuccessful launch in 2011. Quite recently, several satellite instruments with polarimetric capabilities have been deployed by national space agencies. A number of future satellite polarimetric instruments and missions are planned and scheduled for launch in the coming decade.

Many airborne versions of orbital polarimeters have been developed and deployed during field campaigns to test and improve the concept of polarimetric remote sensing. Polarimetric observations of aerosol properties have also been implemented by ground-based radiometer networks. In addition, several in situ and laboratory polar-nephelometer systems have been designed for accurate measurements of spectral, angular, and polarimetric characteristics of light singly scattered by aerosol particles.

Nevertheless, the overall volume of polarimetric observations of the atmosphere remains small compared to that of photometric observations. Furthermore, the currently available polarimetric observations are mostly considered as useful datasets for understanding the potential of polarimetry and for designing future missions rather than as an indispensable source of aerosol information for specific climatological and environmental applications [13]. This situation is undoubtedly the result of the general complexity of polarimetric observations and theory. Firstly, obtaining consistent, highly accurate, simultaneous multi-angular polarimetric observations in a sufficiently wide spectral range is a technically difficult task requiring substantial efforts for designing, building, and implementing adequate detection systems. Secondly, and probably more fundamentally, the interpretation of multi-angular multi-spectral polarimetric data is quite challenging. Polarimetry is highly sensitive to a large number of atmospheric parameters, and accounting adequately for all these sensitivities in the retrieval algorithm is very demanding, especially in satellite applications where large volumes of data need to be processed in near-real time or with a minimal delay. Not surprisingly, applications of conventional algorithm types that performed well with intensity-only satellite data (e.g., Refs. [24,25]) to polarimetric observations failed to realize the significant advantages of aerosol polarimetry [26]. Therefore, the need to develop more robust algorithms for deriv-

ing aerosol properties from polarimetry has been clearly identified by the satellite community. As a result, several such highly optimized algorithms have been developed and demonstrated to provide enhanced aerosol retrievals from satellite polarimetry [27–31]. Yet it remains clear that additional efforts are needed for the understanding and utilization of the full potential of aerosol retrievals from polarimetric observations. As it currently stands, satellite polarimetry remains an underexploited area of aerosol remote sensing which requires more attention and investment from the remote sensing community since advancements in this area are likely to drive progress in aerosol (and overall atmospheric) monitoring.

The main objective of this paper is to support ongoing efforts aimed at the advancement of aerosol polarimetry by gathering detailed information about the available and planned polarimetric observations and providing references to other supplementary information on the existing data products and their distribution. We also summarize recent progress in the areas of forward modeling and retrieval algorithm development, outline the most challenging aspects of polarimetric retrievals, and discuss potentially promising ideas for further advancement of polarimetric retrieval methodologies. Owing to its nature, this paper contains a large number of references (Refs. [1–277]). As such, it can also be considered a representative database of publications relevant to polarimetric remote sensing of tropospheric aerosols.

2. Polarimetric observations

This paper is primarily focused on passive polarimetric observations from satellites. However, the most common airborne, ground-based, and laboratory measurements are also discussed for the sake of completeness. Both currently available and expected future observations are considered. The description of relevant instruments is summarized in four tables using a maximally standardized format. Below we provide a brief description of the most important polarimetric datasets currently available. Pertinent information about instruments under development is also included. The description is separated into sections discussing different types of observation, including orbital, airborne, ground-based, and in situ measurements. Yet the main emphasis is on satellite missions, since every such mission involves a thorough design and development stage and is expected to provide a long data record once launched. In contrast, airborne, ground-based, and in situ measurements often accommodate the development and validation needs of different space missions and hence tend to involve continuous modifications of measurement and data processing concepts.

Relatively little will be said in what follows about differentiating polarimeter designs by how they analyze the polarimetric state. Obviously, there is considerable variability in specific approaches, and this variability has significant consequences, especially in terms of polarization accuracy. We refer the reader to the review by Tyo et al. [225] which outlines categorization that could serve to classify characteristics of each design, for example:

- rotating element: POLDER, 3MI, MAI, DPC;
- co-boresighted: RSP;
- division of amplitude: HARP2/PACE, HARP-cubesat;
- division of time: MAIA, AirMSPI.

It is also important to recognize that essentially all previous and current aerosol–cloud polarimeters have been designed to measure only the first three Stokes parameters (I, Q, and U) describing the intensity and linear polarization state of the diffusely reflected sunlight reaching the orbital instrument. This is usually justified by the fact that the first-order scattering in the atmosphere does not contribute to the value of the fourth Stokes parameter (V). As a consequence, it has a relatively small magnitude and typically carries minimal amont of implicit aerosol information [267].

Table 1

Acronyms and their definitions.

Acronym	Definition
3MI	Multi-View Multi-Channel Multi-Polarization Imaging mission
AATSR	Advanced Along-Track Scanning Radiometer
ACE	Aerosol–Cloud–Ecosystem mission
ACEPOL	Aerosol Characterization from Polarimeter and Lidar
ADEOS	Advanced Earth Observing Satellite
AE	Ångström exponent
AERIS	Données et Services pour l'Atmosphère
AEROCLO-SA	AErosol RAdiation and CLOuds in Southern Africa
AERONET	AErosol RObotic NETwork
AIOFM	Anhui Institute of Optics and Fine Mechanics
AirMSPI	Airborne Multi-angle SpectroPolarimeter Imager
ALMP	ALMucantar with Polarization
AMPR	Atmosphere Multi-angle Polarization Radiometer
AOT	Aerosol Optical Thickness
APS	Aerosol Polarimetry Sensor
ARCTAS	Arctic Research of the Composition of the Troposphere from Aircraft and Satellites
AVHRR	Advanced Very High Resolution Radiometer
BPDF	bidirectional polarization distribution function
BRDF	bidirectional reflection distribution function
BUSOC	Belgian User Support Operations Centre
CALIOP	Cloud–Aerosol Lidar with Orthogonal Polarization
CALIPSO	Cloud–Aerosol Lidar and Infrared Pathfinder Satellite Observations
CAPI	Cloud and Aerosol Polarization Imager
CAS	Chinese Academy of Sciences
CCD	charge-coupled device
CM-1	Carbon Monitoring satellite-1
CNES	Centre National d'Etudes Spatiales
CNSA	Chinese National Space Administration
CTM	chemical transport model
CWV	columnar water vapor
DC3	Deep Convective Clouds and Chemistry
DEVOTE	Development and Evaluation of satellite ValidatiOn Tools by Experimenters
DISCOVER-AQ	Deriving Information on Surface Conditions from COlumn and VERtically Resolved Observations Relevant to Air Quality
DLR	German Aerospace Center
DoLP	degree of linear polarization
DPC	Directional Polarimetric Camera
EC	European Commission
Envisat	Environmental Satellite
EOF	empirical orthogonal function
EOS	Earth Observing System
EOSP	Earth Observing Scanning Polarimeter
EPS-SG	EUMETSAT Polar System – Second Generation
ER-2	Earth Resources-2 aircraft
ERS-2	European Remote-Sensing Satellite-2
ESA	European Space Agency
ESTO InVEST	Earth Science Technology Office In-Space Validation of Earth Science Technologies
EU	European Union
EUMETSAT	European Organisation for the Exploitation of Meteorological Satellites
FMF	fine mode fraction
FOV	field of view
GARRLiC	Generalized Aerosol Retrieval from Radiometer and Lidar Combined data
GCOM-C	Global Change Observation Mission–Climate satellite
GF-5	GaoFen-5 spacecraft
GFDM	High Resolution Multi-Mode satellite
GOME	Global Ozone Monitoring Experiment
GRASP	Generalized Retrieval of Aerosol and Surface Properties
HARP	Hyper-Angular Rainbow Polarimeter
HJ-2	Chinese Environmental Satellite-2
HSRL	High Spectral Resolution Lidar
IASI-NG	Infrared Atmospheric Sounder Interferometer – New Generation
ICARE	Cloud–Aerosol–Water–Radiation Interactions center
IFOV	instantaneous field of view
INTEX-B	Intercontinental Chemical Transport Experiment-B
IPCC	Intergovernmental Panel on Climate Change
IR	infrared (spectral range)
ISS	International Space Station
JAXA	Japan Aerospace Exploration Agency
JPL	Jet Propulsion Laboratory
LIRIC	Lidar-Radiometer Inversion Code
LMOS	Lake Michigan Ozone Study
LOA	Laboratoire d'Optique Atmosphérique
LST	Local Sidereal Time
LUT	look-up table
MAI	Multi-Angle polarization Imager
MAIA	Multi-Angle Imager for Aerosols

Table 1 (*continued*)

Acronym	Definition
MAO	Main Astronomical Observatory
MAP/CO2M	Multi-Angle Polarimeter/CO_2 Monitoring mission
MAPP	Microphysical Aerosol Properties from Polarimeter algoritm
MERIS	MEdium Resolution Imaging Spectrometer
MetOp	Meteorological Operational Satellite
MICROPOL	MICROwavelength POlarimeter
MILAGRO	Megacity Initiative: Local and Global Research Observations
MISR	Multiangle Imaging SpectroRadiometer
MODIS	Moderate-Resolution Imaging Spectroradiometer
MSIP	MultiSpectral Imaging Polarimeter
MVPI	Multi-Viewing Polarimetry Imager
NAAMES	North Atlantic Aerosols and Marine Ecosystems Study
NASA	National Aeronautics and Space Administration
NASU	National Academy of Sciences of Ukraine
NIVR	Dutch Space Agency
NSMC	National Satellite Meteorological Center
NWP	Numerical Weather Prediction
OCI	Ocean Color Imager
OLYMPEX	Olympic Mountain Experiment
OMI	Ozone Monitoring Instrument
ORACLES	ObseRvations of Aerosols above Clouds and their intEractionS
OSIRIS	Observing System Including PolaRisation in the Solar Infrared Spectrum
OTB	Orbital Test Bed
PACE	Pre-Aerosol, Clouds, and ocean Ecosystem mission
PACS	Passive Aerosol and Clouds Suite
PARASOL	Polarization and Anisotropy of Reflectances for Atmospheric Sciences coupled with Observations from a Lidar
PCF	Polarization CrossFire Suite
PI-Neph	Polarized Imaging Nephelometer
PM	particulate matter
PODEX	Polarimeter Definition Experiment
POLDER	Polarization and Directionality of the Earth's Reflectance instrument
POSP	Particulate Observing Scanning Polarimeter
PPP	polarized principal plane
PTA	primary target area
RADEX	Radar Definition Experiment
RIVM	National Institute for Public Health and the Environment
RSP	Research Scanning Polarimeter
SABOR	Ship–Aircraft Bio-Optical Research experiment
ScanPol	Scanning along track Polarimeter
SCIAMACHY	SCanning Imaging Absorption spectroMeter for Atmospheric CHartographY
SEAC4RS	Studies of Emissions and Atmospheric Composition, Clouds and Climate Coupling by Regional Surveys
SEVIRI	Spinning Enhanced Visible and InfraRed Imager
SGLI	Second Generation Global Imager
SMAC	Synchronization Monitoring Atmospheric Corrector
SONET	Sun/sky-radiometer Observation NETwork
SPEX	Spectro-Polarimetric Experiment
SRON	Netherlands Institute for Space Research
SSA	single-scattering albedo
STA	secondary target area
SWIR	short-wave infrared (spectral range)
TanSat	Carbon Observing Satellite
TCAP	Two Column Aerosol Project
TG	Tiangong spacecraft
TIR	thermal infrared
TOMS	Total Ozone Mapping Spectrometer
UMBC	University of Maryland/Baltimore County
USA	United States of America
UV	ultraviolet
VIIRS	Visible Infrared Imaging Radiometer Suite
VIS	visible (spectral range)
VNIR	visible and near-infrared (spectral range)

Tables 2–5 summarize the basic information about the instruments endowed with polarimetric capabilities. The information about past, current, and planned observations from satellites is detailed in Tables 2 and 3, respectively. Table 4 provides a summary of airborne polarimeters, while Table 5 describes ground-based and in situ polarimetric observations.

2.1. Previous and currently operating satellite instruments

Table 2 summarizes the information on previous and present-day orbital polarimeters and their respective datasets.

2.1.1. POLDER-1, -2, and -3

Presently, POLarization and Directionality of the Earth's Reflectance (POLDER) instrument observations have spanned about 10 years and represent the longest record of polarimetric multi-angular observations of the Earth from space. The POLDER instruments [21] consist of a digital camera with a 274×242-pixel CCD detector, wide-field telecentric optics, and a rotating filter wheel enabling measurements in 9 spectral channels with bandwidths between 20 and 40 nm. Because it acquires a sequence of images every 20 seconds, the instrument can observe ground targets

Table 2
Launched or completed space-borne instruments.

Instrument/satellite	Organization/country	Launch date – end of mission	Technical characteristics	Orbit	Data products	Data source	Main publications
POLDER-1/ADEOS I	CNES/France	17 Aug 1996 – Jun 1997	Wavelengths: 443 (polarized), 490, 565, 670 (polarized), 763, 765, 865 (polarized), and 910 nm. Viewing angles: ±43° range along track and ±51° range across track. Number of viewing directions: up to 14 successive measurements of a given target. Spatial resolution: 6 × 7 km at nadir. Global coverage in ~2 days with a swath of 1800 × 2400 km (242 × 274 pixels) along/across track.	797-km-altitude sun-synchronous orbit with a 10:30 am descending node.	*Operational product over ocean*: fine mode AOT, fine mode AE, fine mode effective radius, top altitude. *Operational product over land*: AOT, AE, effective radius, top altitude. *Operational GRASP product over ocean and land*: AOT for fine and coarse modes, AE, SSA, spectral complex refractive index, fraction of non-spherical particles, height of aerosol layer, and aerosol type.	AERIS/ICARE Data and Services Center (http://www.icare.univ-lille1.fr)	[61,109] [28,73]
POLDER-2/ADEOS II	CNES/France	14 Dec 2002 – Oct 2003	Same as POLDER-1	Same as POLDER-1	*Operational product over ocean and land*: same as POLDER-1. *Operational GRASP product over ocean and land*: same as POLDER-1	Same as POLDER-1	
POLDER-3/PARASOL	CNES/France	18 Dec 2004 – Dec 2013	Wavelengths: 443, 490 (polarized), 565, 670 (polarized), 763, 765, 865 (polarized), 910, and 1020 nm. Viewing angles: ±51° range along track and ±43° range across track. Number of viewing directions: up to 16 successive measurements of a given target. Spatial resolution: 5.3 × 6.2 km at nadir. Global coverage in ~2 days, with a swath of 2100 × 1600 km (274 × 242 pixels along/across track).	705-km-altitude sun-synchronous orbit with a 1:30 pm ascending node.	*Operational product over ocean and land*: similar to POLDER-1 and -2. *Operational GRASP product over ocean and land*: same as POLDER-1 and -2.	Same as POLDER-1 and -2 Same as POLDER-1 and -2	[22]
APS/Glory Mission	NASA/USA	4 Mar 2011 (failed launch)	Wavelengths: 410, 443, 555, 670, 865, 910, 1370, 1610, and 2200 nm, all polarized. Stokes parameters: *I, Q,* and *U*. Polarimetric accuracy better than 0.2%. 250 angular views per scene (+60°/−80° with respect to nadir). Spatial resolution 5.6 km at nadir. Along-track angular scanning with a pixel-wide lateral swath.	A-train 705-km-altitude 98.2°-inclination ascending sun-synchronous orbit with a 13:34 LST equatorial crossing time.	*Planned operational product*: AOTs, size distribution parameters, and complex refractive indices for two aerosol modes. Particle morphology. Cloud particle size distribution at cloud tops.	N/A	[23,195]
GOME/ERS-2	ESA/EU	28 June 1995–2 July 2011 (starting from July 2003, products have reduced orbital coverage)	Spectral range: 240–793 nm (resolution 0.2–0.4 nm). One view angle, ground pixel resolution: 40 × 320 km, swath 960 km. State of linear polarization in two orthogonal directions in three broad bands.	780-km-altitude sun-synchronous orbit with a 10:30 am descending node.	AOT, UV absorbing aerosol index	https://earth.esa.int/web/guest/missions/esa-operational-eo-missions/ers/instruments/gome	[95,236,268]

Table 2 (*continued*)

Instrument/satellite	Organization/country	Launch date – end of mission	Technical characteristics	Orbit	Data products	Data source	Main publications
GOME-2/MetOp-A	EUMETSAT	19 Oct 2006 onwards	Spectral range: 240–790 nm (with high spectral resolution between 0.26–0.51 nm). One view angle, $80 \times 40/40 \times 40$-km ground pixel resolution, 1920/960-km swath. State of linear polarization in two orthogonal directions in 15 bands covering the spectral region from 312–800 nm with a 10×40-km footprint.	817-km-altitude sun-synchronous orbit with a 9:30 am descending node.	AOT, aerosol model, UV absorbing aerosol index	EUMETSAT web page https://www.eumetsat.int/.../GOME2 ESA web page http://www.esa.int/.../About_GOME-2	[9,105,271,274]
GOME-2/MetOp-B	EUMETSAT	17 Sept 2012 onwards	As above, but 1920-km swath and 80×40-km pixel size.	As above	As above	As above	As above
GOME-2/MetOp-C	EUMETSAT	7 Nov 2018 onwards	As above	As above	As above	As above	As above
SCIAMACHY/Envisat	ESA/DLR/NIVR/BUSOC	1 Mar 2002 – 8 Apr 2012	Spectral range: 240–2380 nm (resolution 0.2–1.5 nm). One view angle, ground-pixel size variable from 30×60 km to 30×240 km. Also limb view. State of linear polarization in two orthogonal directions in six broad bands, at $\times 8$ higher resolution.	800-km-altitude, sun-synchronous orbit, 10:00 am descending node.	AOT, UV absorbing aerosol index, limb aerosol index.	http://www.sciamachy.org/	[269,270,273]
CALIOP/CALIPSO	NASA/USA–CNES/France	28 Apr 2006 onwards	Wavelengths: 532 (polarized) and 1064 nm	Sun-synchronous orbit with a 1:30 pm ascending node.	AOT (532 nm), layer height, backscatter coefficient, extinction coefficient, lidar ratio	https://www-calipso.larc.nasa.gov/tools/data_avail/	[253]
MAI/TG-2	China	15 Sep 2016 onwards	Wavelengths: 565 (polarized), 670 (polarized), 763, 765, 865 (polarized), and 910 nm. 88° angular range and at least 12 viewing directions. Spatial resolution: 3 km. Swath: 770 km.	TG-2 Space Station orbit: ~400 km altitude.	Not yet available	Not yet available	[100]
CAPI/TanSat	China	22 Dec 2016 onwards	Wavelengths: 380, 670 (polarized), 870, 1375, and 1640 (polarized) nm. Spatial resolution: 1.0 km at nadir. Swath: 400 km. Single-view instrument.	Orbit: ~700-km-altitude 98.2°-inclination sun-synchronous orbit with a 13:30 pm ascending node and a 16-day repeat cycle.	Radiance data	NSMC Data and Services Center (http://satellite.nsmc.org.cn)	[49]
DPC/GF-5	CNSA and CAS/China	9 May 2018 onwards	Wavelengths: 443, 490 (polarized), 565, 670 (polarized), 763, 765, 865 (polarized), and 910 nm. Angles: ±50°, 9–12 successive views of a given target. Spatial resolution: 3.3 km at nadir. Global coverage in ~2 days, with a swath of 1850×1850 km (512×512 pixels along/across track).	705-km-altitude sun-synchronous orbit with a 13:30 pm ascending node.	AOT, AE, FMF, columnar water vapor, cloud mask and cloud properties, land and ocean properties.	Not yet available	[140]

Table 2 (*continued*)

Instrument/satellite	Organization/ country	Launch date – end of mission	Technical characteristics	Orbit	Data products	Data source	Main publications
SGLI/GCOM-C	Japan	23 Dec 2017 onwards	*Polarization sensor VNIR-POL* Wavelengths: 673.5 and 868.5 nm. Swath: 1050 km ($\pm$45°). Spatial resolution: 1000 × 1000 m. Angles: one view. *Non-polarization sensor VNIR-non-POL* Wavelengths: 380, 412, 443, 490, 530, 565, 673.5, 763, and 868.5 nm. Swath: 1050 km ($\pm$45°). Spatial resolution: 250 × 250 m except for 763 nm (1 × 1 km). Angles: one view. *Sensor SWIR* Wavelengths: 1050, 1380, 1630, and 2210 nm. Swath: 1400 km. Spatial resolution: 1000 × 1000 m except for 1630 nm (250 × 250 m). Angles: one view. *Sensor TIR* Wavelengths: 10.8 and 12.0 μm. Swath: 1400 km. Spatial resolution: 250 × 250 m. Angles: one view.	798-km-altitude sun-synchronous orbit with a 10:30 am descending node.	*Over ocean*: AOT, AE, aerosol classification. *Over land*: AOT, AE, soot fraction (VNIR-non-POL), SSA (VNIR-POL).	G-Potal (global poltal system) by JAXA; https://gportal.jaxa.jp/gpr/index/index	[118]
MISR/Terra	NASA/USA	18 Dec 1999 onwards	9 view angles (angles at Earth from 0° to $\pm$70.5°); continuous observations on orbit dayside, global coverage between $\pm$82° latitude in 9 days. Swath width ~400 km. Wavelengths: 446, 558, 672, and 866 nm. Spatial resolution 275 m – 1.1 km.	705-km-altitude sun-synchronous orbit with 10:30 am descending node.	Total AOT, plus fractionated AOTs in fine, medium, and coarse modes, spherical and non-spherical aerosols, and absorbing and non-absorbing aerosols. Cloud-top height and albedo, and cloud-tracked, height-resolved vector winds. Surface bidirectional reflectance factors and albedos.	NASA Langley Atmospheric Science Data Center (https://eosweb.larc.nasa.gov/project/misr/misr_table)	[65,67,121,125,161]

O. Dubovik, Z. Li and M.I. Mishchenko et al./Journal of Quantitative Spectroscopy & Radiative Transfer 224 (2019) 474–511

481

Table 3
Future/planned space-borne polarimetric instruments.

Instrument/Satellite	Organization/Country	Launch date (expected)	Technical characteristics	Orbit	Data products	Main publications
HARP/CubeSat	UMBC/USA	2018	Wavelengths: 440, 550, 670, and 870 nm, all polarized. Three polarizations at 0°, 45°, and 90°. Swath: 94° cross track, 114° along track. 60 view angles along track for 670 nm; 20 view angles along track for 440, 550, and 670 nm.	ISS orbit, ~400 km nominal altitude, 51.6° inclination.	Cloud droplet size distributions and thermodynamic phase using cloudbow measurements. AOT, particle size distribution, and refractive indices using GRASP.	[84,157,158]
HARP2/PACE	UMBC/USA	2022	Wavelengths: 440, 550, 670, and 870 nm, all polarized. Three polarizations at 0°, 45°, and 90°. Swath: 94° cross track, 114° along track. 60 view angles along track for 670 nm; 20 view angles along track for 440, 550, and 670 nm. Spatial resolution: 3 km.	675-km-altitude sun-synchronous 1:00 pm orbit.	Cloud droplet size distributions and thermodynamic phase using cloudbow measurements. AOT, particle sizes, and refractive indices. Atmospheric correction for ocean color retrievals.	Not yet available
POSP/HJ-2	China	2019	Wavelengths: 410, 443, 555, 670, 865, 910, 1380, 1610, and 2250 nm, all polarized. Depending on orbit height, at least 60 views in the angular range $\pm 32.5°$, across track scanning. Spatial resolution: 6 km (at nadir).	644-km-altitude sun-synchronous orbit with 10:30 am descending node.	AOT, AE, FMF, aerosol layer height, columnar water vapor, cloud mask and cloud properties, land and ocean properties.	Not yet available
SMAC/GFDM-1	China	2019	Wavelengths: 490 (polarized), 550, 670 (polarized), 870 (polarized), 910, 1380, 1610 (polarized), and 2250 (polarized) nm. Spatial resolution: 7×8 km, two observing pixels along the cross-track direction.	644-km-altitude sun-synchronous orbit with 10:30 am descending node.	AOT, columnar water vapor, cloud mask.	Not yet available
PCF/GF-5(02)	China	2020	*DPC* FOV: $\pm 50°$. Spatial resolution: 1.7 km. Number of viewing angles: > 15. Detector: 1024×1024 pixels. Wavelengths: 443, 490 (polarized), 565, 670 (polarized), 763, 765, 865 (polarized), and 910 nm. *POSP* FOV: at least 100 viewing directions in angular range: $\pm 50°$. Spatial resolution: better than 10.0 km. Wavelengths: 380, 410, 443, 490, 670, 865, 1380, 1610, and 2250 nm, all polarized.	705-km-altitude sun-synchronous orbit with a 10:30 am descending node.	AOT, AE, FMF, aerosol layer height, $PM_{2.5}$, columnar water vapor, cloud mask and cloud properties, land and ocean properties.	Not yet available
DPC–Lidar/CM-1	China	2020	*DPC* Wavelengths: 443, 490 (polarized), 565, 670 (polarized), 763, 765, 865 (polarized), and 910 nm. FOV: $\pm 50°$ along track and $\pm 40°$ across track. Up to 35 successive angular measurements of a given target. Spatial resolution: 2.37 km (at nadir). Detector: 380×512 pixels along/across track. *Lidar* Wavelengths: 532 (polarized) and 1064 nm. Frequency: 20–40 Hz. Laser pulse width: ≤ 20 ns.	506-km-altitude sun-synchronous orbit with a 10:30 am descending node.	AOT, AE, FMF, aerosol layer height, $PM_{2.5}$, columnar water vapor, cloud mask and cloud properties, land and ocean properties.	Not yet available

Table 3 (*continued*)

Instrument/Satellite	Organization/ Country	Launch date (expected)	Technical characteristics	Orbit	Data products	Main publications
3MI	EUMETSAT/EU	2021 MetOp-SG A1; 2028 MetOp-SG A2; 2035 MetOp-SG A3.	10 to 14 angular views of a scene; angular sampling at 10° increments. 12 spectral channels from 410 to 2130 nm. Multi-polarization (9 channels with –60°, 0°, +60° polarizers).	MetOp-like low-Earth orbit: sun-synchronous, 835-km mean altitude, 09:30 local-time descending node.	*Primary operational products*: AOTs for accumulation, coarse and, total modes at high horizontal resolution. Aerosol particle size for accumulation, coarse, and total modes. Aerosol type through AE, refractive index, and non-sphericity index. Aerosol height index. Aerosol absorption. *Secondary operational products*: Improved cloud characterisation through cloud imagery, cloud optical thickness, cloud top height, and cloud microphysics (phase and effective particle size). Land surface properties: surface albedo and BRDF. Vegetation properties: leaf area index, vegetation type, fraction of vegetated land.	[89,156]
MAIA/OTB-2	NASA/USA	2022	Typically 5–9 view angles per scene in step-and-stare mode (view angles at Earth from 0° to ±70°); continuously varying view angles in sweep mode. Scene dimensions for 5 view angles approx. 235 km (cross-track) × 365 km (along-track) from baseline orbit. Wavelengths: 365, 391, 415, 444 (polarized), 550, 646 (polarized), 750, 763, 866, 943, 1044 (polarized), 1610, 1886, and 2126 nm. Spatial resolution ∼200 m at nadir, increasing with off-nadir angle. Aerosol and PM products to be mapped at 1 km resolution.	Low-Earth, sun-synchronous, polar orbit at a baseline altitude of 740 km, ascending node.	*Aerosol products*: Total AOT, SSA, size distribution, and effective height. Fractionated AOTs in fine, medium, and coarse modes, spherical and non-spherical aerosols, and absorbing and non-absorbing aerosols. Effective radii for fine and coarse mode aerosols. *PM products*: Total $PM_{2.5}$, PM_{10}, and speciated $PM_{2.5}$ for sulfate, nitrate, organic carbon, black carbon, and dust.	[66,145]
SpexOne/PACE	SRON/Netherlands and NASA/USA	2022	Hyperspectral measurements in the range 385–770 nm. Spectral sampling 2–4 nm. Spectral resolution for radiance 2–4 nm, for degree of linear polarization 15–40 nm. 5 viewing angles between ±57°. Spatial sampling 2.5 km, spatial resolution 5 km. Swath ∼100 km.	675-km-altitude sun-synchronous 1 pm orbit.	*Aerosols*: Spectral AOT (±0.03 or ±10%), SSA (±0.025), effective radius (±10%), real refractive index (±0.02), imaginary refractive index (±0.001 or ±15%), aerosol layer height (±500 m), column number, particle shape. *Clouds*: effective radius (±10%), effective variance (±50%), cloud optical thickness (±10%), cloud top height (±300 m).	[106]

O. Dubovik, Z. Li and M.I. Mishchenko et al./Journal of Quantitative Spectroscopy & Radiative Transfer 224 (2019) 474–511

483

Table 3 (*continued*)

Instrument/Satellite	Organization/Country	Launch date (expected)	Technical characteristics	Orbit	Data products	Main publications
ScanPol + MSIP/Aerosol-UA	MAO/Ukraine	2022	*ScanPol* Wavelengths: 370, 410, 555, 865, 1378, and 1610 nm (all polarized). Angles: + 50°/–60° along track and ± 0.25° across track; up to 150 successive measurements of a given target. Spatial resolution: 6.0 km at nadir. *MSIP* Five units: 1–3 polarized, 4–5 photometric. Wavelengths: 410, 555, 865 nm (all polarized), 410, 443, 470, and 490 nm (unit 4); 555, 670, 865, and 910 nm (unit 5). Angles: ± 30° along and across track, at least 15 scattering angles for a given target. Spatial resolution: 6 km in the center of 800 × 800 km field-of-view (at nadir).	705-km altitude sun-synchronous orbit with a 13:30 pm ascending node.	AOT of fine and coarse modes, AE, spectral SSA, spectral complex refractive index, fraction of non-spherical particles, height of aerosol layer and aerosol type. (Expected application of GRASP algorithm.)	[165,167]
MAP/CO2M mission	Copernicus/EU	2026–2040	Two concepts are considered in the on-going feasibility studies. One concept is based on polarimetric measurements in 5 views over the spectral range 385–770 nm. The other concept is based on polarimetric measurements in 40 views in 8 spectral channels between 410 and 865 nm. The spatial resolution is 4 × 4 km off-nadir at 50° viewing angle and at the edge of the swath. The CO_2 monitoring mission targets revisit time at 40° latitude every 2 to 3 days. The required DoLP error is below 0.003 over an observation viewing angle range from –60° to + 60°.	Low-Earth, sun-synchronous, polar orbit at an altitude in the 600–850 km range with a 11:30 am local time in descending node.	The main use of the MAP data is to improve the correction for the effect of aerosol on the photon light path in the CO_2 product retrieval. A dedicated aerosol product can also be retrieved.	

Table 4

Airborne polarimeters.

Instrument	Organization/Country	Deployment period	Technical characteristics	Altitude	Data products	Main publications
RSP	NASA/USA	1999 onward	Wavelengths: 410, 470, 555, 670, 865, 960, 1590, 1880, and 2250 nm, all polarized. Stokes parameters: I, Q, and U. Polarimetric accuracy better than 0.2%. 152 angular views per scene ($\pm 60°$ with respect to nadir). IFOV: 14 mrad. Along-track angular scanning with a pixel-wide lateral swath.	20 km	AOT, size distribution parameters, and complex refractive index for two aerosol modes. Particle morphology. Cloud particle size distribution at cloud tops.	[31,34,42,51,53,56]
AirMSPI	NASA/USA	2010 onward	Wavelengths: 355, 380, 445, 470 (polarized), 555, 660 (polarized), 865 (polarized), and 935 nm. Angles: $\pm 67°$. Spatial resolution: 10 m grid (step-and-stare mode), 25 m (sweep mode). Scene dimensions: 10 km (cross-track) $\times$ 10 km (step-and-stare mode), 80–100 km (sweep mode).	20 km	AOT, SSA, refractive index, size distribution, aerosol layer height, fraction of non-spherical aerosols, cloud optical thickness and cloud-top droplet size.	[29,64,256,257]
AirMSPI-2	NASA/USA	2015 onward	Wavelengths: 367, 386, 445 (polarized), 543, 645 (polarized), 751, 763, 862 (polarized), 945, 1620 (polarized), 1888, and 2185 (polarized) nm.			
Airborne DPC	AIOFM/China	2010	Wavelengths: 495 (polarized), 550, 665 (polarized), 780, 865 (polarized), and 910 nm. Angles: $\pm 60°$, up to 8 successive angular views of a scene. Spatial resolution: 4 m (at nadir). Detector: 1024×1024 pixels along/across track.	4 km	AOT	[50,99]
Airborne SMAC	AIOFM/China	2014	Wavelengths: 490 (polarized), 550, 670 (polarized), 870 (polarized), 910, 1380, 1610 (polarized), and 2250 (polarized) nm. FOV: $1.44° \times 1.44°$, two observing pixels along the cross-track direction	3.5 km	AOT, CWV	Not yet available
AMPR (Airborne POSP)	AIOFM/China	2014	Wavelengths: 490, 555, 665, 865, 960 and 1640 nm, all polarized. Up to 111 successive angular measurements of a given scene in angular range: $\pm 55°$ from nadir. IFOV: 17 mrad. Coverage: along/across track.	3.1–3.6 km	AOT, AE	[198,240,241]
MICROPOL	LOA/CNRS, France	2005–2017	Wavelengths: 380, 410, 490, 670 (polarized), 865 (polarized), 1600 (polarized), and 2200 nm (polarized). Single view (adjustable during the flight): $\pm 45°$ in steps of 15°. Field of view: 1.5°.	10 km		[246,247,251]
OSIRIS	LOA/CNRS, France	2017	Wavelengths: 440, 490, 670, 763, 765, 865, 910, 940, 940, 1020, 1240, 1365, 1600, and 2200 nm, all polarized. Viewing angles: $\pm 57°$ (VIS) and $\pm 52.5°$ (SWIR); number of directions: 20 (VIS) and 19 (SWIR). Pixel size: 18 m (VIS) and 58 m (SWIR) with a swath of 25×19 km (VIS) and 19×15 km (SWIR) at 10-km altitude.	10 km		[36]
SPEX airborne	SRON/Netherlands	2017	Hyperspectral measurements in the range 400–800 nm. Spectral sampling 2–4 nm. Spectral resolution for radiance 2–4 nm, for DoLP 15–40 nm. Nine viewing angles between $\pm 57°$. Spatial sampling 250 m, spatial resolution 250 m. Swath $\sim$3 km.	Up to 20 km		[201]
AirHARP	UMBC/USA	2017	Wavelengths: 440, 550, 670, and 870 nm, all polarized. Three polarizations at 0°, 45°, and 90°. Cross track swath: 94°; along track swath: 114°. 60 view angles along track for 670 nm; 20 view angles along track for 440, 550, and 870 nm. Spatial resolution: 20 m.	Up to 20 km	Cloud droplet size distributions and thermodynamic phase using cloudbow measurements. AOT, particle size distribution, and refractive indices using GRASP.	Not yet available

O. Dubovik, Z. Li and M.I. Mishchenko et al./Journal of Quantitative Spectroscopy & Radiative Transfer 224 (2019) 474–511

485

Table 5
Ground-based and in situ polarimetric instruments.

Instrument	Organization/Country	Deployment period	Technical characteristics	Characteristics	Data products	Data source	Main publications
CE318-2 sun/sky-radiometer	Cimel/France	1992 onward	Wavelengths: 440, 675, 870, 870P1, 870P2, 870P3, 936, and 1020 nm. Polarization is derived from the combination of 870P1, 870P2, and 870P3.	PPP: from –85° to ~85° in solar principal plane.	Radiance, DoLP (870 nm)	AERONET, http://aeronet.gsfc.nasa.gov PHOTONS, http://www-loa.univ-lille1.fr/photons	[96,111]
CE318-DP sun/sky-radiometer	Cimel/France	2010 onward	Wavelengths: 340, 380, 440, 500, 675, 865 (all polarized), 936, 1020 and 1640 (both polarized) nm. FOV: ~1.2°.	PPP: from –85° to ~85°. Polarized almucantar: from 30° to ~330°.	Radiance, DoLP, spectral AOT, AE, FMF, spectral SSA, spectral (1,1) and (1,2) elements of the scattering matrix, spectral asymmetry parameter, lidar ratio, size distribution, spectral real and imaginary refractive index, effective radius, aerosol volume, non-spherical ratio, radiative forcing, radiative forcing efficiency, aerosol water, ammonium sulfate, coarse mode component, fraction of brown carbon, fraction of black carbon.	AERONET, http://aeronet.gsfc.nasa.gov PHOTONS, http://www-loa.univ-lille1.fr/photons SONET, http://www.sonet.ac.cn	[138,141]
GroundMSPI	NASA/USA	2010 onward	Wavelengths: 355, 380, 445, 470 (polarized), 555, 660 (polarized), 865 (polarized), and 935 nm.	Pushbroom camera mounted in a drum and rotated about a horizontal axis to achieve field of view.	Radiance in all bands and Stokes components Q and U in the polarimetric bands.	ACEPOL: https://eosweb.larc.nasa.gov/project/airmspi/groundmspi_acepol_radiance_data_v9	[69,71]
GroundSPEX	RIVM/Netherlands	July and September 2013	Wavelengths: 400–900 nm with ~1 nm resolution for radiance and 10–20 nm for DoLP.	Scanning the principal plane between –60° and + 60° at 25 angles.	*For fine and coarse mode:* effective radius, complex refractive index, particle column. *For coarse mode:* fraction of spherical particles. *Optical properties:* AOT (fine, coarse, total), SSA		
PI-Neph	UMBC/USA	2011 onward	Wavelengths: 473, 532, and 671 nm.	Phase function and polarized phase function measured from 3°–175° in scattering angle at 1° resolution.	Scattering coefficient, asymmetry parameter, SSA, size distribution, real and imaginary refractive index, fraction of spherical particles.	DEVOTE: http://www-air.larc.nasa.gov/cgi-bin/ArcView/devote?BE200=1-DOLGOS.GERGELY/ DISCOVER-AQ: http://doi.org/10.5067/Aircraft/DISCOVER-AQ/Aerosol-TraceGas DC3: http://doi.org/10.5067/Aircraft/DC3/DC8/Aerosol-TraceGas SEAC4RS: http://doi.org/10.5067/Aircraft/SEAC4RS/Aerosol-TraceGas-Cloud	[72,81,82]
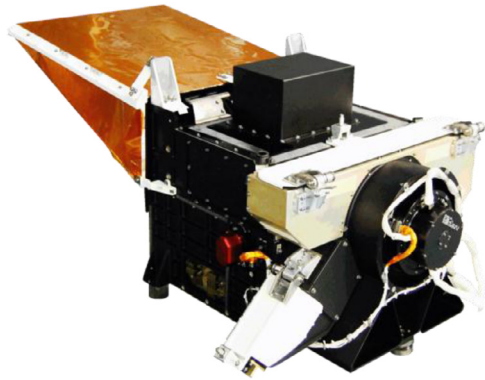
Fig. 1. The Glory APS.

from different viewing directions. The two instruments onboard ADEOS 1 and 2 are identical (Table 2), while the instrument on the PARASOL platform [22] was rotated by 90° to favor multidirectional viewing (a maximum of 16 directions compared to 14) over daily global coverage. Determined by the altitude of the corresponding orbits, the size of the images varies from 2400×1800 km to 1600×2100 km (across/along track) with the respective ground resolutions of 7×6 and 5.3×6.2 km at nadir. The PARASOL platform is part of the A-Train and enables researchers to take advantage of the presence of other instruments in the constellation. The spectral coverage of the three instruments ranges from blue (443 nm) through near IR (910 nm) with three polarized spectral bands. For POLDER-3, the "bluest" polarized channel was moved from 443 to 490 nm, and a 1020-nm channel was added. Innovative techniques [86–88,101] have been developed to calibrate the POLDER instruments in flight.

2.1.2. APS on GLORY

The Aerosol Polarimetry Sensor (Fig. 1, [195]) was launched on the Glory satellite on 4 March 2011. This NASA mission would yield comprehensive and highly accurate data on the chemical, microphysical, and optical properties of aerosols and their spatial and temporal distributions. Unfortunately, due to a malfunction on the launch vehicle, the APS did not reach its intended orbit and hence provided no data. Nonetheless, the development of the APS concept, relevant scientific analyses, and analyses of data from its airborne prototype (e.g., Ref. [44]) have strongly stimulated the progress of and interest in polarimetry as a remote-sensing tool. As a consequence, the conceptual design of several recent polarimeters relies on the APS heritage.

The APS design yields a high polarimetric accuracy (0.2% or better for DoLP), provides a wide range and large number of viewing directions sampled for each scene, and densely covers the relevant VIS–SWIR spectral range. The instrument uses a polarization-compensated scan mirror assembly to scan along the ground track and thereby obtain the requisite range and number of viewing directions. Six boresighted refractive telescopes are paired, with each pair making measurements in three spectral bands. One telescope in each pair makes simultaneous measurements of the linear polarization components of the intensity in orthogonal planes at 0° and 90° to the meridional plane of the instrument, while the other telescope simultaneously measures equivalent intensities in orthogonal planes at 45° and 135°. This approach ensures that the polarization signal is not contaminated by uncorrelated spatial or temporal scene intensity variations during the course of the polarization measurements, which could create false polarization. These measurements in each instantaneous field of view in a scan provide the simultaneous determination of the intensity and the degree and azimuth of linear polarization in all nine spectral bands.

Owing to its very fine angular resolution (250 angular views per scene), the APS design provides the unique capability to profile neutral polarization points that are very sensitive to the height and imaginary refractive index of absorbing aerosols [51], and to sample cloudbows that allow for the retrieval of droplet size distribution in the top layer of clouds with extreme precision [32,34]. Furthermore, this type of fine angular resolution makes possible aerosol retrievals over clouds on the pixel level.

2.1.3. MAI on TG-2

The Multi-Angle polarization Imager onboard the Tiangong-2 spacecraft was launched on 15 September 2016. The TG-2 is the second Chinese space laboratory following TG-1. Its goal is to verify the technology of space rendezvous and docking and also conduct a series of space experiments. The MAI is an Earth observation instrument providing multi-channel multi-angle polarization measurements. It has six channels, including three with polarimetric sensitivity centered at 565, 670, and 865 nm. Observations with 12 different viewing directions for each channel at a resolution of 3 km can be obtained. The instrument can effectively detect the information on clouds (such as cloud phase and top height), aerosols, and atmospheric water content. Its capability for cloud phase identification has been confirmed by the MAI airborne simulator used during a field campaign on 23 October 2015 [100]. During this campaign, a homogeneous stratocumulus cloud layer was overflown at an altitude of 3.7 km above the sea. Three polarization channels of the MAI accurately capture the character of polarized radiation of water clouds (primary cloudbow) near 140° scattering angle. Additionally, due to the non-solar synchronous orbit of the TG-2, polarization observations under different geometry conditions can be obtained, which can provide a unique support for the development of vector radiative transfer models.

2.1.4. CAPI on TanSat

The Cloud and Aerosol Polarization Imager onboard the TanSat mission was launched on 22 December 2016 and is expected to operate for three years. The 620-kg TanSat was sent into a sun-synchronous orbit about 700 km above the earth and aims to monitor the concentration, distribution, and flow of carbon dioxide (CO_2) in the atmosphere to help understand climate change [242]. The CAPI is a 5-channel (380, 670, 870, 1375, and 1640 nm) imager, with additional measurements of linear polarization at 670 and 1640 nm. This instrument was designed to yield cloud and aerosol characteristics to improve the retrieval of greenhouse gases. The CAPI is a push broom system imager using linear detectors, which consists of two units operating in the VIS and SWIR spectral ranges. The radiance measurements from the UV to near IR with additional measurements of the Stokes parameters were designed for the retrieval of aerosol optical and microphysical properties. The stronger sensitivity of polarized measurements to aerosol properties provides additional independent information [48,49].

2.1.5. DPC on GF-5

The Directional Polarimetric Camera onboard the GaoFen-5 spacecraft (Fig. 2), which is the fifth member of the series of China High-resolution Earth Observation System satellites of the CNSA, was launched on 9 May 2018. The GF-5 is also the flagship of the atmospheric environmental monitoring satellites among CNSA on-orbit programs. The DPC was built by the AIOFM of the CAS and consists of a digital camera with a 512×512-pixel CCD matrix. It has eight channels from 443 to 910 nm, including three spectral bands (centered at 490, 670, and 865 nm) yielding polarization measurements. Observations for at least 9 viewing directions for each channel can be obtained when the satellite passes over
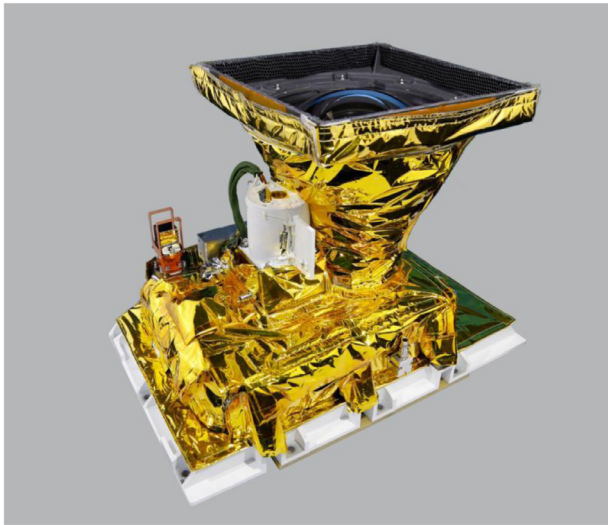
Fig. 2. DPC sensor onboard the GF-5 satellite.

a target. The DPC is designed for the retrieval of spectral properties of atmospheric aerosol, including the spectral AOT, the AE, and the FMF [140]. It can also provide atmospheric correction parameters for the Greenhouse-gases Monitoring Instrument onboard the same satellite GF-5.

2.2. Satellite instruments with multi-angular and/or limited polarimetric capabilities

2.2.1. SGLI on GCOM–C

The Second Generation Global Imager onboard the Global Change Observation Mission–Climate satellite was launched on 23 December 2017 and has been in operation since the spring of 2018. The SGLI is composed of two sensors as the push-broom VNIR radiometer and the whisk-broom infrared scanner instruments. The SGLI measures the Earth's reflectance at 19 wavelengths from the near UV (380 nm) to far IR (12 μm). The polarization optics is included in the VNIR, which can measure I, Q, and U as semi-Stokes parameters at 673.5 and 868.5 nm. The polarization information is taken with three different directions of polarizers ($-60°$, $0°$, and $+60°$). Note that the central polarizer ($0°$) is assigned to the forward direction of the satellite. The VNIR polarization optics has a tilting function that can measure $+45°$ (forward of nadir direction) or $-45°$ (backward) directional information; these large tilting angles are equivalent to forward and backward edge of the POLDER-1 and -2 CCD sensors. The tilting direction is changed with latitude in order to take the measurements at side-scattering angles ($\sim 90°$ to $\sim 120°$), because the magnitude of linear polarization in the backward scattering region is low. Accurately measuring small polarization features at large scattering angles is difficult because each position of the three polarizers in the telescope views slightly different targets. This implies that the SGLI measures synthetic I, Q, and U for targets because of the different positions of the linear CCD arrays in the focal plane of the telescope. Furthermore, the POLDER instruments also measure the synthetic I, Q, and U owing to the difference in acquisition times along the satellite track. Again, in the SGLI case, the angular difference between the three different measurements with a polarizer at $-60°$, $0°$, and $+60°$ is small. Each viewing angle of each polarizer is included in the SGLI level 1B polarization dataset. Also, such small polarization is weak from the signal-to-noise-ratio point of view.

Note that the measurements of I, Q, and U at two wavelengths are only available from one viewing angle, compared to a maximum of 14 directions from POLDER-1 and -2 or 16 directions

from POLDER/PARASOL. However, the non-polarized VNIR optics (i.e., most of observations from 380 nm to 12 μm) always takes nadir-looking measurements. This means that two-directional total reflectances at wavelengths of 673.5 and 868.5 nm are available. The IFOVs of the polarized and non-polarized VNIR optics are 1000 m ($+45°$ or $-45°$ direction) and 250 m, respectively. Although it can be said that the SGLI polarized VNIR sensor is a successor to POLDER, it was not designed for multi-angle observations.

2.2.2. GOME on ERS-2, SCIAMACHY on Envisat, and GOME-2 on MetOp-A/B/C

The Global Ozone Monitoring Experiment instrument operated onboard ESA's ERS-2 satellite launched in July 1995. GOME was a smaller version of the Scanning Imaging Absorption Spectrometer for Atmospheric Chartography which was launched in March 2003 on ESA's Envisat satellite. These instruments were designed to measure trace gases, especially ozone and related gases, by high-resolution spectrometry: GOME from 240–790 nm with a 0.2–0.4 nm resolution, and SCIAMACHY from 240–2380 nm with a 0.2–1.5 nm resolution. The instruments had a scan mirror which enabled cross-track scanning in nadir, as well as sideways viewing for solar and lunar calibration. Since the instruments were sensitive to the polarization of the incoming light, they carried three (GOME) or seven (SCIAMACHY) broad-band polarization sensors to detect the Stokes parameter Q. In this way the incident signal could be corrected for polarization using the on-ground-calibrated polarization sensitivity of the instrument and the measured Q [275]. SCIAMACHY measured not only in nadir but also in limb view [276].

An improved version of GOME is GOME-2 flown on the EU-METSAT's MetOp satellites. MetOp-A, MetOp-B and MetOp-C were launched in October 2006, September 2012 and November 2018, respectively. Like GOME, GOME-2 has 4096 spectral points from four main channels per GOME-2 ground pixel. The footprint size is 80×40 km for the main-channel data. The instrument also measures the state of linear polarization of the Earth's radiance in two perpendicular directions, using linear diode arrays, resulting in the measurement of the spectral Stokes parameters I and Q. The polarization data are down-linked in 15 spectral bands covering the region from 312 to 800 nm for both polarization directions with a footprint of 10×40 km. Although the GOME, SCIAMACHY, and GOME-2 data are primarily aimed at getting a detailed picture of atmospheric chemistry, they are also used for detecting absorbing aerosols [9,95,236,268,277].

2.2.3. MISR on Terra

The Multi-angle Imaging SpectroRadiometer [65] was launched into a polar, sun-synchronous orbit aboard NASA's Terra spacecraft on 18 December 1999. MISR uses nine cameras to image the Earth at nine discrete view angles: $0°$ (nadir) and $26.1°$, $45.6°$, $60.0°$, and $70.5°$ forward and backward of nadir, providing global mapping of aerosols every nine days. Although MISR is not a polarimeter (the cameras include Lyot depolarizers to render them insensitive to scene polarization), it underscores the importance of multi-angle observations for aerosol remote sensing and provides heritage for development of its polarimetric successors, particularly MAIA described in Section 2.3. Multi-angle radiance observations help separate aerosol signals from surface reflection and provide sensitivity to aerosol scattering phase functions, which are governed by particle size, shape, and optical characteristics [67,121,125,126].

2.3. Planned satellite observations

2.3.1. 3MI on EPS-SG

The Multi-View Multi-Channel Multi-Polarization Imaging mission [89,156] planned to fly on the EUMETSAT Polar System – Second Generation platform in the time-frame 2020–2040, is a
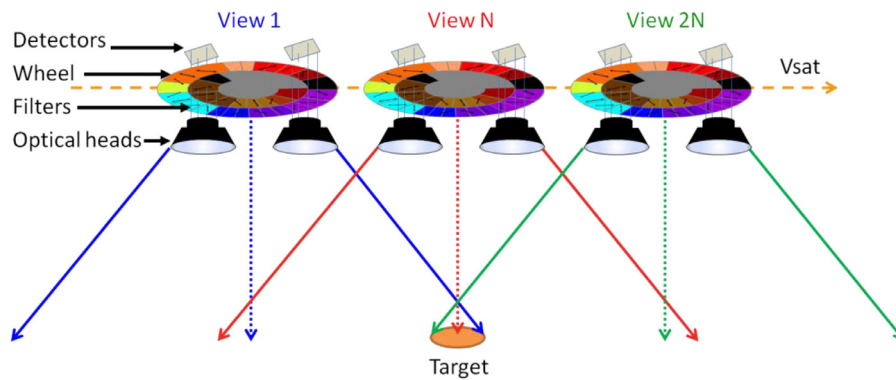
Fig. 3. The 3MI concept of multi-view, multi-spectral, and multi-polarization sampling.

2D wide field of view radiometer dedicated to aerosol and cloud characterization for climate monitoring and atmospheric composition studies, as well as for air quality applications and numerical weather prediction. The instrumental concept of the 3MI is largely inherited from POLDER-3. The purpose of the 3MI is to provide multi-spectral (from 410 to 2130 nm), multi-polarization (–60°, 0°, and +60°), and multi-angular (10 to 14 views) images of the outgoing top-of-atmosphere radiation. The 3MI information on aerosol and cloud properties (and that relevant to aerosol–cloud interaction studies) is expected to far exceed that from the standard radiometers (e.g., MODIS) performing intensity-only measurements at a single viewing angle. The clear shortcoming of the 3MI is the absence of thermal infrared channels. However, these measurements will be available from the METimage and IASI-NG instruments planned to fly on the same satellite platform allowing a synergetic cloud retrieval algorithm to be developed. The Sentinel-5 high-resolution spectrometer will provide information from the UV to the SWIR, through a coarser horizontal sampling. These instruments will provide useful cross calibration (radiometric, spectral, and geometrical) with the 3MI. Indeed, the 3MI has no on-board calibration and thus depends on vicarious techniques using Earth reference scenes as calibration targets. From the POLDER-3 heritage [88,101,156], several methods are available to be adapted and used for the 3MI vicarious calibration during commissioning and operational phases: Rayleigh scattering, sunglint, desert sites, deep convective clouds [87,88], Moon views, and cross calibration with other instruments. These methods are complementary and build a strong toolbox for calibration and validation. This set of methods will also cover vicarious calibration of the new 3MI SWIR channels. The methods are still under improvement (e.g., over Antarctica and using Moon views [86]). However, the performance of these methods has already shown that the requisite calibration accuracy can be achieved.

The 3MI heritage comes from the POLDER/PARASOL missions which are based on a mature technology, with proven reliability fundamental for EUMETSAT operational product policy. The 3MI is a new EUMETSAT mission and has therefore no link to EPS-SG instruments. The 3MI design consists basically of a filter and a polarizer wheel rotating in front of the detectors (Fig. 3). For design purposes, the spectral channels are split into VNIR and SWIR filters and polarizers with dedicated detectors and optical heads. The spectral channels are listed in Table 3. The multi-polarization (three acquisitions within 1 s for the polarized channels) and multi-spectral acquisitions are done within a wheel rotation period of less than 5.5 s. The multi-viewing capability is achieved by successive images of the same spectral channel observing the scene from different angles, allowing up to 14 views per target.

The 3MI products (Table 3) will provide valuable information on the aerosol load in the atmosphere and, e.g., its impact on the
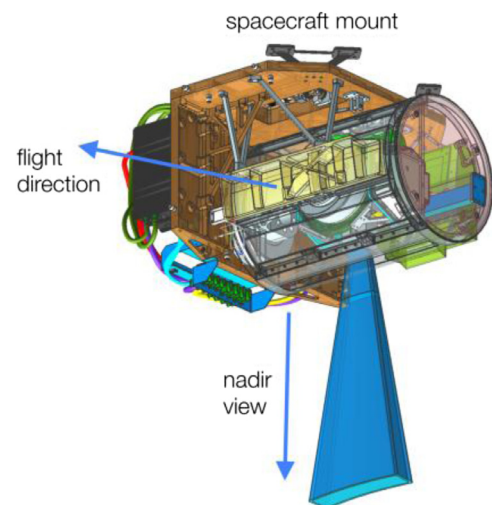
Fig. 4. Computer rendering of the MAIA instrument. The camera field of view is pointable in two axes using a gimbal assembly. Dimensions of the instrument are approximately 0.9 m (W) × 0.7 m (L) × 0.5 m (H).

radiative forcing of the Earth's atmosphere. The 3MI products will as well be beneficial to the NWP by improving sounding and imaging data from METimage, Sentinel-5, and the IASI-NG with a better constraint on the artefacts induced by scattering and polarization of radiation by aerosols and the identification of cirrus clouds. In general, the 3MI products will be used to improve air quality monitoring applications (e.g., aerosol mass load for particles smaller than 2.5 μm ($PM_{2.5}$) or 10 μm (PM_{10})). Combined with the aerosols' absorption index, natural hazards like volcanic ash or fire plumes can also be observed, thereby contributing to now-casting for ash and fire detection.

2.3.2. MAIA

NASA selected the Multi-Angle Imager for Aerosols (Fig. 4) investigation in 2016 as part of its Earth Venture Instrument program. At the heart of the MAIA instrument is a spectropolarimetric camera making use of the same polarimetric retardance modulation technique employed in AirMSPI and AirMSPI-2 (Section 2.4). However, unlike its airborne counterparts in which the camera is mounted on a single-axis gimbal, the MAIA camera will be mounted on a dual-axis gimbal, enabling both along-track multi-angle viewing over a ±70° range (at the Earth's surface) as well as observations of targets displaced in the cross-track direction from the subsatellite ground track. MAIA is to be launched into a low-Earth, sun-synchronous, polar orbit. The baseline orbit altitude and mean local time of equator crossing are 740 km and 10:30

am, respectively. NASA has selected General Atomics Electromagnetic Systems to provide the OTB-2 spacecraft for hosting of the MAIA instrument. Launch is expected to occur in 2022. JPL's MAIA instrument design builds upon the MISR, AirMSPI, and AirMSPI-2 legacies, and incorporates spectral bands from the UV to SWIR (cf. Tables 3 and 4). Unlike MISR, MAIA is a targeted instrument, and would visit at least 10 globally distributed PTAs at a frequency of at least three times per week, using a step-and-stare viewing mode. The PTAs are major population centers designated for conducting investigations of linkages between different types of airborne PM and human health [66,145]. In addition to the PTAs, STAs for other aerosol and cloud science would also be observed, making use of either step-and-stare or sweep mode (see AirMSPI/AirMSPI-2 descriptions in Section 2.4 for definitions of these modes), depending on the measurement objective.

2.3.3. POSP, SMAC, PCF, and DPC-Lidar

The CNSA has approved several space-borne polarimeters in the framework of its Space Infrastructure program. As listed in Table 3, these are the Particulate Observing Scanning Polarimeter, Synchronization Monitoring Atmospheric Corrector, Polarization CrossFire Suite, and Directional Polarimetric Camera with polarized Lidar. The launch of these instruments is planned for the period 2019–2020.

The POSP is a cross-track scanning polarimeter with polarized channels from near-UV to SWIR (410–2250 nm) and without multi-angular capability. Its large scanning angle range (65°) provides wide-swath coverage with intermediate spatial resolution (about 6 km). Polarimetric measurements of the surface-atmosphere system from the POSP provide a unique supplement to other sensors on-board the HJ-2A and -2B satellites. The optical design of the POSP closely follows that of the APS.

The SMAC is a specialized sensor for the purpose of atmospheric correction for high-resolution sensors. It also has a wide spectral range (490–2250 nm) and is equipped with essential polarization bands for aerosol, cloud, and surface monitoring. Notably, its compact size and small weight make it economically affordable. The SMAC on-board the GFDM-1 satellite has two pixels, each having a spatial resolution of about 7 km. By simultaneously measuring atmospheric and surface parameters, it provides a near-real-time correction of high spatial resolution images from the GFDM-1.

The PCF is a heavyweight level polarimeter on-board the next Chinese atmospheric environment flagship satellites (GF-5(02)) and consists of the DPC and POSP. The synergistic and effective design of the combination provides a very wide spectral and polarization range (380–2250 nm) together with the multi-angular capability. The simultaneous UV (380 nm) and SWIR (2250 nm) channels are very useful for improving polarimetric measurements and aerosol monitoring from space. Moreover, the on-board calibration units of the POSP will be used to transfer the highly accurate polarimetric calibration to the DPC.

Finally, the DPC on the CM-1 is deployed alongside a polarized atmospheric Lidar. The Lidar has two spectral channels centered at 532 and 1064 nm; the former is polarization-sensitive. By combing the active and passive polarimetric measurements, the atmospheric parameters are expected to be retrieved with unprecedented precision.

2.3.4. HARP, HARP2 on PACE

The design of the Hyper-Angular Rainbow Polarimeter family focuses on hyperangular polarimetric measurements in different spectral ranges: UV, VNIR, and SWIR. Two satellites are currently funded with the VNIR version of the HARP instrument with four wavelength bands (440, 550, 670, and 865 nm): HARP CubeSat as a technology demonstration and HARP2 as part of the NASA PACE

mission as an operational imaging polarimeter providing global coverage in two days.

The HARP/CubeSat [157,158] satellite funded by the NASA ESTO InVest Program is designed to measure the properties of aerosols and cloud particles from space. The HARP payload is a hyperangular imaging polarimeter that can see Earth simultaneously from multiple viewing angles, four wavelengths, and three polarization angles. It was developed and built at the Earth and Space Institute at UMBC with support from the Joint Center of Earth Systems and Technology and the NASA Goddard Space Flight Center. The HARP spacecraft was designed and built at the Space Dynamics Laboratory in Utah. The HARP polarimeter has no moving parts and is based on a modified Philips prism design [84] providing simultaneous measurements of linear polarization at three orientation angles. The HARP/CubeSat payload is fully programmable and allows for the selection of different spatial resolutions, multiple wavelengths, and tens of along-track viewing angles depending on the science interest and available bandwidth for data to downlink. The different along-track viewing angles from HARP will allow observations of targets on the ground from different viewing perspectives including up to 60 independent angles at 670 nm and up to 20 different viewing angles at the other three wavelengths. The different viewing observations of the same target allow for additional information, thereby facilitating the quantitative retrieval of atmospheric and surface properties such as the aerosol particle amount, aerosol particle size, shape, and complex refractive index, as well as cloud droplet sizes, and specific characteristics of the Earth's surface. HARP/Cubesat will be launched from the International Space Station in 2019 and will produce data with a nominal resolution of 4 km.

The HARP2 instrument onboard the NASA PACE mission is an improved copy of the HARP/CubeSat payload. The main enhancements on HARP2 as compared to HARP/CubeSat are better calibration schemes, improved spatial resolution, and better signal-to-noise ratios resulting in higher measurement accuracy. Fig. 5 shows the 3D rendering of the HARP2 instrument as currently designed for the PACE satellite as well as photographs of the HARP CubeSat payload.

The NASA PACE mission [266], slated for launch in late 2022, will carry three instruments. The primary instrument is the wide-swath (2-day global coverage at 1-km resolution) OCI, which will have sensitivity from 320 nm to 885 nm at 5-nm spectral resolution, and seven discrete channels in the SWIR. It will carry two contributed multi-angle polarimeters on a do-no-harm basis, one of which is HARP2. It will also carry the SpexOne multi-angle polarimeter described in the following section. When launched into its planned 676.5-km, local 13:00 equator crossing orbit, PACE is designed to last three years, with 10 years of fuel. The contrasting, yet complimentary nature of the OCI, HARP2 and SpexOne instruments will provide for a dataset with great potential for remote sensing of aerosols.

2.3.5. SPEX

A family of Spectro-Polarimetric Experiment instruments continues to be developed for ground-based, airborne, and satellite deployment using the same observation concept based on the spectral modulation technique as that described by Snik et al. [218]. The key characteristic of this concept is that the degree and angle of linear polarization are encoded in a modulation of the radiance spectrum. This is achieved by using a set of dedicated optical crystals, an achromatic quarter-wave retarder, an a-thermal multiple order retarder, and a polarizing beam splitter. The quarter-wave retarder and multiple-order retarder ensure that incident linearly polarized light is modulated in the spectral domain. The polarizing beam splitter transforms the spectral polarization modulation into two spectrally modulated intensities $S_+(\lambda)$ and $S_-(\lambda)$, such that the
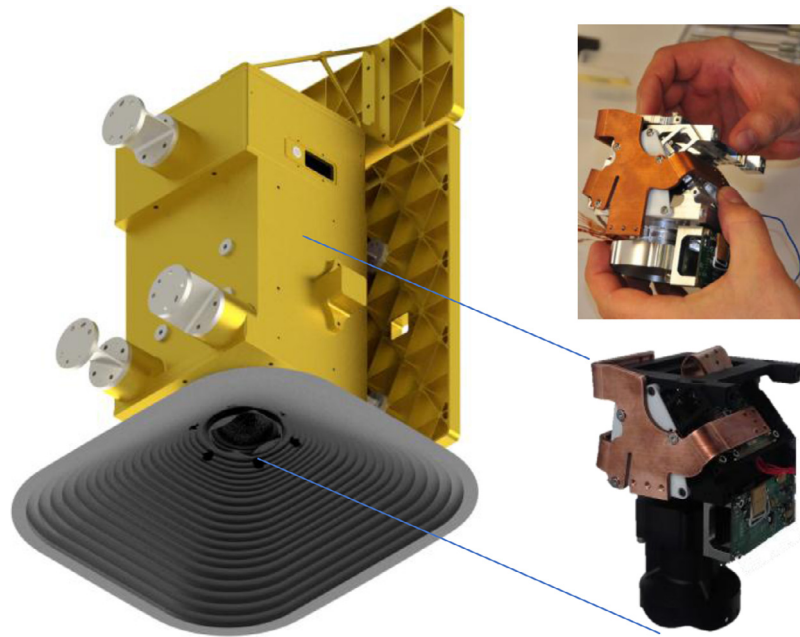
Fig. 5. Left: 3D model of the HARP2 instrument being designed for the PACE spacecraft. Right: actual photographs of the telescope built for the HARP CubeSat satellite with similar dimensions as it will be implemented for HARP2.

amplitude and phase of the modulation are proportional to the degree P and angle φ of linear polarization, respectively, according to

$$I_\pm(\lambda) = \frac{I}{2}\left(1 \pm P(\lambda)\cos\left[\frac{2\pi\,\delta(\lambda)}{\lambda} + \varphi(\lambda)\right]\right). \qquad (1)$$

Here, I is the incident (unmodulated) radiance spectrum and δ is the retardance of the multiple-order retarder. Both S_+ and S_- are recorded, which enables the reconstruction of the unmodulated radiance spectrum at the intrinsic spectral resolution of the spectrometer and allows for a dynamic transmission correction of S_+ and S_-. This, in turn, enables highly accurate polarimetry. Also, this concept allows polarimetry at the intrinsic spectral resolution, enabling, e.g., line polarimetry [232], albeit at a lower accuracy and a spectrally varying efficiency proportional to $\cos[2\pi\,\delta(\lambda)/\lambda + 2\varphi L(\lambda)]$. The advantage of the spectral modulation technique is that it allows for a robust implementation in a space instrument and can yield high polarimetric accuracy because it does not need to combine measurements from different polarization filters that may be spatially and/or temporally misaligned. There are space-borne, airborne, and ground-based SPEX instruments.

The orbital implementation, currently the SpexOne instrument [106,228], is under development. This is a small instrument (compatible with the 12 U cubesat) that is planned to fly on the NASA PACE mission with launch in 2022. The focus of SpexOne is to provide a very high polarimetric accuracy, measurements in the near-UV (down to 385 nm), high spatial sampling, and many measurements per individual ground pixel. This allows for achieving the next step in aerosol characterization needed to improve our understanding of the aerosol–climate effect, albeit with a reduced spatial coverage (swath of ~100 km). In particular, the characteristics of SpexOne allow for unprecedented characterization of aerosol absorption (SSA) and composition through refractive index (e.g., Ref. [10]). The main technical specifications of SpexOne are listed in Table 3. On PACE, the SpexOne hyperspectral polarimetric measurements at five viewing angles have perfect synergy with the hyperangular measurements from HARP and the radiometric measurements from the OCI ranging from the UV to the SWIR. The Spex-

One, HARP, and OCI together will provide a unique capability in aerosol and cloud remote sensing, including a combination of both (aerosols above and in between clouds).

The SpexOne instrument can be transformed into a wide-swath instrument by using separate modules, each with their own detector, for the different viewing angles. This wider-swath realization of SPEX is referred to as the SpexLite instrument [227].

2.3.6. ScanPol and MSIP on Aerosol-UA

The Aerosol-UA instruments include the Scanning along track Polarimeter with six spectral channels, based on the concept and design of the NASA Glory APS [23], and the MultiSpectral Imaging Polarimeter with three polarimetric units and two photometric units, both with four spectral wavebands. The instruments are designed at the Department for Atmospheric Optics and Instrumentation of the MAO/NASU. The multi-channel ScanPol designed for remote sensing of aerosol and cloud properties will measure the Stokes parameters I, Q, and U within the spectral range from the UV to the SWIR in a wide range of scattering angles [165,166,167,221]. The expected ScanPol polarimetric accuracy is ~0.15%, and its photometric accuracy is ~4%. The ScanPol spectral channels are used to estimate the absorption capacity and distribution of tropospheric aerosols over the ocean and land surfaces, the ocean color, and the contribution of the Earth's surface as well as to detect cirrus clouds and stratospheric aerosols caused by volcanic eruptions. A prototype of ScanPol has already been built and is undergoing laboratory tests.

The wide-angle MSIP will collect images of the state of the atmosphere (clouds) and surface (land surface or ocean) in the area overlapping with the ScanPol FOV to retrieve the AOT and polarization properties of aerosol by registration of the first three Stokes parameters simultaneously in three spectral–polarimetric units. Two intensity units of the MSIP will serve to obtain images in eight spectral wavebands to retrieve the AOT. The main feature of the MSIP units is the division of the image by a special prism-splitter into four images on the same image detector in each unit. In that way simultaneous measurements of four polarization components 0°, 45°, 90°, and 135° as images in each of the three polarization units and eight images in eight spectral wavebands in

two intensity units can be achieved. One of the special features of the ScanPol/MSIP concept is the intercalibration of MSIP measurements using ScanPol data in the same FOV. It is expected that the MSIP polarization accuracy should be better than ~1%. The MSIP design has been finalized and one MSIP channel is being tested in the laboratory.

The expected advantages of the Aerosol-UA project are the following: (i) polarization is a relative measurement, which helps achieve high quality of data; (ii) polarimetric ScanPol measurements will be calibrated on-board; (iii) the variation of polarization over many scattering angles and a set of wavelengths provides information on size, refractive index, and shape of aerosol particles; (iv) the synergy of the along-track scanner and the imager will facilitate the retrieval of aerosol properties. The Aerosol-UA mission is planned to be launched in 2022 on a new microsatellite platform "YuzhSat" developed in the Yuzhnoye State Design Office.

2.3.7. MAP/CO2M

As part of the European Copernicus Program, the EC and ESA together with the support of EUMETSAT and the European Centre for Medium-range Weather Forecasts are considering further development of the first generation Copernicus Space Component to include measurements for fossil CO_2 emission monitoring. The greatest contribution to the increase in atmospheric CO_2 comes from emissions from the combustion of fossil fuels and cement production. Current uncertainties associated with their emission estimates at national and regional scales may translate into ill-informed policy decisions and limitations in assessing the effectiveness of CO_2 emission strategies. Satellite and in-situ atmospheric measurements, in addition to bottom-up inventories, would enable the transparent and consistent quantitative assessment of CO_2 emissions and their trends at the scale of megacities, regions, countries, and the globe as well. The space component of the CO_2 Monitoring mission targets to reach global coverage within 2–3 days at mid latitudes, which is expected to be accomplished by a constellation of several satellites with a swath in the range of 250–500 km.

In order to meet the stringent CO2M mission objectives, the retrieved CO_2 data will be obtained also in areas with higher aerosol loadings and shall be only minimally affected by biases. Scattering by clouds and aerosol introduces uncertainties in the optical path length that affect the accuracy of the CO_2 retrieval. The added value of a Multi-Angle Polarimeter has been assessed for correcting this effect on the light path. The bias has been estimated indicating that the high accuracy requirements for CO_2 can be met using these additional MAP observations, which remain valid for larger solar zenith angles and total AOT up to 0.5. Two MAP concepts are considered in the on-going CO2M mission feasibility studies. One concept is based on polarimetric measurements in five views over the spectral range 385–770 nm. The other concept is based on polarimetric measurements in 40 views in 8 spectral channels between 410 and 865 nm. The spatial resolution is 4×4 km off-nadir at a 50° viewing angle and at the edge of the swath. The required DoLP error is below 0.003 over an observation zenith angle range from −60° to +60°

2.4. Airborne observations

Airborne polarimeters are often developed as simulators for space instruments to verify practical performance, validate the measurement concept, and test data processing algorithms. Therefore, the majority of airborne instruments have designs very close to those of their satellite counterparts.

Fig. 6. The NASA RSP.

2.4.1. RSP

The Research Scanning Polarimeter developed by SpecTIR Corporation (Fig. 6) can make either ground-based or aircraft measurements [42–44]. The RSP was developed as the airborne version of the EOSP [14] intended for the initial EOS orbital platform, but not ultimately included owing to budget-dictated restructuring of the EOS program. Two copies of the RSP were built and have been deployed in numerous field campaigns. The expected accuracy of the total reflectance of the RSP is 3% across all spectral bands except for channels located in water vapor absorption bands at 960 (5%) and 1880 nm (8%). The polarimetric accuracy is expected to be better than 0.2% across all bands and is monitored continuously in flight to maintain the level of accuracy. The observations in water vapor absorption bands include complete measurements of the polarization state that provide unique capabilities for determining the physical thickness of clouds using measurements at 960 nm (e.g., Ref. [216]) and for characterizing both thin cirrus and the droplet sizes of mid-level clouds above low-level clouds, such as those observed over the South Atlantic, using measurements at 1880 nm. The observations obtained by the RSP have widely been used for aerosol and cloud particle retrievals as part of comprehensive closure studies, for testing other (less accurate) instruments, and for the development of advanced retrieval algorithms based on passive photopolarimetry alone or in combination with active lidar measurements (e.g., Refs. [31,33,51,53,56,63,129,130,163,215,216,229–231,254,255]).

2.4.2. MICROPOL

The MICROwavelength POlarimeter (Fig. 7) is a single-view multi-spectral airborne polarimeter built at LOA in the 2000s with support from CNES. This instrument is the precursor of the OSIRIS instrument and operates in five bands centered at 490, 670, 865, 1600, and 2200 nm. For each wavelength, there are three separate optical systems composed of a collimator, a lens, an interference filter, a polarizer, and a detector. The angle between the directions of the three polarizers is 60°, the same as for the POLDER and OSIRIS instruments. The total and polarized normalized radiances as well as the angle of polarization are derived using the calibration and the combination of these three simultaneous measure-
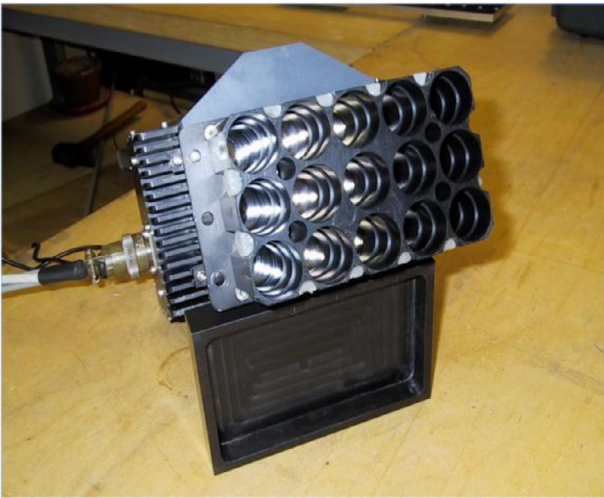
Fig. 7. MICROPOL and its 15 optical systems.

Fig 9. The airborne DPC.

Fig 8. The OSIRIS.

ments. A set of total and polarized normalized radiances at the five wavelengths is accumulated in no more than 7.5 ms. In the 1600 and 2200 nm channels, the detectors are stabilized at a temperature of 10 °C (InGaAs detectors). The absolute accuracy is about 2.5% for the wavelengths 490, 670, 865, and 1600 nm and reaches 6% for the 2200 nm channel. The noise equivalent differential spectral luminances in the total and polarized normalized radiances are better than 10^{-5} and 10^{-4}, respectively. This instrument has participated in several aircraft campaigns over land (north of France, pollution study and surface investigation) and ocean [246,247,251]. This instrument was recently modified to provide additional measurements in the UV (380 and 410 nm) to supplement the OSIRIS measurements acquired during the AEROCLO-SA field experiment held in Namibia in 2017 [85].

2.4.3. OSIRIS

The Observing System Including PolaRisation in the Solar Infrared Spectrum is a recent instrument designed to observe the polarization and directionality of the solar radiation reflected by the surface–atmosphere system (Fig. 8). OSIRIS is based on the same imaging radiometer concept as the POLDER instrument. The original design includes a two-dimensional CCD array of detectors, two rotating wheels carrying spectral filters and polarizers, respectively, and wide FOV telecentric optics [36]. OSIRIS has two optical systems: one for the VIS and near-IR range (440 to 940 nm)

with a ±57° FOV and the other for the SWIR (940 to 2200 nm) with a ±52.5° FOV.

The measurement concept and selection of spectral channels are close to the instrument specifications of the 3MI. OSIRIS has eight spectral bands in the VNIR and six in the SWIR. Owing to the two separated wheels, polarization measurements can be made at all available wavelengths. The DoLP and polarization direction are derived by combining measurements made with three polarizers rotated by a 60° angle relative to each other. The nominal measurement configuration is that no polarization measurements are made within molecular absorption bands (763, 765, 910, 940, and 1365 nm). The OSIRIS calibration was performed in the laboratory. The estimated accuracy in absolute reflectance is better than 4% in the VIS, 6% in the near-IR and shorter SWIR wavelengths, and 10% in longer wavelengths (1220 to 2200 nm).

During the AEROCLO-SA field campaign in Namibia in August–September 2017 [85] aboard the French Falcon-20 aircraft, OSIRIS provided quasi-simultaneous multidirectional radiance measurements of any target giving the opportunity to measure the anisotropy of the reflected (and polarized) solar radiation. The typical aircraft altitude and speed were 10 km and 200–250 m/s, respectively. Under these conditions a target at the ground level is seen from 20 different viewing angles with the VIS optical head and from 19 viewing angles with the SWIR one. Taking into account the characteristics of the detector (number, pixel size) and the FOV of both heads, the pixel size at the ground was 18 and 58 m, respectively, for the VNIR and SWIR. The swath is about 25×19 km for the VIS and 19×15 km for the SWIR at a typical aircraft height of 10 km.

2.4.4. Airborne DPC

The airborne DPC (Fig. 9) is a POLDER-type CCD camera with a significant improvement in the spatial resolution (nadir pixel size: 4×4 m at the 4000-m cruising level). It has spectral bands in the range 495–910 nm with up to three polarized spectral bands (495, 665, and 865 nm). Each polarized band is equipped with a set of three linear polarizers with polarization azimuths separated by 60° angles. The goal of the airborne DPC is to: (i) map atmospheric aerosols, including their sources and transport, and their influence on the air pollution at mega cities in China; and (ii) characterize land surface properties such as the BRDF and BPDF. Campaigns have been conducted over the Pearl River Delta, China during December 2009 to retrieve aerosol properties using multi-angular, multi-spectral, and polarized measurements with high spatial resolution, to quantify the impact of high aerosol loads on climate

Fig. 10. Upper panel: the rotating drum containing the AirMSPI-2 camera is shown mounted to the nose of the ER-2 aircraft. The optical viewport (rectangular slit) through which the camera observes is shown. Lower panel: AirMSPI-2 is shown mounted on the underside of the aircraft in the nose cone just ahead of the extended pitot tubes.

change and air quality. Optical properties of aerosol, including the AOT and AE, were retrieved from the airborne DPC data [50,99].

2.4.5. AirMSPI and AirMSPI-2

The Airborne Multiangle SpectroPolarimetric Imager [64] is an airborne instrument that flies in the nose of NASA's high-altitude ER-2 aircraft. AirMSPI is a prototype of the MAIA satellite instrument (Fig. 10). AirMSPI consists of a single spectropolarimetric camera and acquires multi-angle observations at a programmable set of along-track view angles between $\pm 67°$ off nadir using a motorized gimbal. Images are acquired in eight spectral bands in the UV and VNIR, three of which are polarimetric (see Table 4). The pair of UV bands and measurements of linear polarization are used to enhance the sensitivity to aerosol absorption, height, and microphysical properties. The images are mapped to a 10-m grid in step-and-stare mode and 25 m for sweep mode operations, respectively. Step-and-stare mode covers 10×10 km target areas at a discrete set of view angles beginning with the most forward view and then stepping backward as the aircraft flies downtrack. In sweep mode, the gimbal slews back and forth, enabling more extensive spatial coverage of multi-layered cloud fields. In this mode, the image dimensions range from 10–25 km cross-track and 80–100 km along-track. AirMSPI has been flying aboard the ER-2 since 2010 and has participated in several field campaigns. Polarization is measured by introducing a retardance modulator into the optical path of the AirMSPI camera and by incorporating wiregrid polarizers into the focal plane spectral filter assembly in the polarimetric bands. The retardance modulator consists of a pair of photoelastic modulators and a pair of achromatic quarter waveplates. A high-speed read-out integrated circuit samples the resulting time-modulated signal [68,69]. With this technique, radiance I is measured in all spec-

Fig. 11. The airborne SMAC.

tral bands, while the Stokes parameters Q and U are measured in the polarimetric bands. The ratios $q = Q/I$ and $u = U/I$ are to first order independent of system transmittance or detector gain variations. Pixel averaging (4×4 in the VIS, 8×8 in the near IR) enables achieving an uncertainty of ± 0.005 or better in the degree of linear polarization for typical minimum scene reflectances. This uncertainty requirement has been specified in preformulation studies for NASA's ACE mission [220]. Data products from AirMSPI are available from the NASA Langley Atmospheric Science Data Center, at https://eosweb.larc.nasa.gov/project/airmspi/airmspi_table.

The second generation airborne instrument, AirMSPI-2, underwent test flights in late 2015. Compared to the AirMSPI, this instrument includes a cirrus channel at 1888 nm, polarimetric capability at 1620 and 2185 nm, and narrowband radiance channels in the center and wing of the near-IR O_2 A-band (see Table 4). The AirMSPI-2 camera focal plane contains detectors sensitive to both UV/VNIR and SWIR radiation, and the design has been adapted for use in MAIA. The SWIR channels require cooling the camera focal plane and housing the camera within a vacuum vessel. Due to problems with maintenance of vacuum during the test flights, only imagery in the UV/VNIR channels was obtained. Rework of the instrument is currently in progress, and reflight is expected in 2019. Photographs of the AirMSPI-2 instrument mounted on the ER-2 are shown in Fig. 10.

2.4.6. Airborne SMAC

The airborne SMAC (Fig. 11) is designed to be mounted on an airborne platform and provides essential atmospheric parameters (i.e., aerosols and water vapor) for atmospheric correction of imagery obtained by other instruments. It is intended to be a small and lightweight single-angle radiometer with multi-spectral and polarimetric measurement capabilities. The airborne SMAC observes in eight bands covering the spectral range from 490 to 2250 nm, with five polarized spectral bands and three intensity-only bands. The bands in the VIS (490 (polarized), 550, and 670 (polarized) nm), near IR (870 nm, polarized), and SWIR (1610 nm, polarized) are designed to detect aerosols of different sizes, while the longer polarized 2250-nm band data yield an estimate of the polarized surface reflectance for aerosol retrievals. The 910-nm
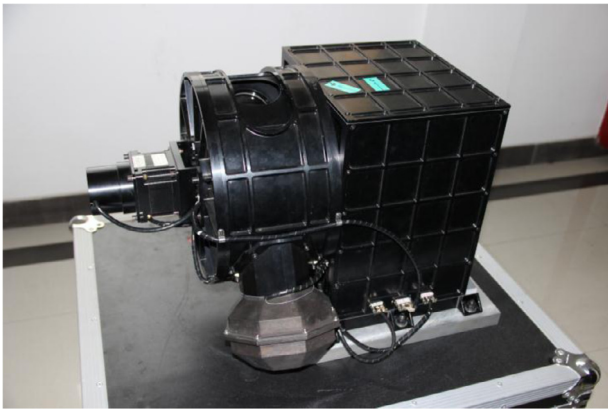
Fig. 12. The AMPR.

band is located in a major water vapor absorption band and is used to derive the atmospheric column vapor content via the differential absorption technique. The 1380-nm band measurements are sensitive to thin cirrus clouds and are used to correct for the cirrus cloud contamination.

2.4.7. AMPR (Airborne POSP)

The Atmosphere Multi-angle Polarization Radiometer (Fig. 12) is an airborne version of the POSP. It provides polarization and intensity measurements in six spectral bands, covering a spectral range from the blue (490 nm) through the SWIR (1640 nm), with full width at half maximum of each band between about 30 to 40 nm. All these bands are designed to detect aerosols and clouds, except for the water vapor band centered at 960 nm. The AMPR uses two Wollaston prisms which are fixed in a relative position as polarization analyzers; then the polarization states in four azimuths (0°, 45°, 90°, and 135°) can be detected simultaneously. This RSP-type design allows for the first three Stokes parameters (I, Q, and U) to be measured simultaneously in six spectral channels. Multiangular measurements are acquired by scanning the fields of view through $\pm 55°$ around nadir, with a sampling interval of 1°, thereby yielding 111 scattering angles per scanning course. The IFOV of the AMPR is 17 mrad, and the pixel size is approximately 60 m at a flight altitude of 3.6 km. The AMPR can be operated to scan in the along-track mode or the cross-track mode depending on the mounting type on the aircraft. The AMPR in the along-track mode provides multi-angular detection of pixels along the ground track, whereas that in the cross-track mode provides single-viewing measurements over the image covering the scanning swath. Also, the AMPR is equipped with a standard light source to monitor the status of the sensor. During a scan course of 0.863 s, about 1/3 of the overall time is taken to acquire the scene signals, and the remaining time is used to collect dark current and onboard calibration records.

2.4.8. SPEX airborne

The SPEX concept has been implemented in the form of an airborne instrument which was deployed on the NASA ER-2 aircraft for engineering flights in February and July 2016 and science flights during the ACEPOL campaign in October–November 2017 (https://www-air.larc.nasa.gov/missions/acepol/index.html). Although based on the same spectral modulation method for polarimetry, SPEX airborne is different from SpexOne – its orbital counterpart – in a number of aspects. (i) The wavelength range of SPEX airborne is 400–800 nm, but the range 750–800 nm is hampered by order overlap of the grating and the range below ~420 nm is hampered by decreased sensitivity. Therefore, the useful spectral range of SPEX airborne is 420–750 nm

while for SpexOne it will be 385–770 nm, where order overlap of the grating is prevented by a filter. (ii) SPEX airborne has a spatial resolution that coarsens with viewing angle, resulting in ground pixels that are a factor of 2–3 larger for the forward and backward view than for nadir. SpexOne will have (almost) the same spatial resolution for all viewing angles. (iii) SPEX airborne has nine viewing angles ranging from −57° to +57° while SpexOne has five angles in the same range, which has been shown to be sufficient for aerosol retrievals [10,254,257]. SPEX airborne did not have a strict design requirement on polarimetric accuracy while for SpexOne the requirement is 0.003 on DoLP. However, laboratory measurements have demonstrated the potential of SPEX airborne to achieve sub-percent polarimetric accuracy [201].

Comparisons of SPEX airborne with RSP measurements during the ACEPOL campaign indicate that SPEX airborne is already capable of achieving polarimetric accuracy of the order of 0.005. This confirms the high expectations for SpexOne/PACE given the different instrumental improvements mentioned above.

2.4.9. AirHARP (Airborne HARP)

The airborne version of the HARP polarimeter family was developed and so far successfully deployed in two observation campaigns: LMOS, onboard the NASA UC12 aircraft, and ACEPOL, onboard the NASA ER2 aircraft. The current VNIR version of the AirHARP instrument is summarized in Table 4 and has similar properties as the previously discussed HARP/CubeSat payload. Fig. 13 shows the configuration of the AirHARP as installed in the NASA ER2 aircraft, and Fig. 14 shows a series of pictures from LAKE Michigan taken during the LMOS experiment. The different perspectives in the images emphasize the variation of the reflection of the sun on the water surface (sunglint) as a function of the viewing angle. At some along-track viewing angles the sunglint disappears while at other angles it appears very intensively.

2.5. Airborne field campaigns and instrument intercomparison

The airborne instruments described in the previous section have been deployed in numerous field campaigns for the purposes of validation of observed and retrieved products, and as a demonstration of the utility of such instrument for scientific investigation. We can distinguish between two types of validation efforts. Validation of the observed radiometric and polarimetric state (which we denote as Level 1 for continuity with orbital data processing terminology) serves as confirmation that the instrument can perform within stated measurement uncertainties. Confirmation of the measurement uncertainty model is as important as the measurements themselves, because the model is often incorporated into the retrieval algorithm to properly weight the observed data. This is especially relevant for multi-angle polarimetry, since uncertainty can be vastly different for radiometric and polarimetric observations, as well as the dependence of this uncertainty on systematic or random sources [13]. Validation of (Level 2) retrieved geophysical parameters is equally important, as this ultimately demonstrates the utility of an instrument, and because comparisons can be made with in situ or other observations that determine geophysical parameters in a different manner (see next section). If geophysical product differences are found at Level 2, it can be difficult to detangle the sources of these differences without a confident assessment of measurement uncertainty for all instruments at Level 1, and an understanding of how the measurement system's information content affects Level 2 uncertainty expectations.

Because of the need to demonstrate measurement utility, most assessments of airborne polarimeter measurement uncertainty have thus far been performed at Level 2. Such field campaigns date back as far as 1999 for the RSP. Generally, these field campaigns have primarily scientific objectives, so geophysical product
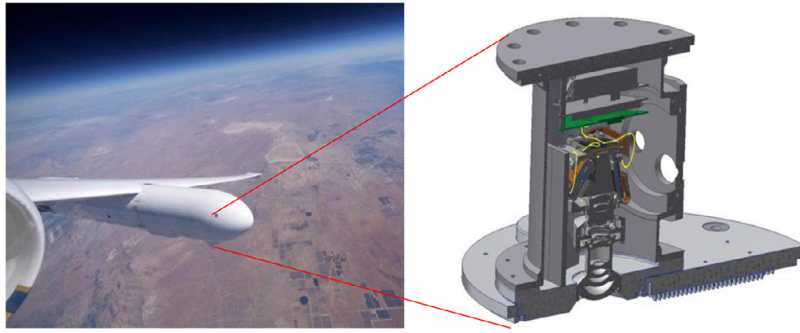
Fig. 13. AirHARP VNIR instrument as installed in the NASA ER2 aircraft during the ACEPOL airborne campaign.
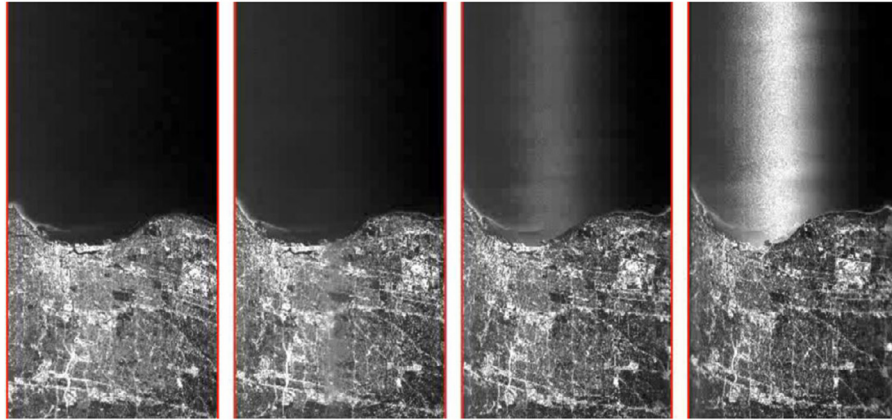

Fig. 14. AirHARP multiangle observations of the sunglint reflected by water of Lake Michigan during the LMOS experiment.

retrieval is performed for this purpose. Examples of large field campaigns deploying the RSP in North America in the last two decades include MILAGRO/INTEX-B [181], ARCTAS [119], SABOR and NAAMES (see the ACE Mission final report for more details). With the creation of AirMSPI, coincident measurements were performed with the RSP during SEAC4RS and ORACLES [265], and campaigns with AirMSPI as the sole polarmeter include RADEX/OLYMPEX, CalWater-22 and Impact-PM. Meanwhile, the AMPR instrument has been deployed in China, and the MICROPOL instrument has been deployed in Europe and Africa. Observations from these field campaigns demonstrated the ability of multi-angle polarimeters to determine aerosol optical properties over the ocean [29–31,51–53,55,56,247], over land [44,63,198,240,241,245,251,254,257], over clouds [129,215,256] and in combination with lidars [130,247]. Algorithm development continues for these and newer instruments (see Section 3). Comparisons of retrieved aerosol properties from airborne polarimeters have not yet been performed, primarily because of the paucity of coincident observations. However, data from the previously mentioned SEAC4RS and ORACLES field campaigns could be used for such purposes, as well as those from the PODEX and ACEPOL field campaigns that were funded by the NASA ACE mission study. The first, PODEX, was performed in southern California in early 2013, and included the RSP, AirMSPI, and PACS (a predecessor to HARP) on the high-altitude ER-2 aircraft. The more recent ACEPOL field campaign was conducted in the same location with the ER-2 in late 2017, and included RSP, AirHARP, SPEX airborne, and AirMSPI.

Level 1 observation validation is less common, partly because characterization of the observed polarimetric state at the aircraft is difficult. Validation of radiometric observations can use the techniques of multispectral instrument systems (e.g., Ref. [163]). However, polarimetric characterization of surface reflectance is less common. Intercomparison of multiple airborne polarimeters may

therefore be the best way of validating at Level 1. Opportunities for such comparison for the RSP and AirMSPI are limited to the aforementioned PODEX, SEAC4RS, and ORACLES field campaigns, while the recent ACEPOL campaign included those two instruments alongside AirHARP and SPEX airborne. Using PODEX and SEAC4RS data, van Harten et al. [234] compared the RSP and AirMSPI and found root-mean-square differences in the DoLP that were largely consistent with the instruments' paired measurement uncertainties. Knobelspiesse et al. [131] performed a more detailed analysis with PODEX data that compared observations by taking per pixel measurement uncertainty expectations into account. The results mostly agree with van Harten et al., but found polarimetric differences between AirMSPI and RSP for dark ocean scenes that were larger than paired measurement uncertainty. This indicates that the measurement uncertainty model for such dark, moderately polarizing scenes is underestimated for one or both of the instruments. The limited nature of these comparisons illustrates the need for concerted efforts to have field campaigns that deploy multiple polarimeters. ACEPOL, in particular, will be valuable for both Level 1 and Level 2 instrument comparisons, and efforts do perform this analysis are underway.

2.6. Ground-based observations

2.6.1. CE318 and CE318-DP

The CE318 sun/sky-radiometer is manufactured by the French Cimel Electronique for measuring atmospheric aerosol and water vapor. The radiometer has been deployed worldwide within the internationally federated network AERONET as a standard instrument since 1992 [111]. The CE318 has had several versions. Some base modifications of the instrument (CE318-2) enabled polarimetric observations at 870 nm in the principal-plane sky scanning mode. The recent CE318-DP automatic multi-wavelength polarization ver-

sion has eight wavelengths (centered at 340, 380, 440, 500, 675, 865, 1020, and 1640 nm) and the capability to measure direct sun, diffuse sky radiation, and polarization. The CE318-DP can perform measurements of multi-wavelength polarization based on a time-sharing combination of polarizers and filters. The CE318-DP has nine polarizers belonging to three groups (each group has three polarizers fitting different wavelength ranges). During polarization measurements, the angles between every two axes of three polarizers are 60°. By combing measurements with three polarizers of each group, the DoLP can be calculated at each wavelength. The spatial distribution of the sky polarization is essentially related to characteristics of aerosols and thus can be employed in the retrieval of aerosol optical and microphysical properties, including particle size, volume, complex refractive index, effective radius, etc. In addition, the CE318-DP can perform unattended automatic observations, functions well under extreme weather conditions (e.g., in polar regions), and can communicate with the server via wires or wirelessly; it is thus well adapted for long-term continuous observations at field sites. The ambient radiation and humidity can cause decay of filters and polarizers; hence the sun/sky radiometers need to be maintained and calibrated routinely (e.g., annually).

In accordance with the operational observation protocol, AERONET CE318 instruments have routinely collected polarimetric data at 870 nm which can be found on the AERONET website. CE318-DP instruments have been deployed by the NASA Goddard Space Flight Center/AERONET and French PHOTONS/AERONET components [96], and the corresponding data are also available on the AERONET web site. The Chinese SONET operating CE318-DP instruments has provided operational multi-wavelength polarimetric observations; the corresponding data are available through an inquiry portal.

2.6.2. GroundSPEX spectropolarimeter

The spectral modulation concept has also been implemented in the form of a ground-based instrument GroundSpex [62,233]. With a single module, pointing at one angle at a time, GroundSPEX samples the scattering phase function in the principal plane in an automated fashion, using a motorized pan/tilt unit and automatic exposure time detection. The instrument samples the intensity and polarization at 360–910 nm in the principal plane defined by the instrument, zenith, and the sun. Each principal plane scan consists of 8 to 25 viewing zenith angles between –60° and +60° degrees. GroundSPEX operated in July and September 2013 at the Cabauw site in The Netherlands. The main purpose of groundSPEX was to demonstrate the spectral modulation method.

2.6.3. GroundMSPI

A ground-based spectropolarimeter, similar in design to AirMSPI and covering the same spectral range, was developed at JPL and the University of Arizona. The GroundMSPI camera [71] is mounted on a two-axis gimbal, enabling pushbroom imagery of the surface and sky by scanning in elevation, and permitting views in different directions by panning to different azimuths. GroundMSPI radiance and polarization data from the ACE-POL campaign are available at the NASA Langley Atmospheric Science Data Center, https://eosweb.larc.nasa.gov/project/airmspi/groundmspi_acepol_radiance_data_v9.

2.7. In situ and laboratory measurements

There has been a number of instruments making measurements of the full aerosol scattering matrix in laboratory conditions (e.g., [153,185,186,238]). Recently, nephelometric instruments which can make ground-based and airborne measurements of single-scattering polarimetric properties of aerosols have also been developed.

2.7.1. PI-Neph

The Polarized Imaging Nephelometer is capable of performing high-accuracy in situ measurements of the phase function and DoLP at three VIS wavelengths and over a wide scattering-angle range from 3° to 177° [72,82]. The resulting inversion yields the particle size distribution which agrees, within experimental errors, with measurements made with commercial optical particle counters. Additionally, the retrieved real part of the refractive index was generally found to be within the predicted error of ± 0.02 from the expected values for three species of humidified salt particles having a refractive index that is well established. PI-Neph airborne measurements were performed during SEAC4RS and other field campaigns.

2.8. Active polarimetric observations

Our main focus is on passive polarimetric observations, which implies that active remote sensing is largely beyond the scope of this review. However, it would be remiss not to recognize that the vertical profiling capability of passive photopolarimeters is inherently limited and may, in fact, be inadequate in many cases. It is therefore appropriate to mention that such important active remote-sensing instruments as lidars [252] can also be endowed with polarimetric measurement capabilities [210]. For example, CALIOP (Table 2) makes measurements of the backscattering depolarization ratio at 552 nm [253]. There is a large number of ground-based and airborne lidars that measure backscattering depolarization in one or more wavelengths (e.g., Refs. [102,162,164]). This characteristic is very sensitive to particle morphology and size [168,175] and can be used for detection and characterization of nonspherical particles. Most often, depolarization is used as a qualitative flag for detecting the presence of nonspherical particles. There are several studies suggesting models for quantitative use of depolarization (e.g., Refs. [37,41,80,177,180,237]). However, the robustness of some of these models may still need improvement for actual lidar applications [184,239].

It has been suggested that combining synergistically active and passive polarimetric remote sensing can improve the detection and accurate quantitative characterization of tropospheric aerosols (e.g., Refs. [130,250]). More recent analyses [35,178] have highlighted the potentially unprecedented retrieval capabilities provided by multistatic polarimetric orbital lidars.

3. Retrieval algorithms

The quality of a remote-sensing retrieval depends critically on the quality of the measurement data as well as on the robustness of the retrieval algorithm. Once an instrument concept has been selected based on various criteria (among which the existence of a heritage instrument, technological feasibility, and especially cost can be dominant), the quality of the resulting observational data cannot be radically improved. The Glory APS appears to be the first passive photopolarimeter that was designed based on a thorough analysis of what it actually takes to significantly improve our knowledge of the aerosol effects on climate [3,7,11,15,23,195]. The unfortunate failure of the Glory launch has delayed the much needed measurements. Yet the process of designing and building the Glory APS had set the stage for a thorough analysis of the requisite instrument requirements as following unequivocally from the meticulously defined science objectives of an aerosol remote-sensing instrument. Otherwise one has to deal with whatever data the instrument in question can actually generate.

Unlike instrument concepts, retrieval algorithms have been evolving much more dynamically. Indeed, while the instrument capability remains fixed once the instrument has been built (this is especially true of orbital instruments), retrieval algorithms,

even those used for processing data from a particular instrument, rarely remain completely unchanged. Usually retrieval algorithms are continuously revised, improved, and updated. Moreover, completely different and independent methods and algorithms can be used for processing data from the same sensor. Therefore, there is a wide variety of algorithms that can be notably different not only due to ingesting data from different instruments but also due to relying on different modeling and retrieval concepts. At the same time, the availability of an operational product – which includes the retrieval product generated for the entire measurement record of an instrument – is vitally important for making a substantial scientific impact. Therefore, the following discussion is largely focused on the retrieval algorithms providing openly available operational products, although research algorithms testing new retrieval ideas and concepts are also mentioned.

3.1. Forward modeling

Any retrieval algorithm includes a forward-modeling module, i.e., a computer program that models what the remote-sensing instrument in question would measure if all the requisite parameters of the atmosphere–surface system were known. This module is traditionally based on the old concepts of the phenomenological radiative transfer theory, the genesis of which is traced by Mishchenko [173]. According to these concepts, the computation can be separated into the calculation of single-scattering properties of aerosol and cloud particles and the solution of the vector radiative transfer equation subject to appropriate boundary/interface conditions [46,103].

Substantial progress has recently been made in the first-principles derivation of the vector radiative transfer theory directly from the Maxwell equations [170,174]. An essential part of this progress has been the fundamental recognition of passive polarimeters as being so-called well-collimated radiometers operating in the wave-propagation rather than "energy-propagation" domain.

Yet many fundamental aspects of the radiative transfer theory currently used in the majority of aerosol/cloud remote-sensing applications remain thoroughly phenomenological. This is especially true of the treatment of particulate surfaces and interfaces, in which case simplistic *ad hoc* models of diffuse reflection and transmission not derived from the Maxwell equations are still invoked. Given the poor state of the underlying phenomenological theory, extensive tests versus direct solutions of the Maxwell equations and/or the results of controlled laboratory experiments are urgently needed. Unfortunately, only two such tests involving very simple scattering geometries have been reported [176,182].

Efficient computer programs based on the Lorenz–Mie solution of the Maxwell equations for spherical particles have been in use for more than half a century. Probably it is owing to the ready availability of these tools that it has taken the remote-sensing community several decades to finally recognize that the extreme morphological complexity of certain types of tropospheric aerosols (such as mineral dust, sea salt, and carbonaceous particles) has a dramatic impact on their single-scattering properties serving as input to computer solvers of the radiative transfer equation. Substantial progress has recently been made in developing efficient and robust solvers of the Maxwell equations applicable to a wide variety of aerosol-particle morphologies [39,40,123,124,151,152,168,169,192,260]. Yet much work is still urgently needed to analyze the implications of these state-of-the-art tools and incorporate them into the direct-modeling modules of operational retrieval algorithms.

Although this may often not be the case, we will assume in what follows that direct modeling is performed adequately and focus on other elements of specific retrieval algorithms.

3.2. Satellite and airborne data

3.2.1. LUT algorithms

The majority of operational satellite algorithms rely on look-up tables of simulated satellite signals pre-computed for a limited set of selected scenarios of aerosol and underlying surface combinations. The modeled scenario that provides the best match of the observed radiances is accepted as the retrieved solution. This approach enables rapid operational processing of large volumes of satellite data. Therefore, with some modifications, this strategy is adopted in aerosol retrievals for all single-view satellite instruments such as AVHRR, MERIS, MODIS, SEVIRI, TOMS, VIIRS, etc. (e.g., Refs. [24,25,110,117,172,223]). The LUT approach is also used for multi-viewing AATSR and MISR instruments as well as for multi-angle polarimeters (Refs. [58,120,122,159,160,196] etc.).

POLDER: The POLDER operational retrieval algorithm over ocean [109] uses total and polarized radiances in two spectral channels (670 and 870 nm). These two channels are sensitive to the scattering by both fine and coarse mode aerosols, are insensitive to vertical variability of aerosol, and are not strongly affected by water-leaving radiation. The POLDER retrieval over land [61] uses only polarized radiances in the same two channels. Such a strategy is used because the contribution of aerosol to the reflected polarized radiances generally dominates over the contribution of the land reflectance, whereas the contribution of the land surface to the total reflected radiance is usually comparable to or stronger than that of aerosol. This was first observed from airborne POLDER measurements [108]. Therefore, as discussed by Deuzé et al. [61], the use of only polarized radiances allows one to derive aerosol properties and to avoid the challenging issue of separation of surface and aerosol contributions to the total reflectance; however, the retrieval is limited to the accumulation mode only. The POLDER algorithm has been updated over the years, and several versions of research algorithms have been developed. For example, the non-sphericity of desert dust particles has been taken into account (e.g., see Refs. [94,109]). Waquet et al. [251] showed that using polarimetirc observations in a wider spectral range is essential for aerosol retrievals over land. Waquet et al. [245,246,251] followed the Deuzé et al. [61] approach and used only polarized radiances. At the same time, the Waquet et al. [245,246,251] algorithm was driven by a large number of unknowns.

SGLI: Although, as mentioned above, the SGLI VNIR-POL sensor is a successor to POLDER, it is a dual-view instrument and does not have the same multi-angle observation capabilities. However, its viewing settings are optimized for aerosol observations. Over ocean, the VNIR-POL looks in a near-sunglint direction in order to capture intermediate scattering angles which are optimal for aerosol characterization over land. Thus, the aerosol retrieval procedure over ocean is similar to the earlier POLDER retrieval approach [97,207,208] but is based on VNIR-non-POL measurements. Over land the SGLI retrieval by Sano [206] relies on polarization, following the approach by Deuzé [61], while the recent retrieval procedure by Sano et al. [205] includes near-UV observations to detect absorbing aerosols such as biomass burning particles and mineral dust and then estimate the SSA from SGLI measurements [183,209].

MISR: Although MISR is not a polarimeter, it stands out among the instruments measuring radiances only owing to its advanced multi-angle capability. Therefore, the MISR retrieval heritage is relevant to the development of retrieval algorithms for its polarimetric successor MAIA and other polarimeters. MISR aerosol retrievals over ocean primarily use radiances in the red and near-IR bands, while retrievals over land use all four bands [160]. The ocean retrievals take advantage of the low reflectance of clear deep waters. The land retrievals use spatial contrasts to derive an EOF representation of the surface contribution to the top-of-the-atmosphere

radiances [160,161] and capitalize on the similarity in the angular shapes of surface BRDFs among the four spectral bands [70]. A LUT consisting of 74 mixtures of aerosol particles having prescribed microphysical and optical properties drives aerosol retrievals over both ocean and land. Several goodness-of-fit metrics are used to compare modeled top-of-the-atmosphere radiances to the MISR observations, providing sensitivity to the total AOT as well as the AOTs corresponding to small, medium, large, absorbing, and non-spherical particles.

GOME, SCIAMACHY, and GOME-2: The polarization capabilities of GOME and SCIAMACHY, which were intended to correct spectra for instrumental polarization sensitivity, were too limited to use for aerosol retrievals. However, GOME-2 has improved polarization performance. From the GOME-2 polarization measuring devices, information on aerosol optical (AOT, SSA) and microphysical (effective radius, refractive index) properties can be derived. However, whether the single-viewing-angle instrument measures at a favorable scattering angle depends strongly on solar zenith and relative azimuth angles. The operational processing for GOME-2 makes use of a LUT for a number of standard aerosol models [105] and yields AOT as its main product and the selected aerosol type as a by-product. The polarization data are also used for the retrieval of a UV absorbing aerosol index in the framework of the EUMETSAT's Atmospheric Composition Satellite Application Facility.

3.2.2. Advanced algorithms

A number of analyses aimed at identifying the most promising passive polarimeter for complete and accurate aerosol characterization have concluded that high-accuracy multi-angle polarimetry in the VIS–SWIR part of the spectrum is the measurement having the greatest potential (e.g., Refs. [6,7,11–13,23,27,107], etc). Based on these and other studies, it is expected that, for a given spectral range, multi-angularity should increase the implicit information content compared to single-view observations, while adding the polarimetric capability increases the information content even further. However, at present, retrieval data products from single-view radiometers such as MODIS [24,25,113,150,200] are by far the most frequently used. Moreover, most of the known comparisons of the aerosol products derived from multi-viewing imagers (such as MISR and POLDER) with the aerosol products from single-view sensors are not necessarily indicative of obvious advantages of multi-angle polarimetric observations (e.g., see Ref. [26]). This result can probably be partially explained by the facts that the amount of available multi-angular and polarimetric data is much smaller than those from single-view radiometers; the available multi-angle and polarimetric sensors have narrower spectral coverage (e.g., MISR and POLDER compared to MODIS); the accuracy of multi-viewing sensors can be limited (e.g., non-simultaneous observations by POLDER in different viewing directions require co-registration, thereby increasing data uncertainty, etc.). At the same time, it is also clear that the complexity of multi-angle polarimetric observations is greater than that of single-view radiometers. For example, POLDER provides more than 150 observations per pixel compared to ~10 for MODIS. Accordingly, this calls for using more rigorous and sophisticated retrieval approaches in order to benefit from richer information content of satellite polarimetry. Indeed, multi-spectral multi-directional polarimetric observations have a notably greater sensitivity to the details of aerosol and surface properties, and the retrieval of a larger number of parameters is expected. By contrast, the LUT concept is designed for quick retrievals from a rather limited number of measurements. Moreover, LUT-based algorithms rely only on selected sub-sets of observations having the greatest sensitivity to aerosol parameters (e.g., using only selected wavelengths, not using both intensity and polarization data) and retrieve a reduced set of characteristics. There-

fore, in recent years, there have been several efforts to develop new-generation retrieval algorithms. Such algorithms tend to implement:

- a statistically optimized search in a continued space of solutions (no LUTs);
- the retrieval of a complete set of aerosol parameters, including aerosol size, shape, refractive index/composition, and vertical distribution; and
- use of the majority of – if not all – available measurements.

Several studies have shown that the new-generation algorithms provide more accurate and more detailed retrievals compared to LUT approaches. On the other hand, the advanced algorithms require significantly more computer time. Therefore, at present the performance of the new retrieval concepts is often demonstrated by using airborne data, while only a few satellite products have been generated.

POLDER: As of today, the POLDER instrument launched on the PARASOL micro-satellite has provided the longest record of multi-angle polarimetric observations. Therefore, the largest number of new retrieval concepts have been developed, in parallel, for the POLDER-3/PARASOL data.

SRON algorithm. An advanced retrieval algorithm making full use of the information content of the multi-angle photopolarimetric observations from POLDER-3/PARASOL has been developed at SRON. This algorithm yields all microphysical characteristics of a bi-modal aerosol ensemble. The aerosol parameters of each mode included in the state vector are the effective radius, effective variance, column number, and real and imaginary parts of the refractive index. For retrievals over ocean, the state vector also includes the wind speed, Chlorophyll-a concentration, and white-cap fraction, while for retrievals over land, the state vector includes the parameters describing the surface BRDF. The retrieval is based on an iterative fitting of a linearized radiative transfer model [9] to the POLDER data, using a cost function containing a misfit term between the forward model and measurement and a regularization term using *a priori* estimates of values of some of the retrieved parameters. The algorithm, including an application to PARASOL measurements over ocean, is described by Hasekamp et al. [27]. More recent refinements are described by Stap et al. [219], Wu et al. [254], and Di Noia et al. [63]. Fu and Hasekamp [90] describe the extension of the SRON algorithm to an arbitrary number of modes, making the algorithm very flexible in its state vector definition. The SRON algorithm makes available new information on aerosol absorption, size, and type. The retrieval results have been used for aerosol type determination by Russel et al. [204] and in studies related to aerosol absorption and direct radiative effect by Lacagnina et al. [133,134]. Currently, the algorithm has been applied to one year (2006) of global aerosol data; the extension to other years is planned. The SRON algorithm is also planned to be used for operational processing of the SpexOne/PACE data.

POLDER/GRASP algorithm. The Generalized Retrieval of Aerosol and Surface Properties is a new-generation algorithm developed for deriving extensive aerosol properties from POLDER-like observations. The overall concept of the algorithm is described by Dubovik et al. [79], while specific aspects are detailed in Dubovik et al. [28]. An open-source GRASP-OPEN software version and documentation are available from https://www.grasp-open.com.

The algorithm is based on highly advanced statistically optimized fitting implemented as multi-term least square minimization [76] that had earlier been successfully implemented (e.g., see Refs. [75,78,80]) for aerosol retrievals from ground-based AERONET radiometers. POLDER/GRASP shares its methodology with AERONET retrievals. For example, for each individual pixel it uses multiple *a priori* constraints such as smoothness limitations on the retrieved continuous functions including the size distribution, spectral

dependencies of the refractive index, and BRDF parameters. At the same time, the POLDER/GRASP concept is more flexible, includes several original features, and enables the implementation of advanced retrieval scenarios. For example, it retrieves both aerosol and underlying surface properties simultaneously from satellite observations using additional *a priori* constraints on the spectral variability of the land BRDF. The more essential novelty is that the POLDER/GRASP retrieval is implemented as a multi-pixel concept wherein the optimized retrieval is performed simultaneously for a large group of pixels [28]. This feature brings additional possibilities for improving the accuracy of retrievals by using known constraints on the inter-pixel variability of retrieved aerosol and surface reflectance parameters. The GRASP retrieval design allows for a stable retrieval using a unique global set of constraints (no location-specific assumptions) starting from a single initial guess globally. As a result, GRASP provides reliable retrievals of detailed aerosol properties that have traditionally been difficult to obtain from satellites, such as aerosol absorption and type. GRASP utilizes radiances in six wavelengths and polarized radiances in three wavelengths and performs radiative-transfer modeling fully accounting for multiple interactions of the scattered solar light in the atmosphere at the native POLDER-1 and -2 ~7 km and POLDER-3 ~6-km resolution. Since these complex computations are done online, significant efforts have been focused on the optimization and acceleration of the GRASP routines and on adapting the code for operational processing of voluminous datasets.

Presently, 18 months of POLDER-1 and -2 and nine years of POLDER-3 observations have been processed and two versions of the retrieval product have been archived at the AERIS/ICARE Data and Services Center (http://www.icare.univ-lille1.fr). Some information is also available from the GRASP-OPEN site (https://www.grasp-open.com). These aerosol products have been evaluated against AERONET data. A detailed description of the POLDER/GRASP product can be found in Dubovik et al. [73]. Also, following the positive POLDER/GRASP retrieval experience, versions 3MI/GRASP, HARP/GRASP, SGLI/GRASP, PCF/GRASP, and Aerosol-UA/GRASP are under development.

Aerosols above clouds with POLDER-3 on PARASOL. Waquet et al. [248,249] have developed an advanced LUT method for retrieving the properties of aerosols above clouds from POLDER/PARASOL polarization measurements. The method for retrieving the above-cloud AOT consists of a comparison between the polarized radiances measured by POLDER at 670 and 865 nm and polarized radiances pre-computed with a successive-order-scattering computer program [135] for different aerosol models. Collocated cloud properties retrieved from MODIS at high resolution (1×1 km at nadir) are used to characterize and select cloudy scenes within the POLDER pixel (6×6 km at nadir). Moreover, Waquet et al. have introduced a mask to correct for cirrus above liquid clouds which makes use of the MODIS brightness temperature difference between the 8.5- and 11-μm spectral bands as well as of MODIS and POLDER cloud top pressure estimates.

The POLDER instrument measures both the total radiances and the polarized radiances, which allows for the development of a complementary method used to determine absorbing properties of aerosols situated above clouds [194]. The input data used in this second retrieval algorithm are the POLDER total radiances at 490 and 865 nm (at the 6×6 km spatial resolution) as well as the previously calculated scattering AOT above cloud and the associated aerosol model. This technique provides the aerosol absorption (assumed to be spectrally neutral between 490 and 865 nm) and the corrected cloud optical thickness.

More information on these algorithms and specific results (accompanied by an estimate of the retrieval accuracy) is provided by Peers et al. [194]. These innovative retrieval methods have recently been used to evaluate simulations of aerosols above clouds in five

AeroCom models over the South East Atlantic Ocean during the fire season [193].

RSP: Several examples by Chowdhary et al. [51–53,55], Stamnes et al. [31], and Gao et al. [30] have demonstrated the capability of retrieving detailed aerosol properties from the multi-spectral multi-angle RSP over water and by Waquet et al. [245,246,251], Cairns et al. [44], and Wu et al. [254,255] over land including over urban surfaces. The bi-modal aerosol size distribution along with the complex refractive index for each mode were retrieved using an optimal estimation framework.

The analysis of RSP observations over land presented in Waquet et al. [245,246] and Cairns et al. [44] only uses polarized reflectances in the retrieval scheme, since uncertainties in the characterization of the polarized reflectance of the land surface are smaller than for the total reflectance, and demonstrated that shorter wavelength (< 500 nm) observations are crucial for determining the aerosols vertical extent and imaginary refractive index from polarization measurements. The optimal estimation scheme was extended to the comprehensive retrieval of aerosol properties above clouds in Knobelspiesse et al. [129]. The retrieval again focused on the use of polarized reflectances, which simplifies the inversion, as once the cloud optical depth is sufficiently large (> 5) its retrieval is not necessary. The use of only polarized measurements in aerosol and cloud retrievals is feasible with RSP observations because all spectral bands provide a complete determination of the polarization state, in contrast with other sensors where only small subsets of bands have a polarization capability.

The RSP Microphysical Aerosol Properties from Polarimeter algorithm by Stamnes et al. [31] is an automated retrieval procedure that inverts multi-angle, multi-channel polarimeter data to produce simultaneous aerosol microphysical properties and ocean color parameters, initially developed for and applied to airborne data. The MAPP is based on optimal estimation and uses NASA high-performance computer resources to do highly accurate Mie and vector radiative transfer calculations on-the-fly. It employs a LUT to efficiently add the contribution from scattering by hydrosols in the ocean sub-surface, as parameterized by Chowdhary et al. [54,56]. The MAPP can be applied to a wide variety of scenarios, including retrieval of microphysical aerosol properties above land surfaces and clouds and for information content studies.

Since the radiative transfer problem of the atmosphere–ocean system is "coupled", errors in the ocean parameters can influence the retrieval of aerosol microphysical parameters such as aerosol SSA, and vice versa. Therefore, both the ocean and the atmosphere must be characterized simultaneously for maximum accuracy, particularly over complex, coastal waters. The RSP MAPP algorithm serves as a building block for the combined polarimeter + lidar (e.g., RSP + HSRL-2) retrieval that has been developed at the NASA Langley Research Center in collaboration with the NASA Goddard Institute for Space Studies.

The retrieved AOT at 532 nm was compared with the results obtained with the HSRL-1 and HSRL-2 during the TCAP and SABOR campaigns, and the majority of retrievals were found to be within ± 0.04. The ocean color parameters were found to strongly correlate with HSRL-1 ocean measurements of the hemispherical particulate backscatter and diffuse attenuation coefficients.

The utility of neural network algorithms for polarimetric retrieval have also been tested with the RSP. Such algorithms offer the promise of very fast results, and may serve as a starting point in a more rigorous iterative retrieval. The combined result is often faster, more accurate, and more likely to converge to a successful solution [63]. This may be especially helpful for otherwise very computationally expensive retrievals, such as for aerosols above clouds [215].

DPC: The first retrieval algorithm for the DPC – the first Chinese multi-angle polarized Earth observation satellite sensor – was

developed based on the experience gained with the MISR and POLDER algorithms. The EOF method was used to decouple land and atmosphere signals, while the AOT was obtained from multi-angle intensity measurements [261,263]. Meanwhile, the fine-mode AOT can be effectively retrieved from multi-angle polarized radiances and then the FMF is calculated as the ratio of these two AOTs [264]. This method has been used in the on-orbit test of the DPC sensor and also provides the basis for the development of a more advanced inversion method. To take full advantage of available radiometric and polarimetric measurements from the DPC, an optimal estimation inversion theoretical framework for the simultaneous retrieval of aerosol and surface parameters has been developed by Li et al. [140]. By constructing an improved BRDF model, wavelength-independent fine-mode and coarse-mode aerosol volumes can be retrieved simultaneously, which enables the subsequent determination of the spectral AOT, AE, and FMF. This optimal-estimation inversion framework can also be applied to space-borne polarimetric measurements in additional SWIR and short-VIS polarized bands, e.g., with POSP and SMAC. Information content analysis results also show that this framework has the potential to retrieve additional aerosol parameters, e.g., size distribution and refractive index [112].

AirMSPI: To exploit the multi-angle, multi-spectral, and polarimetric observations from AirMSPI, optimization-based algorithms [29,256,257] have been developed to simultaneously retrieve aerosol properties over three different types of lower boundaries: ocean, land, and stratocumulus clouds. Conceptually the algorithms are close to those for PARASOL/GRASP while some aspects are refined and extended for the MAIA mission objectives. The first two use step-and-stare imagery while the latter uses sweep imagery. The retrieved aerosol properties include the AOT, SSA, column volume concentration, multi-mode particle size distribution, mean height and half-width of a Gaussian height distribution, complex refractive index, and nonspherical particle fraction. AirMSPI coupled aerosol–ocean retrievals [29] make use of a simplified bio-optical model to estimate normalized water-leaving radiances, followed by an empirical refinement to improve accuracy. The algorithm convergence and stability are achieved by applying constraints on the spatial smoothness of aerosol loading and Chlorophyll-a concentration across neighboring image patches and spectral constraints on aerosol optical properties and water-leaving radiances across relevant bands. In its current form, the algorithm is designed for clear (Case-1) waters, and the extension to turbid coastal (Case-2) waters is under development.

The coupled aerosol–land retrievals [257] impose constraints on the spectral invariance of the BRDF angular shape (capitalizing on MISR experience), and use multiple pixels to invoke surface contrasts as a means of decoupling the surface and atmosphere. They are also capable of constraining the temporal variability of the surface reflectance from multiple target revisits, building upon the work of Dubovik et al. [28]. Precipitable water vapor is simultaneously retrieved by fitting the transmission approximated by the 865- and 935-nm band ratio [91]. Coupled above-cloud aerosol and cloud retrievals [256] simultaneously determine the pixel-scale droplet size distribution and cloud optical thickness along with values of the cloud-top height and above-cloud aerosol properties representative of an entire image domain. The droplet size distribution, the above-cloud aerosol properties, and the cloud-top height are retrieved from polarized radiances at 90°–180° scattering angles, while the cloud optical thickness is retrieved from radiometry based on a 1D radiative-transfer model.

Also, MISR and AirMSPI aerosol retrievals provide heritage for MAIA's data products, which will include both total AOT as well as AOT fractionated by size, absorption, and shape. Geostatistical regression models (e.g., Refs. [146–148]) will be used to relate these parameters to concentrations of near-surface fine and coarse particles, along with the amounts of non-organics (sulfate, nitrate), organic carbon, black or elemental carbon, and mineral dust in the fine-particle mixtures. To generate the spatially and temporally gap-filled PM exposure estimates that are needed to conduct epidemiological studies, the instrument-based PM product, interpolated maps generated from point surface monitor measurements, and PM mass and species fractional concentrations predicted by a chemical transport model will be integrated in ground data processing.

3.3. Ground-based radiometer and in situ nephelometer data

3.3.1. CE318-DP sun/sky radiometer

Ground-based sun/sky radiometers measure direct sunlight and the angular distribution of diffuse sky radiation in several spectral channels (e.g., Ref. [111]). Such measurements of transmitted radiation are traditionally known for high implicit information content regarding detailed aerosol properties which is generally significantly richer than that of reflected radiation measured from satellites. Indeed, satellite-derived AOTs are always fraught with significant uncertainties because they can be inferred from satellite data only indirectly, using a complex inversion procedure. In contrast, direct solar radiation measured from the ground is inverted virtually directly to yield very accurate AOTs. These AOT values not only provide explicit information about aerosol amount but also have traditionally been used for retrieving aerosol size information (e.g., Refs. [127,190,191,222]). In addition, the angular distribution of diffuse radiation measured in aureole carries significant information about the size distribution (even for radii up to 10–15 μm), while measurements at scattering angles from 60° to 150° are sensitive to the refractive index (e.g., see Refs. [75,188]). Therefore, the corresponding retrieval algorithms have always been designed for deriving detailed aerosol properties using rather rigorous inversion techniques [78,127,128,188,224]. For example, the operational AERONET retrieval algorithm [77,78,80] yields the detailed size distribution, spectrally dependent complex refractive index, and fraction of spherical particles.

The interpretation of multi-angular polarimetric data from CE318-DP sun/sky-radiometers is similar to the interpretation of intensity-only multi-angular observations from the earlier version CE318. As shown by Dubovik et al. [80], the same retrieval program [78] updated with polarized radiative-transfer modeling capabilities and aerosol models allowing adequate simulations of the full scattering matrix can be successfully used for inverting multi-angle polarimetric ground-based observations.

The potential advantages of using additional ground-based measurements of polarization are discussed by Li et al. [139] and Fedarenka et al. [83]. These studies have shown that using polarization is mostly beneficial for the characterization of the fine aerosol mode. Specifically, it notably improves the accuracy of retrieving the real part of the refractive index, the shape of the size distribution for small particles, and the fraction of spherical particles. Aerosol retrievals for the cases dominated by desert dust have not shown notable improvements. This can be explained by the fact that desert dust is composed of randomly oriented nonspherical particles that are not strong polarizers of the scattered light (e.g., see the discussion in Section 5.2 of Dubovik et al. [80]). There have been other studies demonstrating the potential use of polarimetric data, such as those by Vermeulen et al. [235] analyzing the use of polarization at 870 nm measured by CE318 as well as Li et al. [138] and Xu et al. [258] analyzing the use of multi-wavelength polarimetric measurements by CE318-DP for retrieving simultaneously aerosol optical and microphysical parameters. The GRASP algorithm also has the ability to invert polarization data from ground-based radiometers; furthermore, these data can be

inverted together with other co-located observations from lidars, satellite imagers, etc. (see the discussion below).

Presently, only the SONET network [141] provides operationally both polarimetric data and aerosol retrievals based on the AERONET algorithm upgraded for using polarimetric data [78,80]. The rather limited use of new polarimetric ground-based observations by presently operational radiometer networks can probably be explained by a significant increase in the effort required to maintain and calibrate the polarimetric instruments and process their data.

3.3.2. GroundSpex radiometer

The PARASOL/SRON retrieval concept has been applied to GroundSpex data collected at the Cabauw site [62,233]. The objective of this study was to invert only diffuse multi-angular intensity and polarization measurements obtained from the ground and demonstrate the potential of the SPEX measurement concept.

3.3.3. PI-Neph

Nephelometers such as the PI-Neph provide direct measurements of the aerosol scattering matrix, total scattering, and absorption. Such measurements are not affected by complex multiple-scattering interactions of light and therefore can be used for validating and verifying aerosol models used in satellite and ground-based retrievals. PI-Neph data can be used for deriving a detailed size distribution, complex refractive index, and information about particle nonsphericity. The retrieval of these properties from PI-Neph data was first demonstrated on laboratory measurements of monodisperse polystyrene spheres by Dolgos and Martins [72]. The GRASP software was later used to extend these retrievals to airborne measurements of polydisperse particles in studies by Espinosa et al. [81,82]. The PI-Neph/GRASP retrieval is based on the earlier work by Dubovik et al. [80] which demonstrated the inversion of scattering matrices measured in the laboratory. At the same time, the PI-Neph/GRASP inversion provides the flexibility to use diverse combinations of data. For example, Espinosa et al. [81] discuss the possibility of a joint interpretation of the scattering matrix elements together with direct measurements of absorption.

3.4. Discussion: achievements, challenges, and perspectives

There is a consensus in the majority of studies on advanced aerosol remote sensing that adding multi-spectral multi-angle polarimetric observation capabilities increases the implicit information content of the measurements. Indeed, as discussed above, there are a number of analyses demonstrating the retrieval of more accurate and complete properties of aerosol (compared to single-view orbital radiometers) using newly developed state-of-the-art algorithms. On the other hand, only nine years of POLDER-3 and eighteen months of POLDER-1 and -2 retrievals provided by GRASP and one year of POLDER-3 retrievals processed by the SRON algorithm are presently available. These products are quite recent and probably need to be extensively validated and used in various applications in order to better understand their full potential and possible issues. Tables 2 and 3 show that several new missions have been launched as well as are being planned. The resulting increase in the available polarimetric data will inevitably stimulate the development of more advanced aerosol retrieval algorithms and products in the near future. However, certain tendencies in the evolution of aerosol retrieval concepts can already be identified.

3.4.1. Achievements

Most existing polarimetric retrievals of aerosols provide an extended set of aerosol properties which includes, in addition to the spectral AOT, size distribution, the spectral SSA,

refractive index, information about aerosol height, and non-sphericity. Usually these parameters do not appear in the lists of aerosol properties retrieved operationally from single-view spectral imagers and even multi-directional radiometers [24,25,58,93,110,113,117,120,122,150,160,172,196,200,223]. Although this remains to be demonstrated via thorough comparisons, many case studies imply that retrievals of the AOT and especially its spectral dependence from multi-angle multi-spectral polarimetry are also expected to have advantages, in particular in challenging situations such as over bright land surfaces. This expectation was clearly demonstrated by Kokhanovsky et al. [12], wherein simulated "error free" data over dark surfaces were processed by a number of algorithms in a "blind test" comparison. Indeed, the POLDER-3/PARASOL results were obviously superior. Certainly real measurements by different satellite instruments differ not only in the number of viewing directions and the availability (or absence) of polarimetric capabilities but also in measurement accuracy, precision, spectral range covered, spatial resolution, etc. Some of these factors can thwart, partially or completely, the increase of information content from doing multi-angular polarimetry. Yet the available aerosol products derived from polarimetry have been recognized in several studies as the most appropriate for characterization of aerosol type [204] and refining emission inventories for different aerosol components [47].

Also, as stated above, the rich information content of multi-spectral multi-angular polarimetry stimulates the use of state-of-the-art algorithms implementing searches in continuous spaces of solutions and optimizing statistical properties of the retrieval in the presence of random noise. This methodology is more sophisticated and difficult for practical implementations compared to LUT approaches, but it potentially provides fundamental advantages such as that it is not limited to a set of preselected solutions, can be adapted for the retrieval of a larger number of parameters, should provide higher retrieval accuracy, can rigorously take advantage of various *a priori* information or co-incident observations, is designed to provide error estimates of the retrieved parameters (covariance matrices), etc. It is fair to say, however, that recently similar algorithms have been applied to single-view imagers as well (see Refs. [73,98]).

3.4.2. Challenges

State-of-the-art polarimetric retrieval algorithms require significantly more computer time than LUT algorithms since they simulate the satellite signal and the Jacobean matrices of first derivatives online. This is the most obvious challenging factor in the development of such advanced algorithms. However, this challenge is unlikely to fundamentally limit the potential use of advanced algorithms for operational processing of data from future polarimetric missions. First, there is clear potential in optimizing the performance of newly developed algorithms. For example, the optimized version of the GRASP algorithm has successfully been used for several re-processing cycles of the full POLDER-3/PARASOL mission archive, and further optimization is underway. Second, due to the rapid progress of technology, the performance of computer systems continuously improves, which implies that even with no specific optimization improvements, the accommodation of demanding calculations will be more feasible in the future.

The second (and most essential) challenge is adequate use of the measurement data. Indeed, there is no doubt that adding new viewing directions and polarimetric capabilities increases the implicit information content of the multi-spectral measurements. Yet this information still remains limited. For example, many sensitivity studies have caused optimism over adding parameters characterizing aerosol absorption, vertical height, etc. to the list of derived parameters (e.g., Refs. [10,23], etc.). It is clear however that many real factors such as inhomogeneity of aerosol particles,

the contribution of nonspherical particles with complex shapes, details of the vertical variability of aerosols, anisotropy of the land reflectance, etc. cannot be fully retrieved and yet affect observations. As a result, any algorithm developer faces the challenge of identifying an adequate set of parameters that can be retrieved uniquely. Polarimetric data are clearly more sensitive to a larger number of parameters than single-view intensity observations, and this increases the difficulty. At the same time this predetermines the diversity of possible approaches. For example, the PARASOL/SRON algorithm retrieves the refractive indices of both fine and coarse modes assuming them spectrally independent and assuming that the size distribution is bi-modal and log-normal. The PARASOL/GRASP and even the AERONET algorithm assumes particles to be homogeneous, while the refractive index can be spectrally dependent and the size distribution is not limited to being bi-modal and log-normal. The analysis by Dubovik et al. [75] showed that allowing different refractive indices for particles of different sizes may lead to ambiguity of the retrieval if the rest of the assumptions remain the same (i.e., there are no additional restrictions on the size distribution and on spectral variability of the refractive index).

The limitations stemming from the use of outdated radiative transfer phenomenology in forward modeling of the measurements and from the frequent nonsphericity and inhomogeneity of real aerosol particles can be profound. For example, many sensitivity studies have shown a high potential of deriving the aerosol complex refractive index from polarimetric imagery. However, the majority of these studies have been based on the assumption of spherical particles [6–8,13,258], whereas accounting for particle nonsphericity even using a rather simple model of polydisperse randomly oriented spheroids [80,171] shows that polarimetry has a rather weak sensitivity to the refractive index of coarse particles. Moreover, Dubovik et al. [80] have also demonstrated that even nonsphericity of small particles needs to be accounted for in adequate simulations of the polarimetric signal. In practice, particles may have more complex shapes than spheroids and be expressly inhomogeneous [38,59,144,179,226]. Therefore, some (or many) of the fine details in the angular polarimetric distribution that can be seen and used in the case of ideal spherical particles may not always be observed and used in practice.

Ambiguities and uncertainties in modeling surface reflectance also add to the simulation uncertainty. Indeed, the effects of directionality of ocean and land surface reflectance are typically accounted for by semi-empirical models driven by a number of internal parameters. There are several *ad hoc* recipes for modeling the BRDF and BPDF, like those by Cox and Munk [57], Ross [202], Li and Strahler [137], Rahman et al. [199], Wanner et al. [244], Nadal and Breón [187], Maignan et al. [154,155], Chowdhary et al. [56], and Litvinov et al. [143]. As comparisons of the models with observations have shown [31,142,143,154,155,246], all models have discrepancies with real observations and even the choice of the best model is not evident. Furthermore, the relevance of these models to first-principles electromagnetic theory remains vague at best.

Polarimetric measurements, especially those at shorter wavelengths, are known to be somewhat sensitive to the vertical distribution of aerosol. This sensitivity stems from the fact that molecular scattering strongly polarizes the scattered light and has a very stable vertical profile. However, the vertical distribution of aerosols can have a rather complex multi-layered structure that cannot be fully adequately assumed or retrieved without additional ancillary information. In the same way, some details of the size distribution, especially for coarse particles, cannot be fully inferred from satellite imagery.

Appropriate characterization of measurement and model uncertainty, and how that knowledge is fit into a retrieval algorithm, is a challenge for many instrument systems. It is particularly relevant, however, for multi-angle polarimetric retrievals of aerosol optical properties. Such retrievals may simultaneously incorporate observations (reflectance, Stokes parameter values, DoLP, etc.) which have dramatically different uncertainty characteristics, and may be correlated; the impact of measurement and model uncertainties may vary with geometry and scene characteristics. The latter may have a strong impact on retrieval capability [13]. Since the forward model is highly nonlinear, the effect of measurement uncertainties may also have a nonlinear impact on the retrieved state [197], which is all the more reason for a precise accounting for measurement uncertainty. Some consumers of aerosol products (e.g., Ref. [196]) use individual retrieval uncertainty estimates if they have been generated, and the fidelity of such retrieval uncertainty estimates depends on that of the original measurement uncertainties as well.

Thus, interpretation of sensitivity tests with ideal/simplified forward models must consider and quantify the implications of those simplifications, and defining realistic and accurate aerosol representations and atmosphere–surface radiation models will likely remain one of the main challenges for future improvements of polarimetric aerosol retrievals. Furthermore, the implementation of first-principles physics in the forward-modeling part of aerosol/surface retrieval algorithms continues to be a fundamental yet thoroughly underappreciated problem.

3.4.3. Perspectives

Taking into account the accumulated experience and the expected increase in the amount of available polarimetric data with the launch of new satellite missions (see Table 3), it is reasonable to anticipate significant progress in the understanding of and benefiting from the aerosol products derived using polarimetry. Specifically, progress can be expected in the following areas.

Multi-spectral multi-angle polarimetry yields more data that allow for the retrieval of a larger set of aerosol parameters than single-view imagery. This is clearly recognized in the new-generation algorithms. For example, all algorithms described in Section 3.2.2 utilize multi-spectral multi-angle measurements of both intensity and polarization, as was recommended in several earlier sensitivity studies [6,7,10]. Also, all these algorithms retrieve a large number of aerosol parameters and implement joint retrievals of land surface properties together with those of aerosols. As mentioned above, Waquet et al. [248] developed the retrieval of aerosols over clouds, while the idea of a joint retrieval of both aerosols and clouds is also being promoted [23].

However, it can also be noted that identifying an optimum set of parameters that can be uniquely retrieved is not an easy task. For example, as mentioned above, POLDER-3/SRON and POLDER-3/GRASP retrieve different sets of parameters. POLDER-3/SRON derives different spectrally independent refractive indices for each aerosol mode, while POLDER-3/GRASP yields a spectrally dependent refractive index that is size independent. At the same time, these two algorithms use different amounts of POLDER-3 data: POLDER-3/SRON is based on four spectral channels, while POLDER-3/GRASP utilizes six channels. Moreover, POLDER/GRASP is a very flexible algorithm that allows for using different assumptions in the retrieval including a multi-component aerosol mixture wherein each component covers a different size range and may have an individual spectrally dependent (or independent) refractive index. Also, the size distribution of each component may be represented as a log-normal function or as a combination of log-normal or triangular size bins (e.g., see Refs. [28,73,222]). This flexibility will be certainly explored further in search for the most adequate assumptions providing the best retrieval results.

Currently there are ongoing studies aimed at investigating the possibility of optimizing the set of retrieved parameters. Similar analyses have been done in other algorithm-development studies

[29,257] and can naturally be expected to continue into the future. One of the main objectives of such efforts will be a clear focus on aerosol type identification. As emphasized by Russell et al. [203,204], a remote sensing retrieval providing a multi-parameter aerosol product is suitable for identifying aerosol type, i.e., information highly desirable for many applications. In the study by Chen et al. [47] the POLDER-3/GRASP aerosol products were used for deriving/correcting emission sources of desert dust and carbonaceous aerosols via an inverse modeling approach. It was shown that the sources of desert dust, black carbon, and organic carbon aerosol emissions can be derived simultaneously using the spectral AOT and aerosol absorption optical thickness derived from POLDER-3/PARASOL observations. Chen et al. showed that the spectral AOT and absorption AOT provided by the POLDER-3/GRASP retrieval yielded sufficient constraints for improving global emissions simultaneously of the above three chemical components at the temporal and special resolutions of transport models. Previous studies relying on the MODIS AOT or OMI results had achieved reliable constraints on only one aerosol component [74,243,262], or used a simplified aerosol model constraining emissions over large areas [114–116] or degraded time resolution [259]. Moreover, in the studies by Schuster et al. [211–214] it has been demonstrated that using a model of aerosols as an internal mixture of different chemical components, it is possible to estimate quantitatively the aerosol composition based on the values of the spectrally dependent complex refractive index provided by AERONET. Following generally the same idea, Li et al. [136] have developed a GRASP/composition retrieval. This modification of the GRASP algorithm derives the fractions of different aerosol components directly instead of the values of the complex refractive index at each wavelength. Li et al. demonstrated the applicability of this algorithm to POLDER-3 and AERONET data. It was shown that other aerosol parameters retrieved from POLDER-3 data, such as the spectral AOT and SSA derived using the GRASP/composition approach, are determined comparably well or even better than when using the retrieval of a spectrally dependent refractive index. This approach can yield not only a new type of parameter but also serve as an improved constraint on the solution. Also, the tool for rigorous calculation of radiative fluxes and aerosol forcing based on the retrieval result has been implemented as and optional module in the GRASP code [60].

Yet one should recognize that aerosol typing as well as the retrieval of chemical composition always contain ambiguities due to limitations of the information content of satellite observations. Therefore, the typing of aerosols and specific assumptions made in relating optical properties to aerosol chemistry and microphysics can also be instrument-dependent since different types of measurement can have very different sensitivities to various aerosol parameters. These approaches should be considered as an effort of the scientific community to optimize the connection between optical remote-sensing data with aerosol chemistry and physics used in climate models. At the same time, in comparisons of different aerosol remote sensing data products the primordial parameters such as aerosol microphysics and complex refractive index should always be the ultimate "measuring stick" [11]. The same parameters enter the aerosol radiative forcing computation and are used fundamentally to parameterize aerosols in CTMs.

Synergistic retrievals constitute another promising direction of research. Due to the common recognition of a high information content of multi-spectral multi-angle polarimetry, there are multiple suggestions to develop retrievals using a combination of polarimetric imagery with other types of observation. For example, the SPEX and HARP polarimetry planned as part of the NASA PACE mission is expected to complement hyperspectral radiance data from the OCI and thereby provide more accurate aerosol information helpful for characterizing ocean surface properties. Such com-

bined observations are anticipated to address critical science questions on ocean–atmosphere interactions [189]. The DPC is expected to provide atmospheric correction parameters for the Greenhouse-gases Monitoring Instrument onboard the same GF-5. Also, the MAP/CO2M EU/Copernicus mission is based on the idea of deploying a polarimeter as part of CO_2 monitoring with the expectation that polarimetry will help reduce the effect of possible aerosol contamination on the derived CO_2 product. Remote sensing of aerosols with small satellites in formation flight is discussed by Knobelspiesse and Nag [132].

There are many suggestions of joint processing of coincident polarimetric and lidar satellite data (e.g., see Refs. [31,130]) as providing complimentary information. It should be noted that in the case of ground-based observations, such combined processing has already been implemented in several algorithms such LIRIC [45] and GARRLiC/GRASP [149]. These algorithms use joint data from a multi-wavelength lidar and an AERONET radiometer and derive vertical profiles of two aerosol components as well as extra parameters of the column-integrated properties of aerosols. The latest version of GARRLiC/GRASP allows for using polarimetric data from both a radiometer and a lidar. There is also potential of improving characterization of both aerosol and surface reflectance using simultaneous synergistic inversion of ground-based up-looking observations with down-looking satellite [217] or airborne observations [92].

Finally, reliable *a priori* information about aerosol chemical composition and spatial distribution from a CTM could help constrain the retrievals of aerosol properties about which observations may have insufficient information, and fill the gap when satellite observations are unavailable or contaminated by the presence of clouds. One technical challenge is that chemical parameterization of speciated aerosols usually means a significant expansion of aerosol parameter space to account for composition, fraction, and microphysical properties (e.g., size distribution) of all species. This motivates the development of reliable mixing mechanisms and hygroscopicity models as well as models linking the physical and optical characteristics of aerosols retrieved from remote sensing with the mass and chemistry representations provided by CTMs.

4. Conclusions

Thus, as discussed extensively in this review, multi-angle multi-spectral polarimetry is among the most promising types of aerosol remote sensing. Without the multi-angle, multi-spectral, and polarimetric capabilities deciphering aerosol properties is highly problematic since the contribution of the underlying reflective surface often overwhelms the measurement. At present orbital multi-spectral multi-angle polarimeters are recognized as satellite instruments capable of providing the most detailed global aerosol products that include such key characteristics as aerosol composition and microphysics. This has been suggested in many theoretical studies as well as demonstrated using the only available long-term record of satellite polarimetric observations provided by the POLDER-3/PARASOL instrument. By now, several aerosol datasets have been generated from nine years worth of archived PARASOL data which are used for in-depth analyses of the global variability of aerosol and validation of products derived from other observations.

Presently, several more satellite polarimetric missions are being flown, including two Chinese polarimeters CAPI/TanSat and DPC/GF-5 as well as the SGLI/GCOM-C launched by Japan. The fleet of polarimeters should increase significantly in next decade following the planned launches of the 3MI/EPS-SG EU instrument, MAP/CO2M EU/Copernicus mission, several USA missions (MAIA, HARP/CubeSat, HARP2/PACE, and SpexOne/PACE), four Chinese instruments (POSP, SMAC, PCF, and DPC-Lidar), and the Ukranian

Aerosol-UA mission, all by 2023. Airborne prototypes are being developed to parallel these satellite instruments. Most of these airborne polarimeters have already been tested and have provided useful data. In addition, ground-based radiometers and in situ nephelometers endowed with polarimetric capabilities have been developed for advanced validation of remote-sensing algorithms and scattering models.

Analyses of polarimetric data have revealed several key issues. Most importantly, it had become evident that advanced algorithms are necessary to take full advantage of the information implicit in complex multi-angle and multi-spectral polarimetric data. Accordingly, several retrieval approaches, such as the GRASP, SRON, MAPP, and JPL state-of-the-art algorithms, have been developed. In contrast to the traditional LUT methodology, these algorithms use rigorous statistical optimization and perform searches in continuous spaces of solutions governed by elaborated sets of *a priori* constraints. As a consequence, such approaches tend to use all or most of the available measurement data and derive significantly more representative sets of parameters with higher accuracy. For example, most of such algorithms derive properties of both the aerosol and the underlying surface and provide information about aerosol absorption and refractive index, i.e., the characteristics that are very difficult to obtain from space.

In addition, the generalized retrieval approaches employed and the corresponding algorithms are highly suitable for exploiting the inherent synergy of different types of observation. Yet the practical implementation of such algorithms and obtaining actual results are rather challenging. First, such algorithms are very complex and need specialized expertise in numerical inversion and atmospheric radiation modeling. Second, these algorithms involve full radiative-transfer calculations as part of the retrieval and therefore are rather time consuming compared to LUT approaches. Also, accurate forward simulation of a multi-angle polarimetric observation requires advanced light scattering models of aerosols and the surface. For example, adequate models of light scattering by nonspherical and heterogeneous particles are vital for the interpretation of polarimetric observations of desert dust [80,168], sea-salt [38], and carbonaceous [144] aerosols. Developing such models is challenging both conceptually and technically. Furthermore, advanced first-principles studies are needed to better understand the physics of radiative transfer, especially in the presence of complex surface types. Therefore, although the outlook on the advancement of polarimetric retrieval algorithms is quite positive, massive research and programming efforts are still required.

The actual aerosol-retrieval capability of an instrument is ultimately constrained by the specific instrument design. Ideally, an orbital aerosol/cloud polarimeter should be designed in such a way as to enable

- retrievals of morphologically complex tropospheric aerosols and multi-modal aerosol populations;
- aerosol retrievals above bright land surfaces and liquid-water clouds;
- tropospheric-aerosol retrievals in the presence of liquid-water clouds, cirrus clouds, and/or volcanic stratospheric aerosols; and
- achieving high precision of the long-term aerosol record for climate applications.

The cumulative body of existing literature demonstrates that among key instrument characteristics are the following:

- the number and total range of scattering angles;
- the spectral range covered and the number of polarization-sensitive spectral channels;
- the availability of specialized polarization-sensitive spectral channels, such as those at 1375 and 2250 nm;

- polarimetric and radiometric accuracy and precision; and
- the availability and long-term stability of on-board polarimetric and radiance calibration.

We have not discussed specifically how the actual designs of the instruments detailed in Tables 2 and 3 define their respective retrieval capabilities. In the final analysis, it is the responsibility of the individual instrument teams to demonstrate to what extent their instruments can yield the requisite aerosol characteristics [11] and thereby improve our understanding of the direct and indirect aerosol forcings of climate.

In summary, the increasing number of polarimeters and rapidly growing volume of polarimetric data, especially from orbital instruments, along with sustainable advances in forward modeling, retrieval methodologies, and algorithms serve as a compelling reason to envision satellite polarimetry as the main tool for global aerosol monitoring and characterization.

References

[1] Kokhanovsky AA, de Leeuw GH, editors. Satellite aerosol remote sensing over land. Berlin: Springer; 2009. doi:10.1007/978-3-540-69397-0.

[2] Lenoble J, Remer L, Tanré D, editors. Aerosol remote sensing. Berlin: Springer; 2010. doi:10.1007/978-3-642-17725-5.

[3] Hansen J, Rossow W, Carlson B, Lacis A, Travis L, Del Genio A, et al. Low-cost long-term monitoring of global climate forcings and feedbacks. Clim Change 1995;31:247–71. doi:10.1007/BF01095149.

[4] Solomon S. Climate change 2007 – the physical science basis: working group I contribution to the fourth assessment report of the IPCC. Cambridge, UK: Cambridge University Press; 2007.

[5] Stocker TF, Qin D, Plattner GK, Tignor MMB, Allen SK, Boschung J, et al. Climate change 2013 – the physical science basis: working group I contribution to the fifth assessment report of the intergovernmental panel on climate change. Cambridge, UK: Cambridge University Press; 2013. doi:10.1017/CBO9781107415324.

[6] Mishchenko MI, Travis LD. Satellite retrieval of aerosol properties over the ocean using polarization as well as intensity of reflected sunlight. J Geophys Res 1997;102:16989–7013. doi:10.1029/96JD02425.

[7] Mishchenko MI, Travis LD. Satellite retrieval of aerosol properties over the ocean using measurements of reflected sunlight: effect of instrumental errors and aerosol absorption. J Geophys Res 1997;102:13543–53. doi:10.1029/97JD01124.

[8] Mishchenko MI, Travis LD, Rossow WB, Cairns B, Carlson BE, Han Q. Retrieving CCN column density from single-channel measurements of reflected sunlight over the ocean: a sensitivity study. Geophys Res Lett 1997;24:2655–8. doi:10.1029/97GL02783.

[9] Hasekamp OP, Landgraf J. Linearization of vector radiative transfer with respect to aerosol properties and its use in satellite remote sensing. J Geophys Res 2005;110:D04203. doi:10.1029/2004JD005260.

[10] Hasekamp OP, Landgraf J. Retrieval of aerosol properties over land surfaces: capabilities of multiple-viewing-angle intensity and polarization measurements. Appl Opt 2007;46:3332–44. doi:10.1364/AO.46.003332.

[11] Mishchenko MI, Cairns B, Hansen JE, Travis LD, Burg R, Kaufman YJ, et al. Monitoring of aerosol forcing of climate from space: analysis of measurement requirements. J Quant Spectrosc Radiat Transf 2004;88:149–61. doi:10.1016/j.jqsrt.2004.03.030.

[12] Kokhanovsky AA, Deuzé JL, Diner DJ, Dubovik O, Ducos F, Emde C, et al. The inter-comparison of major satellite aerosol retrieval algorithms using simulated intensity and polarization characteristics of reflected light. Atmos Meas Tech 2010;3:909–32. doi:10.5194/amt-3-909-2010.

[13] Knobelspiesse K, Cairns B, Mishchenko M, Chowdhary J, Tsigaridis K, van Diedenhoven B, et al. Analysis of fine-mode aerosol retrieval capabilities by different passive remote sensing instrument designs. Opt Express 2012;20:21457–84. doi:10.1364/OE.20.021457.

[14] Travis LD. Remote sensing of aerosols with the Earth Observing Scanning Polarimeter. Proc SPIE 1992;1747:154–64. doi:10.1117/12.138823.

[15] Travis L. Earth Observing System Polarimeter. In: Hansen J, Rossow W, Fung I, editors. Long-term monitoring of global climate forcings and feedbacks; NASA CP-3234. Washington, DC: NASA; 1993. p. 40–6.

[16] Lyot B. Recherches sur la polarisation de la lumière des planetes et de quelques substances terrestres. Ann Obs Paris, Sect Meudon 1929;8(1).

[17] Dollfus A, Coffeen DL. Polarization of Venus. I. Disk observations. Astron Astrophys 1970;8:251–66.

[18] Hansen JE, Hovenier JW. Interpretation of the polarization of Venus. J Atmos Sci 1974;31:1137–60.

[19] Kawabata K, Coffeen DL, Hansen JE, Lane WA, Sato M, Travis LD. Cloud and haze properties from pioneer Venus polarimetry. J Geophys Res 1980;85:8129–40. doi:10.1029/JA085iA13p08129.

[20] West RA, Smith PH. Evidence for aggregate particles in the atmospheres of Titan and Jupiter. Icarus 1991;90:330–3. doi:10.1016/0019-1035(91) 90113-8.

[21] Deschamps P-Y, Bréon F-M, Leroy M, Podaire A, Bricaud A, Buriez J-C, et al. The POLDER mission: instrument characteristics and scientific objectives. IEEE Trans Geosci Remote Sens 1994;32:598–615. doi:10.1109/36.297978.

[22] Tanré D, Bréon FM, Deuzé JL, Dubovik O, Ducos F, François P, et al. Remote sensing of aerosols by using polarized, directional and spectral measurements within the A-Train: the PARASOL mission. Atmos Meas Tech 2011;4:1383–95. doi:10.5194/amt-4-1383-2011.

[23] Mishchenko MI, Cairns B, Kopp G, Schueler CF, Fafaul BA, Hansen JE, et al. Accurate monitoring of terrestrial aerosols and total solar irradiance: introducing the Glory mission. Bull Am Meteorol Soc 2007;88:677–92. doi:10.1175/BAMS-88-5-677.

[24] Kaufman YJ, Tanré D, Remer LA, Vermote EF, Chu A, Holben BN. Operational remote sensing of tropospheric aerosol over land from EOS moderate resolution imaging spectroradiometer. J Geophys Res 1997;102:17051–67. doi:10.1029/96JD03988.

[25] Tanré D, Kaufman YJ, Herman M, Mattoo S. Remote sensing of aerosol properties over oceans using the MODIS/EOS spectral radiances. J Geophys Res 1997;102:16971–88. doi:10.1029/96JD03437.

[26] Kokhanovsky AA, Bréon F-M, Cacciari A, Carboni E, Diner D, Di Nicolantonio W, et al. Aerosol remote sensing over land: a comparison of satellite retrievals using different algorithms and instruments. Atmos Res 2007;85:372–94. doi:10.1016/j.atmosres.2007.02.008.

[27] Hasekamp OP, Litvinov P, Butz A. Aerosol properties over the ocean from PARASOL multiangle photopolarimetric measurements. J Geophys Res 2011;116:D14204. doi:10.1029/2010JD015469.

[28] Dubovik O, Herman M, Holdak A, Lapyonok T, Tanré D, Deuzé JL, et al. Statistically optimized inversion algorithm for enhanced retrieval of aerosol properties from spectral multi-angle polarimetric satellite observations. Atmos Meas Tech 2011;4:975–1018. doi:10.5194/amt-4-975-2011.

[29] Xu F, Dubovik O, Zhai P-W, Diner DJ, Kalashnikova OV, Seidel FC, et al. Joint retrieval of aerosol and water-leaving radiance from multispectral, multiangular and polarimetric measurements over ocean. Atmos Meas Tech 2016;9:2877–907. doi:10.5194/amt-9-2877-2016.

[30] Gao M, Zhai P-W, Franz BA, Hu Y, Knobelspiesse KD, Werdell PJ, et al. Retrieval of aerosol properties and water-leaving reflectance from multi-angular polarimetric measurements over coastal waters. Opt Express 2018;26:8968–89.

[31] Stamnes S, Hostetler C, Ferrare R, Burton S, Liu X, Hair J, et al. Simultaneous polarimeter retrievals of microphysical aerosol and ocean color parameters from the "MAPP" algorithm with comparison to high-spectral-resolution lidar aerosol and ocean products. Appl Opt 2018;57:2394–413. doi:10.1364/AO.57.002394.

[32] Alexandrov MD, Cairns B, Mishchenko MI. Rainbow Fourier transform. J Quant Spectrosc Radiat Transf 2012;113:2521–35. doi:10.1016/j.jqsrt.2012.03.025.

[33] Alexandrov MD, Cairns B, Emde C, Ackerman AS, van Diedenhoven B. Accuracy assessments of cloud droplet size retrievals from polarized reflectance measurements by the research scanning polarimeter. Remote Sens Environ 2012;125:92–111. doi:10.1016/j.rse.2012.07.012.

[34] Alexandrov MD, Cairns B, Sinclair K, Wasilewski AP, Ziemba L, Crosbie E, et al. Retrievals of cloud droplet size from the research scanning polarimeter data: validation using in situ measurements. Remote Sens Environ 2018;210:76–95. doi:10.1016/j.rse.2018.03.005.

[35] Alexandrov MD, Mishchenko MI. Information content of bistatic lidar observations of aerosols from space. Opt Express 2017;25:A134–50. doi:10.1364/OE.25.00A134.

[36] Auriol F, Léon J-F, Balois J-Y, Verwaerde C, François P, Riedi J, et al. Multidirectional visible and shortwave infrared polarimeter for atmospheric aerosol and cloud observation: OSIRIS (Observing System Including PolaRisation in the Solar Infrared Spectrum). Proc SPIE 2008;7149:71491D. doi:10.1117/12.806421.

[37] Bi L, Lin W, Liu D, Zhang K. Assessing the depolarization capabilities of nonspherical particles in a super-ellipsoidal shape space. Opt Express 2018;26:1426–39. doi:10.1364/OE.26.001726.

[38] Bi L, Lin W, Wang Z, Tang X, Zhang X, Yi B. Optical modeling of sea salt aerosols: the effects of nonsphericity and inhomogeneity. J Geophys Res Atmos 2018;123:543–58. doi:10.1002/2017JD027869.

[39] Bi L, Yang P, Kattawar GW, Mishchenko MI. Efficient implementation of the invariant imbedding T-matrix method and the separation of variables method applied to large nonspherical inhomogeneous particles. J Quant Spectrosc Radiat Transf 2013;116:169–83. doi:10.1016/j.jqsrt.2012.11.014.

[40] Bi L, Yang P, Kattawar GW, Mishchenko MI. A numerical combination of extended boundary condition method and invariant imbedding method applied to light scattering by large spheroids and cylinders. J Quant Spectrosc Radiat Transf 2013;123:17–22. doi:10.1016/j.jqsrt.2012.11.033.

[41] Burton SP, Hair JW, Kahnert M, Ferrare RA, Hostetler CA, Cook AL, et al. Observations of the spectral dependence of linear particle depolarization ratio of aerosols using NASA Langley airborne High Spectral Resolution Lidar. Atmos Chem Phys 2015;15:13453–73. doi:10.5194/acp-15-13453-2015.

[42] Cairns B, Russell EE, LaVeigne JD, Tennant PMW. Research scanning polarimeter and airborne usage for remote sensing of aerosols. Proc SPIE 2003;5158:33–44. doi:10.1117/12.518320.

[43] Cairns B, Russell EE, Travis LD. Research Scanning Polarimeter: calibration and ground-based measurements. Proc SPIE 1999;3754:186–96. doi:10.1117/12.366329.

[44] Cairns B, Waquet F, Knobelspiesse K, Chowdhary J, Deuzé J-L. Polarimetric remote sensing of aerosols over land surfaces. In: Kokhanovsky A, de Leeuw G, editors. Satellite aerosol remote sensing over land. Berlin: Springer; 2009. p. 295–325. doi:10.1007/978-3-540-69397-0_10.

[45] Chaikovsky A, Dubovik O, Holben B, Bril A, Goloub P, Tanré D, et al. Lidar-Radiometer Inversion Code (LIRIC) for the retrieval of vertical aerosol properties from combined lidar/radiometer data: development and distribution in EARLINET. Atmos Meas Tech 2016;9:1181–205. doi:10.5194/amt-9-1181-0_16.

[46] Chandrasekhar S. Radiative transfer. Oxford: Oxford University Press; 1950.

[47] Chen C, Dubovik O, Henze DK, Lapyonak T, Chin M, Ducos F, et al. Retrieval of desert dust and carbonaceous aerosol emissions over Africa from POLDER/PARASOL products generated by the GRASP algorithm. Atmos Chem Phys 2018;18:12551–80. doi:10.5194/acp-18-12551-2018.

[48] Chen X, Yang D, Cai Z, Liu Y, Spurr R. Aerosol retrieval sensitivity and error analysis for the cloud and aerosol polarimetric imager on board TanSat: the effect of multi-angle measurement. Remote Sens 2017;9:183. doi:10.3390/rs9020183.

[49] Chen X, Wang J, Liu Y, Xu X, Cai Z, Yang D, et al. Angular dependence of aerosol information content in CAPI/TanSat observation over land: effect of polarization and synergy with A-train satellites. Remote Sens Environ 2017;196:163–77. doi:10.1016/j.rse.2017.05.007.

[50] Cheng TH, Gu XF, Xie DH, Li ZQ, Yu T, Chen XF. Simultaneous retrieval of aerosol optical properties over the Pearl River Delta, China using multiangular, multi-spectral, and polarized measurements. Remote Sens Environ 2011;115:1643–52. doi:10.1016/j.rse.2011.02.020.

[51] Chowdhary J, Cairns B, Mishchenko MI, Hobbs PV, Cota GF, Redemann J, et al. Retrieval of aerosol scattering and absorption properties from photopolarimetric observations over the ocean during the CLAMS experiment. J Atmos Sci 2005;62:1093–117. doi:10.1175/JAS3389.1.

[52] Chowdhary J, Cairns B, Mishchenko MI, Travis LD. Using multi-angle multispectral photo-polarimetry of the NASA Glory mission to constrain optical properties of aerosols and clouds: results from four field experiments. Proc SPIE 2005;5978:59780G. doi:10.1117/12.631201.

[53] Chowdhary J, Cairns B, Mishchenko M, Travis L. Retrieval of aerosol properties over the ocean using multispectral and multiangle photopolarimetric measurements from the Research Scanning Polarimeter. Geophys Res Lett 2001;28:243–6. doi:10.1029/2000GL011783.

[54] Chowdhary J, Cairns B, Travis LD. Contribution of water-leaving radiances to multiangle, multispectral polarimetric observations over the open ocean: bio-optical model results for case 1 waters. Appl Opt 2006;45:5542–67. doi:10.1364/AO.45.005542.

[55] Chowdhary J, Cairns B, Travis LD. Case studies of aerosol retrievals over the ocean from multiangle, multispectral photopolarimetric remote sensing data. J Atmos Sci 2002;59:383–97.

[56] Chowdhary J, Cairns B, Waquet F, Knobelspiesse K, Ottaviani M, Redemann J, et al. Sensitivity of multiangle, multispectral polarimetric remote sensing over open oceans to water-leaving radiance: analyses of RSP data acquired during the MILAGRO campaign. Remote Sens Environ 2012;118:284–308. doi:10.1016/j.rse.2011.11.003.

[57] Cox C, Munk W. Measurement of the roughness of the sea surface from photographs of the sun's glitter. J Opt Soc Am 1954;44:838–50. doi:10.1364/JOSA.44.000838.

[58] de Leeuw G, Holzer-Popp T, Bevan S, Davies WH, Descloitres J, Grainger RG, et al. Evaluation of seven European aerosol optical depth retrieval algorithms for climate analysis. Remote Sens Environ 2015;162:295–315. doi:10.1016/j.rse.2013.04.023.

[59] Derimian Y, Choël M, Rudich Y, Deboudt K, Dubovik O, Laskin A, et al. Effect of sea breeze circulation on aerosol mixing state and radiative properties in a desert setting. Atmos Chem Phys 2017;17:11331–53. doi:10.5194/acp-17-11331-2017.

[60] Derimian Y, Dubovik O, Huang X, Lapyonok T, Litvinov P, Kostinski AB, et al. Comprehensive tool for calculation of radiative fluxes: illustration of shortwave aerosol radiative effect sensitivities to the details in aerosol and underlying surface characteristics. Atmos Chem Phys 2016;16:5763–80. doi:10.5194/acp-16-5763-2016.

[61] Deuzé JL, Bréon FM, Devaux C, Goloub P, Herman M, Lafrance B, et al. Remote sensing of aerosols over land surfaces from POLDER-ADEOS-1 polarized measurements. J Geophys Res 2001;106:4913–26. doi:10.1029/2000JD900364.

[62] Di Noia A, Hasekamp OP, van Harten G, Rietjens JHH, Smit JM, Snik F, et al. Use of neural networks in ground-based aerosol retrievals from multi-angle spectropolarimetric observations. Atmos Meas Tech 2015;8:281–99. doi:10.5194/amt-8-281-2015.

[63] Di Noia A, Hasekamp OP, Wu L, van Diedenhoven B, Cairns B, Yorks JE. Combined neural network/Phillips–Tikhonov approach to aerosol retrievals over land from the NASA Research Scanning Polarimeter. Atmos Meas Tech 2017;10:4235–52. doi:10.5194/amt-10-4235-2017.

[64] Diner DJ, Xu F, Garay MJ, Martonchik JV, Rheingans BE, Geier S, et al. The Airborne Multiangle Spectropolarimetric Imager (AirMSPI): a new tool for aerosol and cloud remote sensing. Atmos Meas Tech 2013;6:2007–25. doi:10.5194/amt-6-2007-2013.

[65] Diner DJ, Beckert JC, Reilly TH, Bruegge CJ, Conel JE, Kahn RA, et al. Multiangle Imaging SpectroRadiometer (MISR) instrument description and experiment overview. IEEE Trans Geosci Remote Sens 1998;36:1072–87. doi:10.1109/36.700992.

[66] Diner DJ, Boland SW, Brauer M, Bruegge C, Burke KA, Chipman R, et al. Advances in multiangle satellite remote sensing of speciated airborne particulate matter and association with adverse health effects: from MISR to MAIA. J Appl Remote Sens 2018;12:042603. doi:10.1117/1.JRS.12.042603.

[67] Diner DJ, Braswell BH, Davies R, Gobron N, Hu J, Jin Y, et al. The value of multiangle measurements for retrieving structurally and radiatively consistent properties of clouds, aerosols, and surfaces. Remote Sens Environ 2005;97:495–518. doi:10.1016/j.rse.2005.06.006.

[68] Diner DJ, Davis A, Hancock B, Geier S, Rheingans B, Jovanovic V, et al. First results from a dual photoelastic-modulator-based polarimetric camera. Appl Opt 2010;49:2929–46. doi:10.1364/AO.49.002929.

[69] Diner DJ, Davis A, Hancock B, Gutt G, Chipman RA, Cairns B. Dual-photoelastic-modulator-based polarimetric imaging concept for aerosol remote sensing. Appl Opt 2007;46:8428–45. doi:10.1364/AO.46.008428.

[70] Diner DJ, Martonchik JV, Kahn RA, Pinty B, Gobron N, Nelson DL, et al. Using angular and spectral shape similarity constraints to improve MISR aerosol and surface retrievals over land. Remote Sens Environ 2005;94:155–71. doi:10.1016/j.rse.2004.09.009.

[71] Diner D, Xu F, Martonchik J, Rheingans B, Geier S, Jovanovic V, et al. Exploration of a polarized surface bidirectional reflectance model using the ground-based multiangle spectropolarimetric imager. Atmosphere 2012;3:591–619. doi:10.3390/atmos3040591.

[72] Dolgos G, Martins JV. Polarized Imaging Nephelometer for in situ airborne measurements of aerosol light scattering. Opt Express 2014;22:21972–90. doi:10.1364/OE.22.021972.

[73] Dubovik O, et al. GRASP algorithm: concept and application to remote sensing observations. J Quant Spectrosc Radiat Transf 2019.

[74] Dubovik O, Lapyonok T, Kaufman YJ, Chin M, Ginoux P, Kahn RA, et al. Retrieving global aerosol sources from satellites using inverse modeling. Atmos Chem Phys 2008;8:209–50. doi:10.5194/acp-8-209-2008.

[75] Dubovik O, Smirnov A, Holben BN, King MD, Kaufman YJ, Eck TF, et al. Accuracy assessments of aerosol optical properties retrieved from Aerosol Robotic Network (AERONET) Sun and sky radiance measurements. J Geophys Res 2000;105:9791–806. doi:10.1029/2000JD900040.

[76] Dubovik O. Optimization of numerical inversion in photopolarimetric remote sensing. In: Videen G, Yatskiv Y, Mishchenko M, editors. Photopolarimetry in remote sensing. Dordrecht, Netherlands: Kluwer; 2004. p. 65–106. doi:10.1007/1-4020-2368-5_3.

[77] Dubovik O, Holben B, Eck TF, Smirnov A, Kaufman YJ, King MD, et al. Variability of absorption and optical properties of key aerosol types observed in worldwide locations. J Atmos Sci 2002;59:590–608.

[78] Dubovik O, King MD. A flexible inversion algorithm for retrieval of aerosol optical properties from Sun and sky radiance measurements. J Geophys Res Atmos 2000;105:20673–96. doi:10.1029/2000JD900282.

[79] Dubovik O, Lapyonok T, Litvinov P, Herman M, Fuertes D, Ducos F, et al. GRASP: a versatile algorithm for characterizing the atmosphere. SPIE Newsroom 2014:2–5. doi:10.1117/2.1201408.005558.

[80] Dubovik O, Sinyuk A, Lapyonok T, Holben BN, Mishchenko M, Yang P, et al. Application of spheroid models to account for aerosol particle nonsphericity in remote sensing of desert dust. J Geophys Res 2006;111:D11208. doi:10.1029/2005JD006619.

[81] Espinosa WR, Martins JV, Remer LA, Dubovik O, Lapyonok T, Fuertes D, et al. Retrievals of aerosol size distribution, spherical fraction and complex refractive index from airborne in situ angular light scattering and absorption measurements. J Geophys Res Atmos 2019.

[82] Espinosa WR, Remer LA, Dubovik O, Ziemba L, Beyersdorf A, Orozco D, et al. Retrievals of aerosol optical and microphysical properties from imaging polar nephelometer scattering measurements. Atmos Meas Tech 2017;10:811–24. doi:10.5194/amt-10-811-2017.

[83] Fedarenka A, Dubovik O, Goloub P, Li Z, Lapyonok T, Litvinov P, et al. Utilization of AERONET polarimetric measurements for improving retrieval of aerosol microphysics: GSFC, Beijing and Dakar data analysis. J Quant Spectrosc Radiat Transf 2016;179:72–97. doi:10.1016/j.jqsrt.2016.03.021.

[84] Fernandez-Borda R, Waluschka E, Pellicori S, Martins VJ, Izquierdo LR, Cieslak JD. Evaluation of the polarization properties of a Philips-type prism for the construction of imaging polarimeters. Proc SPIE 2009;7461:746113.

[85] Formenti P. Le projet aerosols, radiation and clouds in Southern Africa (Aeroclo-SA). La Météorologie 2017;99:6. doi:10.4267/2042/63581.

[86] Fougnie B. Improvement of the PARASOL radiometric in-flight calibration based on synergy between various methods using natural targets. IEEE Trans Geosci Remote Sens 2016;54:2140–52. doi:10.1109/TGRS.2015.2496322.

[87] Fougnie B, Bach R. Monitoring of radiometric sensitivity changes of space sensors using deep convective clouds: operational application to PARASOL. IEEE Trans Geosci Remote Sens 2009;47:851–61. doi:10.1109/TGRS.2008.2005634.

[88] Fougnie B, Bracco G, Lafrance B, Ruffel C, Hagolle O, Tinel C. PARASOL in-flight calibration and performance. Appl Opt 2007;46:5435–51. doi:10.1364/AO.46.005435.

[89] Fougnie B, Marbach T, Lacan A, Lang R, Schlüssel P, Poli G, et al. The multi-viewing multi-channel multi-polarisation imager–overview of the 3MI polarimetric mission for aerosol and cloud characterization. J Quant Spectrosc Radiat Transf 2018;219:23–32. doi:10.1016/j.jqsrt.2018.07.008.

[90] Fu G, Hasekamp O. Multi-mode retrievals for aerosol microphysical and optical properties. Atmos Meas Tech Discuss 2018. doi:10.5194/amt-2018-306.

[91] Gao B-C, Kaufman YJ. Water vapor retrievals using Moderate Resolution Imaging Spectroradiometer (MODIS) near-infrared channels. J Geophys Res 2003;108:4389. doi:10.1029/2002JD003023.

[92] Gatebe CK, Dubovik O, King MD, Sinyuk A. Simultaneous retrieval of aerosol and surface optical properties from combined airborne- and ground-based direct and diffuse radiometric measurements. Atmos Chem Phys 2010;10:2777–94. doi:10.5194/acp-10-2777-2010.

[93] Geogdzhayev IV, Mishchenko MI, Rossow WB, Cairns B, Lacis AA. Global two-channel AVHRR retrievals of aerosol properties over the ocean for the period of NOAA-9 observations and preliminary retrievals using NOAA-7 and NOAA-11 data. J Atmos Sci 2002;59:262–78.

[94] Gérard B, Deuzé J-L, Herman M, Kaufman YJ, Lallart P, Oudard C, et al. Comparisons between POLDER 2 and MODIS/Terra aerosol retrievals over ocean. J Geophys Res 2005;110:D24211. doi:10.1029/2005JD006218.

[95] Gleason JF, Hsu NC, Torres O. Biomass burning smoke measured using backscattered ultraviolet radiation: SCAR-B and Brazilian smoke interannual variability. J Geophys Res 1998;103:31969–78.

[96] Goloub P, Li Z, Dubovik O, Blarel L, Podvin T, Jankowiak I, et al. PHOTONS/AERONET sunphotometer network overview: description, activities, results. Proc SPIE 2008;9636:96360V. doi:10.1117/12.783171.

[97] Goloub P, Tanré D, Deuzé JL, Herman M, Marchand A, Bréon FM. Validation of the first algorithm applied for deriving the aerosol properties over the ocean using the POLDER/ADEOS measurements. IEEE Trans Geosci Remote Sens 1999;37:1575–85. doi:10.1109/36.763270.

[98] Govaerts Y, Luffarelli M. Joint retrieval of surface reflectance and aerosol properties with continuous variations of the state variables in the solution space: Part 1: theoretical concept. Atmos Meas Tech Discuss 2017. doi:10.5194/amt-2017-29.

[99] Gu X, Cheng T, Xie D, Li Z, Yu T, Chen H. Analysis of surface and aerosol polarized reflectance for aerosol retrievals from polarized remote sensing in PRD urban region. Atmos Environ 2011;45:6607–12. doi:10.1016/j.atmosenv.2011.06.047.

[100] Guo J, Yao Z, Han Z, Zhao Z, Yin D, Yan W. Airborne experiment of TG-2 multi-angle polarization imager for cloud phase identification. Remote Sens Technol Appl 2018:439–48 in Chinese.

[101] Hagolle O, Goloub P, Deschamps PY, Cosnefroy H, Briottet X, Bailleul T, et al. Results of POLDER in-flight calibration. IEEE Trans Geosci Remote Sens 1999:1550–66. doi:10.1109/36.763266.

[102] Hair JW, Hostetler CA, Cook AL, Harper DB, Ferrare RA, Mack TL, et al. Airborne High Spectral Resolution Lidar for profiling aerosol optical properties. Appl Opt 2008;47:6734–52. doi:10.1364/AO.47.006734.

[103] Hansen JE, Travis LD. Light scattering in planetary atmospheres. Space Sci Rev 1974;16:527–610. doi:10.1007/BF00168069.

[104] Hasekamp OP. Capability of multi-viewing-angle photo-polarimetric measurements for the simultaneous retrieval of aerosol and cloud properties. Atmos Meas Tech 2010;3:839–51. doi:10.5194/amt-3-839-2010.

[105] Hasekamp O, Tuinder O, Stammes P. Final report of the O3M-SAF activity: aerosol retrieval from GOME-2: improving computational efficiency and first application; 2008.

[106] Hasekamp OP. Aerosol measurements by SPEXone on the NASA PACE Mission: expected retrieval capabilities. J Quant Spectrosc Radiat Transf 2019.

[107] Hasekamp OP, Landgraf J. Retrieval of aerosol properties over the ocean from multispectral single-viewing-angle measurements of intensity and polarization: retrieval approach, information content, and sensitivity study. J Geophys Res 2005;110:D20207. doi:10.1029/2005JD006212.

[108] Herman M, Deuzé JL, Devaux C, Goloub P, Bréon FM, Tanré D. Remote sensing of aerosols over land surfaces including polarization measurements and application to POLDER measurements. J Geophys Res 1999;102:17039–49. doi:10.1029/96JD02109.

[109] Herman M. Aerosol remote sensing from POLDER/ADEOS over the ocean: improved retrieval using a nonspherical particle model. J Geophys Res 2005;110:D10S02. doi:10.1029/2004JD004798.

[110] Higurashi A, Nakajima T. Development of a two-channel aerosol retrieval algorithm on a global scale using NOAA AVHRR. J Atmos Sci 1999;56:924–41.

[111] Holben BN, Eck TF, Slutsker I, Tanré D, Buis JP, Setzer A, et al. AERONET—a federated instrument network and data archive for aerosol characterization. Remote Sens Environ 1998;66:1–16. doi:10.1016/S0034-4257(98)00031-5.

[112] Hou W, Li Z, Wang J, Xu X, Goloub P, Qie L. Improving remote sensing of aerosol microphysical properties by near-infrared polarimetric measurements over vegetated land: information content analysis. J Geophys Res Atmos 2018;123:2215–43. doi:10.1002/2017JD027388.

[113] Hsu NC, Jeong M-J, Bettenhausen C, Sayer AM, Hansell R, Seftor CS, et al. Enhanced deep blue aerosol retrieval algorithm: the second generation. J Geophys Res Atmos 2013;118:9296–315. doi:10.1002/jgrd.50712.

[114] Huneeus N, Schulz M, Balkanski Y, Griesfeller J, Prospero J, Kinne S, et al. Global dust model intercomparison in AeroCom phase I. Atmos Chem Phys 2011;11:7781–816. doi:10.5194/acp-11-7781-2011.

[115] Huneeus N, Chevallier F, Boucher O. Estimating aerosol emissions by assimilating observed aerosol optical depth in a global aerosol model. Atmos Chem Phys 2012;12:4585–606. doi:10.5194/acp-12-4585-2012.

[116] Huneeus N, Boucher O, Chevallier F. Atmospheric inversion of SO_2 and primary aerosol emissions for the year 2010. Atmos Chem Phys 2013;13:6555–73. doi:10.5194/acp-13-6555-2013.

[117] Ignatov A, Stowe L. Aerosol retrievals from individual AVHRR channels. Part I: retrieval algorithm and transition from Dave to 6S radiative transfer model. J Atmos Sci 2002;59:313–34.

[118] Imaoka K, Kachi M, Fujii H, Murakami H, Hori M, Ono A, et al. Global Change Observation Mission (GCOM) for monitoring carbon, water cycles, and climate change. Proc IEEE 2010;98:717–34. doi:10.1109/JPROC.2009.2036869.

[119] Jacob DJ, Crawford JH, Maring H, Clarke AD, Dibb JE, Emmons LK, et al. The Arctic Research of the Composition of the Troposphere from Aircraft and Satellites (ARCTAS) mission: design, execution, and first results. Atmos Chem Phys 2010;10:5191–212. doi:10.5194/acp-10-5191-2010.

[120] Kahn RA, Nelson DL, Garay MJ, Levy RC, Bull MA, Diner DJ, et al. MISR Aerosol product attributes and statistical comparisons with MODIS. IEEE Trans Geosci Remote Sens 2009;47:4095–114. doi:10.1109/TGRS.2009.2023115.

[121] Kahn RA, Gaitley BJ. An analysis of global aerosol type as retrieved by MISR. J Geophys Res Atmos 2015;120:4248–81. doi:10.1002/2015JD023322.

[122] Kahn RA, Garay MJ, Nelson DL, Yau KK, Bull MA, Gaitley BJ, et al. Satellite-derived aerosol optical depth over dark water from MISR and MODIS: comparisons with AERONET and implications for climatological studies. J Geophys Res 2007;112:D18205. doi:10.1029/2006JD008175.

[123] Kahnert FM. Numerical methods in electromagnetic scattering theory. J Quant Spectrosc Radiat Transf 2003;79–80:775–824. doi:10.1016/S0022-4073(02)00321-7.

[124] Kahnert M. Numerical solutions of the macroscopic Maxwell equations for scattering by non-spherical particles: a tutorial review. J Quant Spectrosc Radiat Transf 2016;178:22–37. doi:10.1016/j.jqsrt.2015.10.029.

[125] Kalashnikova OV, Kahn R, Sokolik IN, Li W-H. Ability of multiangle remote sensing observations to identify and distinguish mineral dust types: optical models and retrievals of optically thick plumes. J Geophys Res 2005;110:D18S14. doi:10.1029/2004JD004550.

[126] Kalashnikova OV, Kahn R. Ability of multiangle remote sensing observations to identify and distinguish mineral dust types: 2. Sensitivity over dark water. J Geophys Res 2006;111:D11207. doi:10.1029/2005JD006756.

[127] King MD, Byrne DM, Herman BM, Reagan JA. Aerosol size distributions obtained by inversions of spectral optical depth measurements. J Atmos Sci 1978;35:2153–67.

[128] King MD, Dubovik O. Determination of aerosol optical properties from inverse methods. In: Lenoble J, Remer L, Tanré D, editors. Aerosol remote sensing. Berlin: Springer; 2013. p. 101–36. doi:10.1007/978-3-642-17725-5_5.

[129] Knobelspiesse K, Cairns B, Redemann J, Bergstrom RW, Stohl A. Simultaneous retrieval of aerosol and cloud properties during the MILAGRO field campaign. Atmos Chem Phys 2011;11:6245–63. doi:10.5194/acp-11-6245-2011.

[130] Knobelspiesse K, Cairns B, Ottaviani M, Ferrare R, Hair J, Hostetler C, et al. Combined retrievals of boreal forest fire aerosol properties with a polarimeter and lidar. Atmos Chem Phys 2011;11:7045–67. doi:10.5194/acp-11-7045-2011.

[131] Knobelspiesse K, Tan Q, Bruegge C, Cairns B, Chowdhary J, van Diedenhoven B, et al. Intercomparison of airborne multi-angle polarimeter observations from the Polarimeter Definition Experiment (PODEX). Appl Opt 2018.

[132] Knobelspiesse K, Nag S. Remote sensing of aerosols with small satellites in formation flight. Atmos Meas Tech 2018;11:3935–54. doi:10.5194/amt-11-3935-2018.

[133] Lacagnina C, Hasekamp OP, Bian H, Curci G, Myhre G, van Noije T, et al. Aerosol single-scattering albedo over the global oceans: comparing PARASOL retrievals with AERONET, OMI, and AeroCom models estimates. J Geophys Res Atmos 2015;120:9814–36. doi:10.1002/2015JD023501.

[134] Lacagnina C, Hasekamp OP, Torres O. Direct radiative effect of aerosols based on PARASOL and OMI satellite observations. J Geophys Res Atmos 2017;122:2366–88. doi:10.1002/2016JD025706.

[135] Lenoble J, Herman M, Deuzé JL, Lafrance B, Santer R, Tanré D. A successive order of scattering code for solving the vector equation of transfer in the Earth's atmosphere with aerosols. J Quant Spectrosc Radiat Transf 2007;107:479–507. doi:10.1016/j.jqsrt.2007.03.010.

[136] Li L, Dubovik O, Derimian Y, Schuster GL, Lapyonok T, Litvinov P, et al. Retrieval of aerosol composition directly from satellite and ground-based measurements. J Quant Spectrosc Radiait Transf 2019.

[137] Li X, Strahler AH. Geometric-optical bidirectional reflectance modeling of the discrete crown vegetation canopy: effect of crown shape and mutual shadowing. IEEE Trans Geosci Remote Sens 1992;30:276–92. doi:10.1109/36.134078.

[138] Li Z, Goloub P, Devaux C, Gu X, Deuzé J-L, Qiao Y, et al. Retrieval of aerosol optical and physical properties from ground-based spectral, multi-angular, and polarized sun-photometer measurements. Remote Sens Environ 2006;101:519–33. doi:10.1016/j.rse.2006.01.012.

[139] Li Z, Goloub P, Dubovik O, Blarel L, Zhang W, Podvin T, et al. Improvements for ground-based remote sensing of atmospheric aerosol properties by additional polarimetric measurements. J Quant Spectrosc Radiat Transf 2009;110:1954–61. doi:10.1016/j.jqsrt.2009.04.009.

[140] Li Z, Hou W, Hong J, Zheng F, Luo D, Wang J, et al. Directional Polarimetric Camera (DPC): monitoring aerosol spectral optical properties over land from satellite observation. J Quant Spectrosc Radiat Transf 2018;218:21–37. doi:10.1016/j.jqsrt.2018.07.003.

[141] Li Z, Xu H, Li K, Li D, Xie Y, Li L, et al. Comprehensive study of optical, physical, chemical, and radiative properties of total columnar atmospheric aerosols over China: an overview of sun–sky radiometer observation network (SONET) measurements. Bull Am Meteorol Soc 2018;99:739–55. doi:10.1175/BAMS-D-17-0133.1.

[142] Litvinov P, Hasekamp O, Cairns B, Mishchenko M. Reflection models for soil and vegetation surfaces from multiple-viewing angle photopolarimetric measurements. J Quant Spectrosc Radiat Transf 2010;111:529–39. doi:10.1016/j.jqsrt.2009.11.001.

[143] Litvinov P, Dubovik O, Cairns B. Model for land surface reflectance treatment: physical derivation, application for bare soil and evaluation on airborne and satellite measurements. J Quant Spectrosc Radiat Transf 2012;113:2023–39. doi:10.1016/j.jqsrt.2012.06.027.

[144] Liu L, Mishchenko M. Scattering and radiative properties of morphologically complex carbonaceous aerosols: a systematic modeling study. Remote Sens 2018;10:1634. doi:10.3390/rs10101634.

[145] Liu Y, Diner DJ. Multi-angle imager for aerosols: a satellite investigation to benefit public health. Public Health Rep 2017;132:14–17. doi:10.1177/0033354916679983.

[146] Liu Y, Koutrakis P, Kahn R. Estimating fine particulate matter component concentrations and size distributions using satellite-retrieved fractional aerosol optical depth: Part 1–method development. J Air Waste Manag Assoc 2007;57:1351–9. doi:10.3155/1047-3289.57.11.1351.

[147] Liu Y, Koutrakis P, Kahn R, Turquety S, Yantosca RM. Estimating fine particulate matter component concentrations and size distributions using satellite-retrieved fractional aerosol optical depth: part 2–a case study. J Air Waste Manag Assoc 2007;57:1360–9.

[148] Liu Y, Schichtel BA, Koutrakis P. Estimating particle sulfate concentrations using MISR retrieved aerosol properties. IEEE J Sel Top Appl Earth Obs Remote Sens 2009;2:176–84. doi:10.1109/JSTARS.2009.2030153.

[149] Lopatin A, Dubovik O, Chaikovsky A, Goloub P, Lapyonok T, Tanré D, et al. Enhancement of aerosol characterization using synergy of lidar and sun-photometer coincident observations: the GARRLiC algorithm. Atmos Meas Tech 2013;6:2065–88. doi:10.5194/amt-6-2065-2013.

[150] Lyapustin A, Wang Y, Laszlo I, Kahn R, Korkin S, Remer L, et al. Multiangle implementation of atmospheric correction (MAIAC): 2. Aerosol algorithm. J Geophys Res 2011;116:D03211. doi:10.1029/2010JD014986.

[151] Mackowski DW. A general superposition solution for electromagnetic scattering by multiple spherical domains of optically active media. J Quant Spectrosc Radiat Transf 2014;133:264–70. doi:10.1016/j.jqsrt.2013.08.012.

[152] Mackowski DW, Mishchenko MI. A multiple sphere *T*-matrix Fortran code for use on parallel computer clusters. J Quant Spectrosc Radiat Transf 2011;112:2182–92. doi:10.1016/j.jqsrt.2011.02.019.

[153] Maconi G, Penttilä A, Kassamakov I, Gritsevich M, Helander P, Puranen T, et al. Non-destructive controlled single-particle light scattering measurement. J Quant Spectrosc Radiat Transf 2018;204:159–64. doi:10.1016/j.jqsrt.2017.09.005.

[154] Maignan F, Bréon FM, Lacaze R. Bidirectional reflectance of Earth targets: evaluation of analytical models using a large set of spaceborne measurements with emphasis on the Hot Spot. Remote Sens Environ 2004;90:210–20. doi:10.1016/j.rse.2003.12.006.

[155] Maignan F, Bréon F-M, Fédèle E, Bouvier M. Polarized reflectances of natural surfaces: spaceborne measurements and analytical modeling. Remote Sens Environ 2009;113:2642–50. doi:10.1016/j.rse.2009.07.022.

[156] Marbach T, Riedi J, Lacan A, Schlüssel P. The 3MI mission: multi-viewing-channel-polarisation imager of the EUMETSAT polar system: second generation (EPS-SG) dedicated to aerosol and cloud monitoring. Proc SPIE 2015;9613:961310. doi:10.1117/12.2186978.

[157] Martins JV, Fernandez-Borda R, McBride B, Remer L, Barbosa HMJ. The HARP hyperangular imaging polarimeter and the need for small satellite payloads with high science payoff for Earth science remote sensing. In: Proceeding of the IEEE International Geoscience and Remote Sensing Symposium; 2018. p. 6304–7.

[158] Martins JV. SmallSat revolution: tiny satellites poised to make big contributions to essential science. The Conversation 2017. https://theconversation.com/smallsat-revolution-tiny-satellites-poised-to-make-big-contributions-to-essential-science-71440.

[159] Martonchik JV, Diner DJ, Crean KA, Bull MA. Regional aerosol retrieval results from MISR. IEEE Trans Geosci Remote Sens 2002;40:1520–31. doi:10.1109/TGRS.2002.801142.

[160] Martonchik JV, Diner DJ, Kahn RA, Ackerman TP, Verstraete MM, Pinty B, et al. Techniques for the retrieval of aerosol properties over land and ocean using multiangle imaging. IEEE Trans Geosci Remote Sens 1998;36:1212–27. doi:10.1109/36.701027.

[161] Martonchik JV, Kahn RA, Diner DJ. Retrieval of aerosol properties over land using MISR observations. In: Kokhanovsky A, de Leeuw G, editors. Satellite

aerosol remote sensing over land. Berlin: Springer; 2009. p. 267–93. doi:10.1007/978-3-540-69397-0_9.

[162] Mattis I, Ansmann A, Müller D, Wandinger U, Althausen D. Multiyear aerosol observations with dual-wavelength Raman lidar in the framework of EAR-LINET. J Geophys Res 2004;109:D13203. doi:10.1029/2004JD004600.

[163] McCorkel J, Cairns B, Wasilewski A. Imager-to-radiometer in-flight cross calibration: RSP radiometric comparison with airborne and satellite sensors. Atmos Meas Tech 2016;9:955–62. doi:10.5194/amt-9-955-2016.

[164] McCormick MP, Leavor KR. Active lidar remote sensing. In: Lenoble J, Remer L, Tanré D, editors. Aerosol remote sensing. Berlin: Springer; 2013. p. 283–313. doi:10.1007/978-3-642-17725-5_10.

[165] Milinevsky G, Oberemok Y, Syniavskyi I, Bovchaliuk A, Kolomiets I, Fesyanov I. Polarimetric modeling and calibration of the Aerosol-UA space mission instruments. J Quant Spectrosc Radiait Transf 2019.

[166] Milinevsky G, Yatskiv Y, Degtyaryov O, Syniavskyi I, Ivanov Y, Bovchaliuk A, et al. Remote sensing of aerosol in the terrestrial atmosphere from space: new missions. Adv Astron Space Phys 2015;5:11–16. doi:10.17721/2227-1481.5.11-16.

[167] Milinevsky G, Yatskiv Y, Degtyaryov O, Syniavskyi I, Mishchenko M, Rosenbush V, et al. New satellite project Aerosol-UA: remote sensing of aerosols in the terrestrial atmosphere. Acta Astronaut 2016;123:292–300. doi:10.1016/j.actaastro.2016.02.027.

[168] Mishchenko MI, Travis LD, Lacis AA. Scattering, absorption, and emission of light by small particles. Cambridge, UK: Cambridge University Press; 2002.

[169] Mishchenko MI, Hovenier JW, Travis LD, editors. Light scattering by nonspherical particles: theory, measurements, and applications. San Diego: Academic Press; 2000.

[170] Mishchenko MI, Travis LD, Lacis AA. Multiple scattering of light by particles: radiative transfer and coherent backscattering. Cambridge, UK: Cambridge University Press; 2006.

[171] Mishchenko MI, Travis LD, Kahn RA, West RA. Modeling phase functions for dustlike tropospheric aerosols using a shape mixture of randomly oriented polydisperse spheroids. J Geophys Res 1997;102:16831–47. doi:10.1029/96JD02110.

[172] Mishchenko MI, Geogdzhayev IV, Cairns B, Rossow WB, Lacis AA. Aerosol retrievals over the ocean by use of channels 1 and 2 AVHRR data: sensitivity analysis and preliminary results. Appl Opt 1999;38:7325–41. doi:10.1364/AO.38.007325.

[173] Mishchenko MI. Directional radiometry and radiative transfer: the convoluted path from centuries-old phenomenology to physical optics. J Quant Spectrosc Radiat Transf 2014;146:4–33. doi:10.1016/j.jqsrt.2014.02.033.

[174] Mishchenko MI. Electromagnetic scattering by particles and particle groups: an introduction. Cambridge, UK: Cambridge University Press; 2014.

[175] Mishchenko MI, Liu L, Mackowski DW. T-matrix modeling of linear depolarization by morphologically complex soot and soot-containing aerosols. J Quant Spectrosc Radiat Transf 2013;123:135–44. doi:10.1016/j.jqsrt.2012.11.012.

[176] Mishchenko MI, Goldstein DH, Chowdhary J, Lompado A. Radiative transfer theory verified by controlled laboratory experiments. Opt Lett 2013;38:3522–5. doi:10.1364/OL.38.003522.

[177] Mishchenko MI, Dlugach JM, Liu L. Linear depolarization of lidar returns by aged smoke particles. Appl Opt 2016;55:9968–73. doi:10.1364/AO.55.009968.

[178] Mishchenko MI, Alexandrov MD, Cairns B, Travis LD. Multistatic aerosol–cloud lidar in space: a theoretical perspective. J Quant Spectrosc Radiat Transf 2016;184:180–92. doi:10.1016/j.jqsrt.2016.07.015.

[179] Mishchenko MI, Dlugach JM, Liu L. Applicability of the effective-medium approximation to heterogeneous aerosol particles. J Quant Spectrosc Radiat Transf 2016;178:284–94. doi:10.1016/j.jqsrt.2015.12.028.

[180] Mishchenko MI, Sassen K. Depolarization of lidar returns by small ice crystals: an application to contrails. Geophys Res Lett 1998;25:309–12. doi:10.1029/97GL03764.

[181] Molina LT, Madronich S, Gaffney JS, Apel E, de Foy B, Fast J, et al. An overview of the MILAGRO 2006 campaign: Mexico City emissions and their transport and transformation. Atmos Chem Phys 2010;10:8697–760. doi:10.5194/acp-10-8697-2010.

[182] Muinonen K, Mishchenko MI, Dlugach JM, Zubko E, Penttilä A, Videen G. Coherent backscattering verified numerically for a finite volume of spherical particles. Astrophys J 2012;760:118. doi:10.1088/0004-637X/760/2/118.

[183] Mukai S, Fujito T, Nakata M, Sano I. Role of near ultraviolet wavelength measurements in the detection and retrieval of absorbing aerosols from space. Proc SPIE 2017;10424:104240X. doi:10.1117/12.2277826.

[184] Müller D, Veselovskii I, Kolgotin A, Tesche M, Ansmann A, Dubovik O. Vertical profiles of pure dust and mixed smoke–dust plumes inferred from inversion of multiwavelength Raman/polarization lidar data and comparison to AERONET retrievals and in situ observations. Appl Opt 2013;52:3178–202. doi:10.1364/AO.52.003178.

[185] Muñoz O, Moreno F, Guirado D, Dabrowska DD, Volten H, Hovenier JW. The Amsterdam–Granada light scattering database. J Quant Spectrosc Radiat Transf 2012;113:565–74. doi:10.1016/j.jqsrt.2012.01.014.

[186] Muñoz O, Moreno F, Guirado D, Ramos JL, López A, Girela F, et al. Experimental determination of scattering matrices of dust particles at visible wavelengths: the IAA light scattering apparatus. J Quant Spectrosc Radiat Transf 2010;111:187–96. doi:10.1016/j.jqsrt.2009.06.011.

[187] Nadal F, Bréon F-M. Parameterization of surface polarized reflectance derived from POLDER spaceborne measurements. IEEE Trans Geosci Remote Sens 1999;37:1709–18. doi:10.1109/36.763292.

[188] Nakajima T, Tonna G, Rao R, Boi P, Kaufman Y, Holben B. Use of sky brightness measurements from ground for remote sensing of particulate polydispersions. Appl Opt 1996;35:2672–86. doi:10.1364/AO.35.002672.

[189] Neukermans G, Harmel T, Galí M, Rudorff N, Chowdhary J, Dubovik O, et al. Harnessing remote sensing to address critical science questions on ocean–atmosphere interactions. Elem Sci Anth 2018;6:71. doi:10.1525/elementa.331.

[190] O'Neill NT, Dubovik O, Eck TF. Modified Ångström exponent for the characterization of submicrometer aerosols. Appl Opt 2001;40:2368–75. doi:10.1364/AO.40.002368.

[191] O'Neill NT, Eck TF, Holben BN, Smirnov A, Dubovik O, Royer A. Bimodal size distribution influences on the variation of Ångström derivatives in spectral and optical depth space. J Geophys Res 2001;106:9787–806. doi:10.1029/2000JD900245.

[192] Panetta RL, Liu C, Yang P. A pseudo-spectral time domain method for light scattering computation. Light Scatt Rev 2013;8:139–88. doi:10.1007/978-3-642-32106-1_4.

[193] Peers F, Bellouin N, Waquet F, Ducos F, Goloub P, Mollard J, et al. Comparison of aerosol optical properties above clouds between POLDER and AeroCom models over the South East Atlantic ocean during the fire season. Geophys Res Lett 2016;43:3991–4000. doi:10.1002/2016GL068222.

[194] Peers F, Waquet F, Cornet C, Dubuisson P, Ducos F, Goloub P, et al. Absorption of aerosols above clouds from POLDER/PARASOL measurements and estimation of their direct radiative effect. Atmos Chem Phys 2015;15:4179–96. doi:10.5194/acp-15-4179-2015.

[195] Peralta RJ, Nardell C, Cairns B, Russell EE, Travis LD, Mishchenko MI, et al. Aerosol polarimetry sensor for the Glory Mission. Proc SPIE 2007;6786:67865L. doi:10.1117/12.783307.

[196] Popp T, de Leeuw G, Bingen C, Brühl C, Capelle V, Chedin A, et al. Development, production and evaluation of aerosol climate data records from European satellite observations (Aerosol_cci). Remote Sens 2016;8:421. doi:10.3390/rs8050421.

[197] Povey AC, Grainger RG. Known and unknown unknowns: uncertainty estimation in satellite remote sensing. Atmos Meas Tech 2015;8:4699–718. doi:10.5194/amt-8-4699-2015.

[198] Qie L, Li Z, Sun X, Sun B, Li D, Liu Z, et al. Improving remote sensing of aerosol optical depth over land by polarimetric measurements at 1640 nm: airborne test in North China. Remote Sens 2015;7:6240–56. doi:10.3390/rs70506240.

[199] Rahman H, Pinty B, Verstraete MM. Coupled surface-atmosphere reflectance (CSAR) model: 2. Semiempirical surface model usable with NOAA/AVHRAA data. J Geophys Res 1993;98:20791–801.

[200] Remer LA, Kaufman YJ, Tanré D, Mattoo S, Chu DA, Martins JV, et al. The MODIS aerosol algorithm, products, and validation. J Atmos Sci 2005;62:947–73. doi:10.1175/JAS3385.1.

[201] Rietjens JHH, Smit JM, Snik F, di Noia A, Hasekamp OP, van Harten G, et al. SPEX: a highly accurate spectropolarimeter for atmospheric aerosol characterization. Proc SPIE 2017;10563:1056344. doi:10.1117/12.2304227.

[202] Ross J. The radiation regime and architecture of plant stands. The Haque: Dr. W. Junk Publishers; 1981.

[203] Russell PB, Bergstrom RW, Shinozuka Y, Clarke AD, DeCarlo PF, Jimenez JL, et al. Absorption Ångström exponent in AERONET and related data as an indicator of aerosol composition. Atmos Chem Phys 2010;10:1155–69. doi:10.5194/acp-10-1155-2010.

[204] Russell PB, Kacenelenbogen M, Livingston JM, Hasekamp OP, Burton SP, Schuster GL, et al. A multiparameter aerosol classification method and its application to retrievals from spaceborne polarimetry. J Geophys Res Atmos 2014;119:9838–63. doi:10.1002/2013JD021411.

[205] Sano I, Okada Y, Mukai M, Mukai S. Retrieval algorithm based on combined use of POLDER and GLI data for biomass aerosols. J Remote Sens Soc Jpn 2009;29:54–9.

[206] Sano I. Optical thickness and Ångström exponent of aerosols over the land and ocean from space-borne polarimetric data. Adv Space Res 2004;34:833–7. doi:10.1016/j.asr.2003.06.039.

[207] Sano I, Mukai S. Algorithm description of system flow for global aerosol distribution. Appl Math Comput 2000;116:79–91. doi:10.1016/S0096-3003(99)00196-4.

[208] Sano I, Mukai S. Polarimetric properties of aerosol particles. Earth Planets Space 1998;50:513–19. doi:10.1186/BF03352143.

[209] Sano I, Mukai S, Nakata M. An effective method for retrieval of three kinds of aerosol properties focusing on a coming GCOM-C1/SGLI in December of 2017. Proc SPIE 2017;10424:1042403. doi:10.1117/12.2278159.

[210] Sassen K. LIDAR backscatter depolarization technique for cloud and aerosol research. In: Mishchenko MI, Hovenier JW, Travis LD, editors. Light scattering by nonspherical particles: theory, measurements, and applications. San Diego: Academic Press; 2000. p. 393–416.

[211] Schuster GL, Dubovik O, Arola A. Remote sensing of soot carbon – Part 1: distinguishing different absorbing aerosol species. Atmos Chem Phys 2016;16:1565–85. doi:10.5194/acp-16-1565-2016.

[212] Schuster GL, Dubovik O, Arola A, Eck TF, Holben BN. Remote sensing of soot carbon – Part 2: understanding the absorption Ångström exponent. Atmos Chem Phys 2016;16:1587–602. doi:10.5194/acp-16-1587-2016.

[213] Schuster GL. Inferring black carbon content and specific absorption from Aerosol Robotic Network (AERONET) aerosol retrievals. J Geophys Res 2005;110:D10S17. doi:10.1029/2004JD004548.

[214] Schuster GL, Lin B, Dubovik O. Remote sensing of aerosol water uptake. Geophys Res Lett 2009;36:L03814. doi:10.1029/2008GL036576.

[215] Segal-Rozenhaimer M, Miller DJ, Knobelspiesse K, Redemann J, Cairns B, Alexandrov MD. Development of neural network retrievals of liquid cloud properties from multi-angle polarimetric observations. J Quant Spectrosc Radiat Transf 2018;220:39–51. doi:10.1016/j.jqsrt.2018.08.030.

[216] Sinclair K, van Diedenhoven B, Cairns B, Alexandrov M, Moore R, Crosbie E, et al. Polarimetric retrievals of cloud droplet number concentrations. Remote Sens Environ 2019.

[217] Sinyuk A, Dubovik O, Holben B, Eck TF, Bréon F-M, Martonchik J, et al. Simultaneous retrieval of aerosol and surface properties from a combination of AERONET and satellite data. Remote Sens Environ 2007;107:90–108. doi:10.1016/j.rse.2006.07.022.

[218] Snik F, Karalidi T, Keller CU. Spectral modulation for full linear polarimetry. Appl Opt 2009;48:1337–46. doi:10.1364/AO.48.001337.

[219] Stap FA, Hasekamp OP, Röckmann T. Sensitivity of PARASOL multi-angle photopolarimetric aerosol retrievals to cloud contamination. Atmos Meas Tech 2015;8:1287–301. doi:10.5194/amt-8-1287-2015.

[220] Starr D Aerosol, Cloud, and Ecosystem (ACE) proposed mission study report http://acemission.gsfc.nasa.gov/Study_Report_2010.html.

[221] Syniavskyi II, Milinevsky GP, Ivanov YS, Sosonkin MG, Danylevsky VO, Rosenbush VK, et al. Methodology, hardware implementation, and validation of satellite remote sensing of atmospheric aerosols: first results of the Aerosol-UA space experiment development. Kosmichna Nauka Tehnol 2015;21:9–17. doi:10.15407/knit2015.03.009.

[222] Torres B, Dubovik O, Fuertes D, Schuster G, Cachorro VE, Lapyonok T, et al. Advanced characterisation of aerosol size properties from measurements of spectral optical depth using the GRASP algorithm. Atmos Meas Tech 2017;10:3743–81. doi:10.5194/amt-10-3743-2017.

[223] Torres O, Bhartia PK, Herman JR, Ahmad Z, Gleason J. Derivation of aerosol properties from satellite measurements of backscattered ultraviolet radiation: theoretical basis. J Geophys Res 1998;103:17099–110. doi:10.1029/98JD00900.

[224] Twomey S. Introduction to the mathematics of inversion in remote sensing and indirect measurements. Amsterdam: Elsevier; 1977.

[225] Tyo JS, Goldstein DL, Chenault DB, Shaw JA. Review of passive imaging polarimetry for remote sensing applications. Appl Opt 2006;45:5453–69. doi:10.1364/AO.45.005453.

[226] Unga F, Choël M, Derimian Y, Deboudt K, Dubovik O, Goloub P. Microscopic observations of core-shell particle structure and implications for atmospheric aerosol remote sensing. J Geophys Res Atmos 2018. doi:10.1029/2018JD028602.

[227] van Amerongen AH, Rietjens J, Smit M, van Loon D, van Brug H, Esposito M, et al. SPEX: the Dutch roadmap towards aerosol measurement from space. Proc SPIE 2017;10562:1056210. doi:10.1117/12.2296227.

[228] van Amerongen AH. SPEXone: a compact multi-angle spectro-polarimeter. In: Proceedings of the ICSO; 2018.

[229] van Diedenhoven B, Cairns B, Fridlind AM, Ackerman AS, Garrett TJ. Remote sensing of ice crystal asymmetry parameter using multi-directional polarization measurements – Part 2: application to the research scanning polarimeter. Atmos Chem Phys 2013;13:3185–203. doi:10.5194/acp-13-3185-2013.

[230] van Diedenhoven B, Cairns B, Geogdzhayev IV, Fridlind AM, Ackerman AS, Yang P, et al. Remote sensing of ice crystal asymmetry parameter using multi-directional polarization measurements – Part 1: methodology and evaluation with simulated measurements. Atmos Meas Tech 2012;5:2361–74. doi:10.5194/amt-5-2361-2012.

[231] van Diedenhoven B, Fridlind AM, Cairns B, Ackerman AS, Yorks JE. Vertical variation of ice particle size in convective cloud tops. Geophys Res Lett 2016;43:4586–93. doi:10.1002/2016GL068548.

[232] van Harten G, Snik F, Rietjens JHH, Smit JM, Keller CU. Spectral line polarimetry with a channeled polarimeter. Appl Opt 2014;53:4187–94. doi:10.1364/AO.53.004187.

[233] van Harten G, De Boer J, Rietjens JHH, Di Noia A, Snik F, Volten H, et al. Atmospheric aerosol characterization with a ground-based SPEX spectropolarimetric instrument. Atmos Meas Tech 2014;7:4341–51. doi:10.5194/amt-7-4341-2014.

[234] van Harten G, Diner DJ, Daugherty BJS, Rheingans BE, Bull MA, Seidel FC, et al. Calibration and validation of Airborne Multiangle SpectroPolarimetric Imager (AirMSPI) polarization measurements. Appl Opt 2018;57:4499–513. doi:10.1364/AO.57.004499.

[235] Vermeulen A, Devaux C, Herman M. Retrieval of the scattering and microphysical properties of aerosols from ground-based optical measurements including polarization. I. Method. Appl Opt 2000;39:6207–20. doi:10.1364/AO.39.006207.

[236] Veefkind JP, de Leeuw G, Stammes P, Koelemeijer RBA. Regional distribution of aerosol over land, derived from ATSR-2 and GOME. Remote Sens Environ 2000;74:377–86.

[237] Veselovskii I, Dubovik O, Kolgotin A, Lapyonok T, Di Girolamo P, Summa D, et al. Application of randomly oriented spheroids for retrieval of dust particle parameters from multiwavelength lidar measurements. J Geophys Res 2010;115:D21203. doi:10.1029/2010JD014139.

[238] Volten H, Muñoz O, Rol E, de Haan JF, Vassen W, Hovenier JW, et al. Scattering matrices of mineral aerosol particles at 441.6 nm and 632.8 nm. J Geophys Res 2001;106:17375–401. doi:10.1029/2001JD900068.

[239] Wagner J, Ansmann A, Wandinger U, Seifert P, Schwarz A, Tesche M, et al. Evaluation of the Lidar/Radiometer Inversion Code (LIRIC) to determine microphysical properties of volcanic and desert dust. Atmos Meas Tech 2013;6:1707–24. doi:10.5194/amt-6-1707-2013.

[240] Wang H, Sun X, Sun B, Liang T, Li C, Hong J. Retrieval of aerosol optical properties over a vegetation surface using multi-angular, multi-spectral, and polarized data. Adv Atmos Sci 2014;31:879–87. doi:10.1007/s00376-013-3100-5.

[241] Wang H, Yang L, Deng A, Du W, Liu P, Sun X, et al. Remote sensing of aerosol optical depth using an airborne polarimeter over North China. Remote Sens 2017;9:979. doi:10.3390/rs9100979.

[242] Wang X, Guo Z, Huang Y, Fan H, Li W. A cloud detection scheme for the Chinese Carbon Dioxide Observation Satellite (TANSAT). Adv Atmos Sci 2017;34:16–25. doi:10.1007/s00376-016-6033-y.

[243] Wang J, Xu X, Henze DK, Zeng J, Ji Q, Tsay S-C, et al. Top-down estimate of dust emissions through integration of MODIS and MISR aerosol retrievals with the GEOS-Chem adjoint model. Geophys Res Lett 2012;39:L08802. doi:10.1029/2012GL051136.

[244] Wanner W, Li X, Strahler AH. On the derivation of kernels for kernel-driven models of bidirectional reflectance. J Geophys Res 1995;100:21077–89.

[245] Waquet F, Cairns B, Knobelspiesse K, Chowdhary J, Travis LD, Schmid B, et al. Polarimetric remote sensing of aerosols over land. J Geophys Res 2009;114:D01206. doi:10.1029/2008JD010619.

[246] Waquet F, Léon J-F, Cairns B, Goloub P, Deuzé J-L, Auriol F. Analysis of the spectral and angular response of the vegetated surface polarization for the purpose of aerosol remote sensing over land. Appl Opt 2009;48:1228–36. doi:10.1364/AO.48.001228.

[247] Waquet F, Léon J-F, Goloub P, Pelon J, Tanré D, Deuzé J-L. Maritime and dust aerosol retrieval from polarized and multispectral active and passive sensors. J Geophys Res 2005;110:D10S10. doi:10.1029/2004JD004839.

[248] Waquet F, Cornet C, Deuzé J-L, Dubovik O, Ducos F, Goloub P, et al. Retrieval of aerosol microphysical and optical properties above liquid clouds from POLDER/PARASOL polarization measurements. Atmos Meas Tech 2013;6:991–1016. doi:10.5194/amt-6-991-2013.

[249] Waquet F, Peers F, Ducos F, Goloub P, Platnick S, Riedi J, et al. Global analysis of aerosol properties above clouds. Geophys Res Lett 2013;40:5809–14. doi:10.1002/2013GL057482.

[250] Waquet F, Riedi J, Labonnote LC, Goloub P, Cairns B, Deuzé J-L, et al. Aerosol remote sensing over clouds using A-Train observations. J Atmos Sci 2009;66:2468–80. doi:10.1175/2009JAS3026.1.

[251] Waquet F, Goloub P, Deuzé J-L, Léon J-F, Auriol F, Verwaerde C, et al. Aerosol retrieval over land using a multiband polarimeter and comparison with path radiance method. J Geophys Res 2007;112:D11214. doi:10.1029/2006JD008029.

[252] Weitkamp C, editor. Lidar: range-resolved optical remote sensing of the atmosphere. Berlin: Springer; 2005.

[253] Winker DM, Vaughan MA, Omar A, Hu Y, Powell KA, Liu Z, et al. Overview of the CALIPSO mission and CALIOP data processing algorithms. J Atmos Ocean Technol 2009;26:2310–23. doi:10.1175/2009JTECHA1281.1.

[254] Wu L, Hasekamp O, Van Diedenhoven B, Cairns B. Aerosol retrieval from multiangle, multispectral photopolarimetric measurements: importance of spectral range and angular resolution. Atmos Meas Tech 2015;8:2625–38. doi:10.5194/amt-8-2625-2015.

[255] Wu L, Hasekamp O, van Diedenhoven B, Cairns B, Yorks JE, Chowdhary J. Passive remote sensing of aerosol layer height using near-UV multiangle polarization measurements. Geophys Res Lett 2016;43:8783–90. doi:10.1002/2016GL069848.

[256] Xu F, van Harten G, Diner DJ, Davis AB, Seidel FC, Rheingans B, et al. Coupled retrieval of liquid water cloud and above-cloud aerosol properties using the Airborne Multiangle SpectroPolarimetric Imager (AirMSPI). J Geophys Res Atmos 2018;123:3175–204. doi:10.1002/2017JD027926.

[257] Xu F, van Harten G, Diner DJ, Kalashnikova OV, Seidel FC, Bruegge CJ, et al. Coupled retrieval of aerosol properties and land surface reflection using the Airborne Multiangle SpectroPolarimetric Imager. J Geophys Res Atmos 2017;122:7004–26. doi:10.1002/2017JD026776.

[258] Xu X, Wang J, Zeng J, Spurr R, Liu X, Dubovik O, et al. Retrieval of aerosol microphysical properties from AERONET photopolarimetric measurements: 2. A new research algorithm and case demonstration. J Geophys Res Atmos 2015;120:7079–98. doi:10.1002/2015JD023113.

[259] Xu X, Wang J, Henze DK, Qu W, Kopacz M. Constraints on aerosol sources using GEOS-Chem adjoint and MODIS radiances, and evaluation with multisensor (OMI, MISR) data. J Geophys Res Atmos 2013;118:6396–413. doi:10.1002/jgrd.50515.

[260] Yurkin MA, Hoekstra AG. The discrete-dipole-approximation code ADDA: capabilities and known limitations. J Quant Spectrosc Radiat Transf 2011;112:2234–47. doi:10.1016/j.jqsrt.2011.01.031.

[261] Zhang J, Shao J, Yan C. Cloud and aerosol polarimetric imager. Proc SPIE 2013;9142:91420X. doi:10.1117/12.2054572.

[262] Zhang L, Henze DK, Grell GA, Carmichael GR, Bousserez N, Zhang Q, et al. Constraining black carbon aerosol over Asia using OMI aerosol absorption optical depth and the adjoint of GEOS-Chem. Atmos Chem Phys 2015;15:10281–308. doi:10.5194/acp-15-10281-2015.

[263] Zhang Y, Li Z, Qie L, Hou W, Liu Z, Zhang Y, et al. Retrieval of aerosol optical depth using the Empirical Orthogonal Functions (EOFs) based on PARASOL multi-angle intensity data. Remote Sens 2017;9:578. doi:10.3390/rs9060578.

[264] Zhang Y, Li Z, Qie L, Zhang Y, Liu Z, Chen X, et al. Retrieval of aerosol fine-mode fraction from intensity and polarization measurements by PARASOL over East Asia. Remote Sens 2016;8:417. doi:10.3390/rs8050417.

[265] Zuidema P, Redemann J, Haywood J, Wood R, Piketh S, Hipondoka M, et al. Smoke and clouds above the Southeast Atlantic: upcoming field cam-

paigns probe absorbing aerosol's impact on climate. Bull Am Meteorol Soc 2016;97:1131–5. doi:10.1175/BAMS-D-15-00082.1.

[266] Cetinic I, McClain CR, Werdell PJ, editors. Pre-Aerosol, Clouds, and ocean ecosystem (PACE) mission science definition team report. NASA/TM-2018-219027/Vol. 2, 2018. https://pace.oceansciences.org/docs/PACE_TM2018-219027_Vol_2.pdf.

[267] Hansen JE. Circular polarization of sunlight reflected by clouds. J Atmos Sci 1971;28:1515–16.

[268] de Graaf M, Stammes P, Torres O, Koelemeijer RBA. Absorbing aerosol index: sensitivity analysis, application to GOME and comparison with TOMS. J Geophys Res 2005;110:D01201. doi:10.1029/2004JD005178.

[269] de Graaf M, Stammes P, Aben EAA. Analysis of reflectance spectra of UV-absorbing aerosol scenes measured by SCIAMACHY. J Geophys Res 2007;112:D02206. doi:10.1029/2006JD007249.

[270] Gottwald M, Bovensmann H, editors. SCIAMACHY–exploring the changing earth's atmosphere. Berlin: Springer; 2010.

[271] Munro R, Lang R, Klaes D, Poli G, Retscher C, Lindstrot R, et al. The GOME-2 instrument on the Metop series of satellites: instrument design, calibration, and level 1 data processing – an overview. Atmos Meas Tech 2016;9:1279–301. doi:10.5194/amt-9-1279-2016.

[272] Schutgens NAJ, Tilstra LG, Stammes P, Bréon F-M. On the relationship between Stokes parameters Q and U of atmospheric ultraviolet/visible/near-infrared radiation. J Geophys Res 2004;109:D09205. doi:10.1029/2003JD004081.

[273] Tilstra LG, deGraaf M, Aben I, Stammes P. In-flight degradation correction of SCIAMACHY UV reflectances and Absorbing Aerosol Index. J Geophys Res 2012;117:D06209. doi:10.1029/2011JD016957.

[274] Tilstra LG, Lang R, Munro R, Aben I, Stammes P. Contiguous polarisation spectra of the Earth from 300 to 850 nm measured by GOME-2 onboard MetOp-A. Atmos Meas Tech 2014;7:2047–59. doi:10.5194/amt-7-2047-2014.

[275] Lichtenberg G, Kleipool Q, Krijger JM, van Soest G, van Hees R, Tilstra LG, et al. SCIAMACHY Level 1 data: calibration concept and in-flight calibration. Atmos Chem Phys 2006;6:5347–67. doi:10.5194/acp-6-5347-2006.

[276] Liebing P, Bramstedt K, Noël S, Rozanov V, Bovensmann H, Burrows JP. Polarization data from SCIAMACHY limb backscatter observations compared to vector radiative transfer model simulations. Atmos Meas Tech 2013;6:1503–20. doi:10.5194/amt-6-1503-2013.

[277] de Graaf M, Tilstra LG, Wang P, Stammes P. Retrieval of the aerosol direct radiative effect over clouds from spaceborne spectrometry. J Geophys Res 2012;117:D07207. doi:10.1029/2011JD017160.